APPLICATION OF FUNCTIONALIZED CELLULOSE NANOCRYSTALS TO IMPROVE THEIR DISPERSION IN POLYMER MATRIX AND ENHANCE THE THERMO-MECHANICAL PROPERTIES OF POLYMER COMPOSITES

by

Saptaparni Chanda

A dissertation submitted in partial fulfillment
of the requirements for the degree

of

Doctor of Philosophy

in

Mechanical Engineering

MONTANA STATE UNIVERSITY
Bozeman, Montana

July 2023

ACKNOWLEDGEMENTS

I would like to thank the researchers who have helped me with experiments, answered questions or provided valuable discussion- Seth Kane, Ashton Chan, Riad Rezaul, Daniel Collins, Dalton Nold, Hayden Pritchard, Daniel Blake. Many professors have provided me with mentorship during the research, particularly I would like to thank Dr. Ladean McKittrick and Dr. Stephan Warnat for helping me in tensile testing of composite materials and electrical impedance spectra analysis of composite materials, respectively. I would like to thank my committee members- Dr. Cecily Ryan, Dr. Kirsten Matteson, Dr. Sreekala Bajwa – for their excellent mentorship throughout my doctorate journey. Finally, I would like to thank my advisor Dr. Dilpreet Bajwa, for all of the mentorship and guidance he gave me. The research is funded by U.S. National Institute of Standards and Technology (NIST), grant number 70NANB18H256N.

TABLE OF CONTENTS

1. INTRODUCTION 1

2. A REVIEW OF CURRENT PHYSICAL TECHNIQUES FOR DISPERS ION OF CELLULOSE NANOMATERIALS IN POLYMER MATRICES 4

Contribution of Authors & Co-Authors 4
Manuscript Information Page 5
Abstract 6
Introduction 7
Cellulose Nanocrystals 8
Cellulose Nanofibrils 9
Bacterial Nanocellulose 10
Significance of surface modification 11
Chemical-aided dispersion of cellulose nanomaterials (CNM) 12
Polymer grafting 12
Silylation 14
Other chemical treatments 16
Physical-aided dispersion of cellulose nanomaterials (CNM) 18
Plasma induced surface modification 18
Ultrasonication 22
Magnetic force induced alignment 25
Electric discharge 28
Electrospinning 29
Drawing 32
Quantum dot treatment 35
Conclusion and future direction 37

3. SILANE COMPATIBILIZATION TO IMPROVE THE DISPERSION, THERMAL AND MECHANICAL PROPERTIES OF CELLULOSE NANOCRYSTALS IN POLY(ETHYLENE OXIDE) 39

Contribution of Authors & Co-Authors 39
Manuscript Information Page 40
Abstract 41
Introduction 42
Experimental 45
Results and discussion 48
Conclusion 58

TABLE OF CONTENTS CONTINUED

4. NANO BORON OXIDE AND NANO ZINC OXIDE INCORPORATION TO CELLULOSE NANOCRYSTALS TO IMPROVE THE THERMAL, MECHA NICAL, FLAMMABILITY PROPERTIES OF HIGH-DENSITY POLY(ETHY LENE) POLYMER....60

Contribution of Authors & Co-Authors....60
Manuscript Information Page....61
Abstract....62
Introduction....63
Experimental....66
Results and discussion....70
Conclusion....87

5. NANO BORON OXIDE AND NANO ZINC OXIDE INCORPORATION TO LIGNIN CONTAINING CELLULOSE NANOCRYSTALS TO IMPROVE THE THERMAL, MECHANICAL, FLAMMABILITY PROPERTIES OF HIGH-DENSITY POLY (ETHYLENE) POLYMER....88

Contribution of Authors & Co-Authors....88
Manuscript Information Page....89
Abstract....90
Introduction....91
Experimental section....94
Results and discussion....98
Conclusion....115

6. GRAPHENE QUANTUM DOTS INCORPORATION TO IMPROVE DISPERSI ON OF CELLULOSE NANOCRYSTALS AND THERMAL, PHYSICAL AND MECHANICAL PROPERTIES OF HIGH-DENSITY POLY (ETHYL ENE) POLYMER COMPOSITES....117

Contribution of Authors & Co-Authors....117
Manuscript Information Page....118
Abstract....119
Introduction....120
Experimental section....122
Results and discussion....125
Conclusion....141

REFERENCES CITED....143

LIST OF TABLES

Table Page

2.1. Formulation of nanocomposite samples 46

2.2. Grafting degree of each formulation from TGA....51

2.3. Crystallization behavior of each formulation from DSC....54

2.4. Dynamic mechanical properties of each formulation from DMA....55

2.5. Storage modulus of other CNC composites with similar filler loadings 57

3.1. Formulations of composite samples 68

3.2. Thermal properties of each formulation (CNC/ZnO) from TGA 72

3.3. Thermal properties of each formulation (CNC/ B_2O_3) from TGA 73

3.4. Crystallization behavior of each formulation (CNC/ZnO) from DSC....74

3.5. Crystallization behavior of each formulation (CNC/B_2O_3) from DSC....75

3.6. Dynamic mechanical properties and mean comparison (Fisher LSD) of each formulation (CNC/ZnO) (p= 0.05)....76

3.7. Dynamic mechanical properties and mean comparison (Fisher LSD) of each formulation (CNC/B_2O_3) (p= 0.05)....77

3.8. Young's modulus and mean comparison (Fisher LSD) of each formulation (CNC/ZnO) (p= 0.05)....79

3.9. Elongation at break (%) and mean comparison (Fisher LSD) of each formulation (CNC/ZnO) (p= 0.05)....80

3.10. Young's modulus and mean comparison (Fisher LSD) of each formulation (CNC/ B_2O_3) (p= 0.05)....81

3.11. Elongation at break (%) and mean comparison (Fisher LSD) of each formulation (CNC/ B_2O_3) (p= 0.05)....81

LIST OF TABLES CONTINUED

Table Page

3.12. Mean comparison (Fisher LSD) of flame spread rate (mm/s) of (CNC/ZnO) composites (p= 0.05) 83

3.13. Mean comparison (Fisher LSD) of flame spread rate (mm/s) of (CNC/B_2O_3) composites (p= 0.05) 83

3.14. Mean comparison (Fisher LSD) of weight loss (%) of (CNC/ZnO) composites (p= 0.05) 83

3.15. Mean comparison (Fisher LSD) of weight loss (%) of (CNC/B_2O_3) composites (p= 0.05) 83

3.16. Mean comparison (Fisher LSD) of HR capacity (J/gK) of HDPE composites (p= 0.05) 84

3.17. Mean comparison (Fisher LSD) of peak HRR capacity (W/g) of HDPE composites (p= 0.05) 85

3.18. Microcalorimetry test results of neat HDPE and the composites 86

4.1. Formulations of composite samples 95

4.2. Thermal properties of each formulation (LCNC/ZnO) from TGA 100

4.3. Thermal properties of each formulation (LCNC/B_2O_3) from TGA 100

4.4. Crystallization behavior of each formulation (LCNC/ZnO) from DSC 102

4.5. Crystallization behavior of each formulation (LCNC/B_2O_3) from DSC 102

4.6. Dynamic mechanical properties and mean comparison (Fisher LSD) of each formulation (LCNC/ZnO) (p= 0.05) 104

4.7. Dynamic mechanical properties and mean comparison (Fisher LSD) of each formulation (LCNC/B_2O_3) (p= 0.05) 105

LIST OF TABLES CONTINUED

Table Page

4.8. Young's modulus and mean comparison (Fisher LSD) of each formulation (LCNC/ZnO) (p= 0.05) 107

4.9. Elongation at break (%) and mean comparison (Fisher LSD) of each formulation (LCNC/ZnO) (p= 0.05) 107

4.10. Young's modulus and mean comparison (Fisher LSD) of each formulation (LCNC/B_2O_3) (p= 0.05) 108

4.11. Elongation at break (%) and mean comparison (Fisher LSD) of each formulation (LCNC/B_2O_3) (p= 0.05) 109

4.12. Mean comparison (Fisher LSD) of flame spread rate (mm/s) of (LCNC/ZnO) composites (p= 0.05) 110

4.13. Mean comparison (Fisher LSD) of flame spread rate (mm/s) of (LCNC/B_2O_3) composites (p= 0.05).....110

4.14. Mean comparison (Fisher LSD) of weight loss (%) of (LCNC/ZnO) composites (p= 0.05) 111

4.15. Mean comparison (Fisher LSD) of weight loss (%) of (LCNC/B_2O_3) composites (p= 0.05) 111

4.16. Mean comparison (Fisher LSD) of HR capacity (J/gK) of HDPE composites (p= 0.05) 112

4.17. Mean comparison (Fisher LSD) of peak HRR capacity (W/g) of HDPE composites (p= 0.05) 113

4.18. Microcalorimetry test results of neat HDPE and the composites 114

5.1. Formulations of composite samples 123

5.2. Characteristics of D and G bands of CNC/GQD inclusion complexes 127

5.3. Atomic percentages of different elements of CNC/GQD inclusion complexes 128

LIST OF TABLES CONTINUED

Table Page

5.4. O to C ratio and FWHM of CNC/GQD inclusion complex 128

5.5. Thermal properties of each formulation (CNC/GQD) from TGA 133

5.6. Crystallization behavior of each formulation from DSC 134

5.7. Dynamic mechanical properties and mean comparison (Fisher LSD) of composites (p= 0.05) 136

5.8. Young's modulus and mean comparison (Fisher LSD) of each formulation (CNC/GQD) (p= 0.05) 138

5.9. Elongation at break (%) and mean comparison (Fisher LSD) of each formulation (CNC/GQD) (p= 0.05) 139

LIST OF FIGURES

Figure Page

1.1. Types of nanocellulosic materials from woody/non-woody biomass.....8

1.2. SEM micrographs of freeze-fractured surfaces of (a) CNC-g-PHBH (1.0 wt%) blend and (b) CNC-g-PHBH (2.0 wt%) blend.....15

1.3. FESEM micrographs of CNCs modified with different acids: (a) sulfuric acid, (b) hydrochloric acid, (c) phosphoric acid and (d) nitric acid 16

1.4. Fracture surface of broken tensile specimens of (a) CNC_d, (b) CNC_h and (c) CNC_a 18

1.5. SEM images of fractured samples (a) PHB-MCC Ar, (b) PHB-MCC Ar/N_2, (c) PHB-MCC Ar/O_2, (d) PHB-MCC Ar/CAN 20

1.6. Change in transparency of CNF samples (a) before and (b) after ultrasonication.....23

1.7. SEM images of ACNF/PCC nanopapers before (a) and after (b)-(c) ultrasonication. The images (b), (c) represent images of composites after use of 80% ultrasonicator power and 30 and 60 min treatment, respectively 24

1.8. FESEM micrographs of fracture surfaces of polymer nanocomposites (a) lower magnification image, (b) enlarged view and (c) higher magnification image under the influence of an external magnetic field.....26

1.9. Polarized light microscopy images of (a) 5 v/v% CNW reinforced composite within the magnetic field, (b) 5 v/v% CNW reinforced composite rotated by 45º to the polarization axis.....27

1.10. AFM image of electric field oriented CNC films 29

1.11. SEM images of (a) aligned B-CA nanofibers and (b) CNFs after regeneration 30

1.12. SEM images of CNF/CNC nanocomposite nanofibers: (a) 0% CNC, (b) 5% CNC, (c) 12.5% CNC and (d) 20% CNC 32

1.13. SEM images of a fractured cross section of a drawn and strongly aligned film, DR = 2.5, acquired (a) perpendicular to and (b) within the drawing direction (scale bars are 500 nm), 2D WAXD data to characterize

LIST OF FIGURES CONTINUED

Figure Page

the extent of alignment, (c) DR = 2.5. (d) Orientation index, π, and order parameter, as a function of DR, establishing a direct link between drawing and orientation of the reinforcements 33

1.14. AFM micrographs of surfaces of (a) a reference undrawn TEMPO-NFC nanopaper sample (DR = 1), (b) a drawn TEMPO-NFC nanopaper at DR = 1.4.....34

1.15. AFM image of GQDs, (b) AFM image of CQDs 36

2.1. Reaction mechanism of silane grafting onto CNC surface 45

2.2. Transmission spectra of PEO, untreated CNC incorporated PEO, (1:1) silane treated, (1:2.5) silane treated and (1:5) silane treated CNC incorporated samples using FTIR 49

2.3. SEM images of PEO-CNC composite films :(a) 1PEO/1CNC, (b) 1PEO/1CNC/1Silane, (c) 1PEO/1CNC/2.5Silane and (d) 1PEO/1CNC/5Silane samples 50

2.4. TGA thermogram of PEO, untreated CNC incorporated PEO, (1:1) silane treated, (1:2.5) silane treated and (1:5) silane treated CNC incorporated samples 52

2.5. Derivative thermogravimetric (DTG) curves of PEO, untreated CNC incorporated PEO, (1:1) silane treated, (1:2.5) silane treated and (1:5) silane treated CNC incorporated samples 52

2.6. DSC thermograms of PEO, untreated CNC incorporated PEO, (1:1) silane treated, (1:2.5) silane treated and (1:5) silane treated CNC incorporated samples.....52

2.7. Representative curve of storage modulus as a function of temperature of PEO, untreated CNC incorporated PEO, (1:1) silane treated and (1:2.5) silane treated CNC incorporated samples 55

2.8. Tan δ curves as a function of temperature for PEO, untreated CNC incorporated, (1:1) silane treated and (1:2.5) silane treated CNC incorporated samples 56

LIST OF FIGURES CONTINUED

Figure Page

3.1. Transmission spectra of (a) ZnO coated CNC composites and (b) B_2O_3 coated CNC composites 71

3.2. SEM images of HDPE composites cross-sections: (a) CNC-ZnO, (b) CNC- B_2O_3 (agglomerations shown in red circles) (c) elemental mapping of Zn, and (d) elemental mapping of B (shown in red circles)……71

3.3. DSC thermograms of (a) ZnO coated CNC composites and (b) B_2O_3 coated CNC composites……74

3.4. Representative curves of storage modulus as a function of temperature of (a) ZnO coated CNC composites and (b) B_2O_3 coated CNC composites……76

3.5. Representative box plots of statistical analysis of (a) ZnO coated CNC composites and (b) B_2O_3 coated CNC composites……77

3.6. Bar graphs comparison of tensile properties of (a) ZnO coated CNC composites and (b) B_2O_3 coated CNC composites…….....78

3.7. Representative box plots of statistical analysis of (a) elastic modulus and (b) elongation at break (%) of ZnO coated CNC composites……80

3.8. Representative box plots of statistical analysis of B_2O_3 coated CNC composites……82

3.9. Weight loss (%) graphs of (a) ZnO coated CNC composites and (b) B_2O_3 coated CNC composites……82

3.10. (a) Heat release rate graph of neat HDPE, C1B1 and CS1Z2 formulations and (b) statistical comparison of peak heat release rate of the three formulations (significance level = 0.05) ……85

LIST OF FIGURES CONTINUED

Figure Page

4.1. Transmission spectra of (a) ZnO coated LCNC composites and (b) B_2O_3 coated LCNC composites.....98

4.2. SEM images of HDPE composites cross-sections: (a) LCNC-ZnO, (b) LCNC- B_2O_3 (agglomerations shown in red circles) (c) elemental mapping of Zn, and (d) elemental mapping of B (shown in red circles)……..99

4.3. DSC thermograms of (a) ZnO coated LCNC composites and (b) B_2O_3 coated LCNC composites 101

4.4. Representative curves of storage modulus as a function of temperature of (a) ZnO coated LCNC composites and (b) B_2O_3 coated LCNC composites…….104

4.5. Representative box plots of statistical analysis of (a) ZnO coated LCNC composites and (b) B_2O_3 coated LCNC composites……...105

4.6. Graphical representation of the tensile properties of (a) ZnO coated LCNC composites and (b) B_2O_3 coated LCNC composites…….106

4.7. Representative box plots of statistical analysis of (a) elastic modulus and (b) elongation at break (%) of ZnO coated LCNC composites……108

4.8. Representative box plots of statistical analysis of (a) elastic modulus and (b) elongation at break (%) of B_2O_3 coated LCNC composites……...109

4.9. Weight loss (%) graphs of (a) ZnO coated LCNC composites and (b) B_2O_3 coated LCNC composites…….....111

4.10. (a) Statistical comparison of peak heat release rate of the three formulations (significance level=0.05) and (b) heat release rate graph of neat HDPE, LC1Z1 and LC1B2…….114

LIST OF FIGURES CONTINUED

Figure Page

5.1. Raman spectra of GQD/CNC inclusion complexes.....127

5.2. XPS survey spectra of CNC/GQD inclusion complex…….129

5.3. High resolution C1s spectra of CNC/GQD inclusion complexes.....129

5.4. X-Ray diffraction patterns of CNC and CNC/GQD inclusion complex.....131

5.5. SEM micrographs of the cryo-fractured cross-sections of (a) HDPE/CNC (2 μm), (b) HDPE/CNC/GQD (2 μm) and (c) HDPE/CNC/GQD (1 μm) 131

5.6. TGA thermograms of Neat HDPE, untreated CNC incorporated HDPE and GQD incorporated composite samples…….133

5.7. DSC thermograms of composite samples of (a) heating cycle and (b) cooling cycle……..135

5.8. Representative curves of storage modulus as a function of temperature of composite samples……...136

5.9. Representative box plots of the statistical analysis of the storage modulus of the composite samples……..137

5.10. Representative box plots of statistical analysis of (a) elastic modulus and (b) elongation at break (%) of HDPE composites……138

5.11. Nyquist plot for electrical impedance spectra of neat HDPE and CNC/GQD composites…….140

5.12. Bode plot for electrical impedance spectra of (a) neat HDPE and (b) CNC/GQD composites……..141

ABSTRACT

In the past few years, Cellulose nanocrystals (CNC) and its derivatives are exploited as potential bio-based nanofillers for functional polymer composites. The main challenge for manufacturing CNC-based composites is to disperse CNC uniformly in the hydrophobic polymer matrix. The hydrophilicity of CNC hindered their uniform distribution in the matrix and reduced the overall thermal, mechanical, and physical properties of the composite system. To overcome this challenge, several methods have been developed, such as physical and chemical modification of CNC. Also, polymer-based composites are highly flammable in nature and can cause severe life-threatening incidence. The flame-retardants available commercially should be added to the composite for a very high add-on% and toxic in nature, which is not eco-friendly and can be dangerous for humans. In this study, two critical research gaps are addressed: 1) uniform dispersion of CNC in a hydrophobic matrix, and 2) improving fire-retardancy of polymer composites by using non-toxic inorganic oxides. In the first part, a chemical compound, aminosilane was used as a dispersing agent for CNC in polyethylene oxide (PEO) based composite films and their thermo-chemical properties were analyzed. In the next part, the silanated CNCs are coated with nano ZnO and nano B_2O_3 and added as a functional filler to manufacture high density polyethylene (HDPE) based composites. The ZnO coated composites showed a significant improvement in thermo-mechanical properties of the composites even at a low add-on%, due to the smaller size and higher surface area of nano ZnO. The lignin containing CNC (LCNC) was also used as a functional additive along with nano ZnO and B_2O_3. The hydrophobic character of lignin could not improve the dispersion of LCNC in the HDPE matrix because of the reduction of the aspect ratio and aggregate formation of LCNC/inorganic oxides during freeze drying. The role of the new age material graphene quantum dots (GQD) as a dispersing agent for CNC was also exploited. The CNC/GQD inclusion complex showed excellent dispersion behavior in HDPE matrix along with the significant improvement in thermo-mechanical properties of the composites, even at very low add-on% of GQD. The preliminary idea of using CNC/GQD inclusion complex as an energy storage device was also developed. Overall, the current work addresses the two main challenges which hindered the functional application of CNC based polymer composites and developed safe, effective, and eco-friendly methods to overcome those challenges. CNC based polymer composites have strong potential to be used in various industrial applications from fire-retardant material to energy storage device.

Keywords: Polymer-matrix composites, dispersion of cellulose nanocrystals, Silane functionalization, Fire retardant additives, Graphene quantum dot

CHAPTER ONE

INTRODUCTION

Recently, biodegradable and renewable materials have received special attention from both scientific and industrial communities. The use of conventional petroleum-based products has posed severe ecological threats to the world environment and caused global warming and plastic pollution. To cope with the effect of global warming and pollution, the use of 'green' materials is the present trend followed by researchers. Cellulose is the most abundant bio-based polymer and has been used as a potential solution to resolve these issues. In the last few decades, nanostructured cellulose materials have become the new field of interest because of the specific physical and chemical properties of these materials. The development of high performance/functional composites using nanofillers has become a prominent area of recent research. The selection of nanofillers has raised serious concerns and there is an immense need to introduce sustainable and bio-degradable nanofillers. Nanocellulose materials are potential candidates to fill this gap. Cellulose nanocrystals (less than 100 nm in one dimension) are widely exploited in polymer composites as filler because they are highly crystalline material with Young's modulus near 150 GPa and tensile strength 10 GPa. They exhibit surface charge, chiral nematic and amphiphilic properties, and serve to modify rheological, optical, and electrical properties of polymers [1]. The central challenge regarding the mixing of CNCs with polymers is their poor dispersion. Commercial polymers are generally hydrophobic in nature and low in surface energy, whereas the CNCs are hydrophilic and have high surface energy. Because of this reason, the polymers cannot adequately interact with the surface of CNCs and effectively disperse them throughout the matrix [2].

The growth of fossil-fuel derived polymeric materials in every sector of modern life also brings additional hazard with it: hydrocarbon based polymeric materials are inherently highly flammable and release toxic gases during combustion. Loss of property and lives has become a continuous reminder of the need to find a suitable solution to limit flammability of materials [3]. The combustion of polymers is an endothermic pyrolysis to flammable and toxic gases, which ignite in contact with air and lead to exothermic processes of flame propagation and heat release. The modes of action of flame retardancy are mainly in the condensed phase and vapor phase [4]. Different types of flame retardants (FRs) are used to cope the flammability of polymers which generally act chemically and/or physically in the condensed or vapor phase to interfere with the combustion process during heating, pyrolysis, ignition, or flame spread []. Inorganic oxides are very popular as flame retardants because of their low toxicity and low smoke evolution [5].

To address the above-mentioned issues, the current study addresses two specific objectives: 1) improving the dispersion behavior of CNC in a hydrophobic polymer matrix with the help of different types of dispersing agents, and 2) improving the thermo-mechanical properties of the overall composite system.

In the first chapter, literature review, different types of dispersion techniques used for cellulose nanomaterials and the findings of the research papers related to this topic were discussed. The second chapter includes a manuscript which demonstrates the effect of a dispersing agent, silane, on the dispersion of CNC and the overall thermo-mechanical properties of poly(ethylene) oxide based composite films.

The third chapter is also a manuscript where silane functionalized CNC and two different inorganic oxides are used as functional additives for high density poly(ethylene) (HDPE) based

composites. These composites are manufactured via melt blending extrusion and are characterized to analyze their thermal, physical, and mechanical properties. The manuscript of the fourth chapter demonstrated the effect of lignin containing CNC (LCNC) and inorganic oxide incorporation on the thermo-mechanical properties of HDPE based composites.

The fifth chapter also includes a manuscript which demonstrates the role of graphene quantum dots (GQD) as a dispersing agent for CNC and as a functional additive for HDPE based composites. In this manuscript the characteristics of the CNC/GQD inclusion complex were also discussed along with the composite properties. Also, a preliminary idea of using CNC/GQD inclusion complex as an energy storage device was also developed.

CHAPTER TWO

A REVIEW OF CURRENT PHYSICAL TECHNIQUES FOR DISPERSION OF CELLULOSE NANOMATERIALS IN POLYMER MATRICES

Contribution of Authors and Co-Authors

Manuscript in Chapter 2

Author: Saptaparni Chanda

Contributions: Investigation, Analysis, Writing – Original draft, Visualization

Co-Author: Dilpreet S. Bajwa

Contributions: Supervision, Writing – Review, Editing

Manuscript Information

Saptaparni Chanda, and Dilpreet S. Bajwa

Reviews on Advanced Materials Science

Status of Manuscript:
____ Prepared for submission to a peer-reviewed journal
____ Officially submitted to a peer-reviewed journal
____ Accepted by a peer-reviewed journal
__X__ Published in a peer-reviewed journal

Publisher: De Gruyter; 60.1: 325-341, DOI: https://doi.org/10.1515/rams-2021-0023

Abstract

Cellulose nanomaterials (CNMs) exist in biomass. Recent developments in nanotechnology and extraction procedure of CNMs open up a new era in the polymer composites industry. Abundant, renewable, biodegradable, transparent, light weight and most importantly low cost make CNMs the ideal material for packaging, automotive, construction and infrastructure applications. CNMs are generally used as materials for polymer matrix reinforcement in the composites industry. The industrial-scale manufacturing of CNM/thermoplastic composites remains an unsolved puzzle for both academics and industries. The dispersion of nanocellulose in polymer matrix is the central problem inhibiting the manufacturing of CNM/polymer composites at an industrial scale. Several attempts were made to disperse nanocellulose effectively in a polymer matrix and improve compatibility between the matrix and CNMs. Chemical aided surface modification of CNMs have been effective in several cases, however chemical toxicity, high price, critical control of reactions make them unsuitable. This current review paper focuses on novel eco-friendly physical dispersion techniques of CNMs and their future scope of research. The physical dispersion techniques such as plasma induced surface modification, ultrasonication, magnetic and electric field discharge, electrospinning or drawing can visibly improve the dispersion state of CNMs. But several factors affect physical techniques' performance, e.g. CNM type and forms, process conditions and parameters etc. Moreover, the material related factors interplay with the process related factors. This review addresses the current state of knowledge on the physical dispersion techniques for CNMs and identifies challenges that are critical to adoption of these novel materials at commercial scale for future applications.

Keywords: Polymer-matrix composites, dispersion of nanocellulose, chemical aided surface modification, physical dispersion techniques

Introduction

Polymer materials are widely used in various industrial sectors for a variety of applications. Most petroleum-based materials are not biodegradable. The lack of biodegradability of fossil-based non-biodegradable products is a growing concern in today's world. Increased greenhouse gas emission, air and water pollution and the severity of global climate change have compelled scientists to find ecofriendly alternatives to these petroleum-based materials. The most common and sustainable bio-based material is cellulose. Cellulose is the most abundant and natural polymer on earth [1]. Cellulose is the most abundant, natural polymer on earth [6]. Chemically, cellulose is a high molecular weight homopolysaccharide composed of β-1,4-anhydro-D-glucopyranose units. Each cellulose chain has a hemiacetal group, a chemically reducing functionality in one end. The other end has a pendant hydroxyl group as a reducing group. The degree of polymerization of cellulose (DP) varies depending on its origin, starting from 10000 to 15000. Each monomer of cellulose contains three hydroxyl groups, which play a major role in fibrillar and semicrystalline packing governing important physical properties [7].

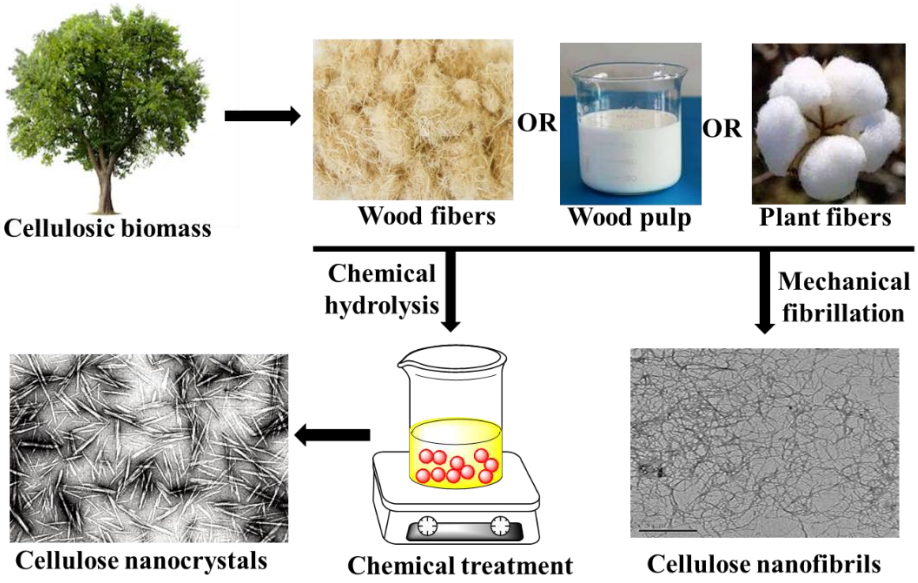

Fig. 1.1. Types of nanocellulosic materials from woody/non-woody biomass

When cellulose is mechanically fibrillated or chemically hydrolyzed under specific conditions, nanoscale materials are generated as shown in Fig. 1[8-10]. There are three types of nanocelluloses: cellulose nanocrystals, cellulose nanofibrills, bacterial nanocellulose.

Cellulose Nanocrystals

Cellulose nanocrystals (CNC), also known as nanocrystalline cellulose or cellulose nano whiskers is a nanocellulose with high strength. Additionally, CNCs have limited flexibility because of their high crystallinity (54-88%). CNCs have a short rod-like or whisker shape with a diameter of 2-20 nm and length of 100-500 nm. The nanocrystalline cellulose is prepared by hydrolysing and removing the amorphous part of cellulose using highly concentrated acids. The dimension of CNC and crystallinity depend on the conditions of extraction and source of cellulose. Higher crystallinity is exhibited by CNCs extracted from pure cellulosic materials. During

hydrolysis, the nature of the acid used is extremely important because it affects the dispersion property. If hydrochloric or hydrobromic acid is used, the dispersion is very limited and subsequently, the aqueous suspensions tend to flocculate. However, in case of sulfuric and phosphoric acids, the hydroxyl groups of cellulose surface yield sulfate or phosphate esters which improve dispersion of CNC in water [11-15].

CNC exhibits excellent mechanical properties as a result of higher crystallinity. The theoretical tensile strength of CNC ranges between of 7.5-7.7 GPa, which is much higher than steel and Kevlar and the elastic moduli is ~150 GPa. The experimental Young's moduli of cotton CNC's and tunicate CNC's are ~105 GPa and ~143 GPa, respectively [16]. CNCs can be successfully functionalized to reduce their hydrophilicity and to promote incorporation of modified nanoparticles in a hydrophobic matrix.

Cellulose Nanofibrils

Cellulose nanofibrills (CNF) are also known as nanofibrillated cellulose, cellulose microfibrill, microfibrillated cellulose or cellulose nanofiber etc. CNFs consist of long, flexible bundles of elementary nanofibrills composed of alternating amorphous and crystalline domains. CNFs can be of 1-100 nm in diameter and 500-2000 nm in length. CNFs are generally extracted from pure cellulosic material such as wood pulp, by the cleavage of fibrils in High Pressure Homogenizer (HPH) without any pre-treatment, or after chemical or enzymatic pre-treatment. In the amorphous domains of cellulose or hemi-cellulose, at first some of inter-fibrillar hydrogen bonding are broken due to mechanical shearing. Afterwards, the inter-molecular bonding of van dar waal's forces are also broken. CNFs having a spaghetti-like shape, contain both cellulose and hemicellulose, with a medium range of crystallinity (51-69%) [11-15].

CNFs tend to show gel-like characteristics in aqueous solution even at low concentration (2 wt%). There are two reasons behind this phenomenon. The first one is a large number of hydrogen bond formation because of the surface hydroxyl groups present in its structure. The second one is significant increase in the surface area due to reduction in size. Agglomeration is induced in CNF suspension because of the strong hydrogen interaction and high hydrophilicity of the material by virtue of their structure. The effective dispersion and distribution of CNFs are the most crucial challenges faced when they are used as reinforcement in polymer matrices [17]. The most feasible solution is to modify the surface functional groups of cellulose to avoid hydroxyl interactions and to increase interfacial compatibility with different types of polymer matrices. The axial strength and modulus of CNFs are estimated to be ~3 GPa and ~136 GPa, respectively [10].

Bacterial Nanocellulose

Unlike plant cellulose, bacterial nanocellulose (BNC) is produced in the pure form, devoid of lignin, hemicellulose, pectin, or any other compound commonly present in plant pulp. BNC does not contain any contaminant of animal origin [18]. The anhydroglucose units and various BNC fibrils interact to form a crystalline structure through internal and external hydrogen bondings. These thin nanofibers have a diameter range of 20-100 nm [19]. BNC is a highly crystalline linear polymer of glucose, synthesized mainly by *Gluconacetobacter xylinus.* During cellulose production, *G. xylinus* builds a nanofibrillar film with dense lateral surface and a gelatinous layer on the opposite side [20]. Despite numerous studies, the metabolic pathways through which the microorganisms regulate BNC production remain unclear.

There are two main methods of BNC production using microorganisms: static culture and stirred culture. In case of static culture, there is an accumulation of a thick, leather-like white BNC pellicle at the air-liquid interface. In stirred culture, BNC is produced in a dispersed manner in the culture medium, forming irregular pellets or suspended fibers [21].

The high mechanical strength of BNC's can be attributed to its fibrillar structure. BNCs exhibit a hydrogel like behaviour as they can bind water. Additionally, BNC is not degradable in human bodies making them suitable for biomedical applications [22].

Significance of Surface Modification

The excellent mechanical properties of cellulose nanomaterials (CNMs) comparable to conventional materials like glass fiber, carbon fiber and Kevlar fiber, make them potential candidates for green replacement of the synthetic fibers in the composites industry [23]. Polymer matrix nanocomposites are the new age materials and are regarded as the future of the composites industry. The main advantages of polymer composites are that they are flexible, stretchable, and even reconfigurable [24]. Polymer composites have gained special attentions from both researchers and industry for their unique properties such as high strength to weight ratio. During manufacturing, the major parameters to take care of are: filler/reinforcement alignment and loading, nature of reinforcement, nature of matrices, and good filler-to-matrix adhesion [25]. The incompatibility between filler and matrix materials may cause bond weakening or even debonding. Bond weakening will result in less effectiveness of the filler material, which in turn adversely affect the mechanical properties of the resultant composite material [24]. With the recent advancement of nanotechnology, cellulose nanomaterials are exploited as a reinforcement for polymer composites along with other ones because of the special attributes such as

biodegradability, light weight, transparency, and relatively low cost [26]. Thermoplastic polymers are used as matrix materials in major cases (90%), and the rest being thermosets [27]. Though thermoplastics are recyclable in nature, they are not mechanically robust like thermosets. For this reason, fillers are used to reinforce the thermoplastics to create stronger composites [28]. The main issue regarding the mixing of CNMs with thermoplastics is the limited dispersion of CNMs in the polymer matrices. Thermoplastics are usually hydrophobic in nature and have low surface energy, while the CNMs are hydrophilic with high surface energy. Because of this reason, thermoplastics cannot adequately interact (wet) with the surface of CNMs and effectively disperse them throughout the polymer matrices [29]. All surface modifications are mainly conducted to (1) introduce stable negative or positive electrostatic charges on the surface of the CNMs, (2) tune the surface energy characteristics to enhance compatibility with the polymeric matrices, especially non-polar or hydrophobic ones, and (3) change only the surface characteristics of the CNMs keeping the original morphology intact to avoid any polymorphic conversion [28]. Surface modifications can induce charges or tune the surface energy characteristics of CNMs by decreasing energy consumption and clogging and confer new properties to CNMs [30]. Therefore, many efforts have been spent on the surface modification of CNMs either by chemical or physical means. Currently, there is no efficient single physical or chemical method available to improve dispersibility of CNMs in the polymer matrices for enhancement of the mechanical properties.

Chemical-aided Dispersion of Cellulose Nanomaterials (CNMs)

The chemical modification of the surface of CNMs can be divided into two categories depending on the locations of attack: either on the surface hydroxyl groups or AGU ring opening [31]. In some cases, charged groups generate repulsive forces to weaken the cohesion of hydrogen bonds. In other ones, osmotic pressure produced by the difference in ionic concentration facilitates fibre swelling and reduction in the interfibrillar cohesion which in turn enhances breakage of the cell walls [31]. There are different types of chemical surface modifications reported in recent years: polymer grafting, silanization, acetylation, esterification etc. In the following section a brief discussion on these methods is presented.

Polymer Grafting

In polymer grafting method, functional polymer brushes are grafted on the surface of nanocelluloses by "grafting onto" and "grafting from" approaches. The "grafting onto" method involves attachment of pre-synthesized polymer chains with reactive groups onto the surface hydroxyl groups of cellulose. On the other hand, the "grafting from" approach uses ring opening polymerization (ROP) method to grow polymer brushes *in situ* on nanocelluloses using the surface hydroxyl groups as initiating sites [32]. In "grafting onto" approach, high grafting densities cannot be obtained because of the steric hindrance of the polymer chains. The main advantage of this method is that the properties of the resulting material can be controlled judiciously as the molecular weight of the attached polymer can be characterized before grafting [33]. For example, Anirudhan et al. synthesized a novel multi-component superabsorbant polymer composite by grafting the vinyl monomers onto magnetite nanocellulose composite (MNCC). Methacrylic acid (MAA) and vinyl sulfonic acid (VSA) were chosen because of their anionic character, which increases the

swelling capacity of the resultant material. The FTIR spectra showed the characteristic absorption bands of cellulose retained in MNCC with a small decrease in intensity. This indicated the degradation of hydrogen bonds between the cellulose chains during the acid hydrolysis treatment [34]. The "grafting from" approach normally provides higher grafting efficiency due to lower steric hindrance produced by small monomers, compared to the shielding effect on reaction sites in "grafting onto" approach. Wang et al. grafted poly(methyl methacrylate) (PMA) from the CNC-macroinitiator achieving almost six times the mass of grafted PMA (with respect to CNC) within only 30 min. The resulting PMA-grafted CNC showed excellent dispersibility in a number of organic solvents. From FTIR spectra, it can be seen that the hydrogen absorption band showed a gradual decrease with reaction time, almost disappeared at 30 min. This indicated that the CNC surface was covered gradually by the growing PMA chains [35]. In another study polycaprolactone diol (PCL) was grafted on the surface of oxidized nanocelluloses to enhance the compatibility between the hydrophobic polymer matrix and hydrophilic cellulose. This grafting was done by using click chemistry. The reaction produced polycaprolactone grafted oxidized nanocellulose (ONC-g-PCL), which improved the interfacial adhesion of composite material. The TEM image of the ONC-g-PCL shows significant increase in the width of the grafted ONC fibres (25-30 nm). The increase in width clearly indicates successful grafting of PCL chains onto the surface of the ONC fibrils [28]. There is no visual evidence of the improvement in dispersion of the CNMs in the polymer matrix in "grafting onto" method.

Silylation

Silanes are another widely used coupling agent that can be used for polymer composites to improve the interfacial compatibility between nanocellulose and the polymer matrix. One of the

major benefits of using silane is the reaction can be a water/alcohol-based system, instead of the harmful organic solvents. First, the alkoxy end group of the bifunctional silanes should be converted to silanols before reacting with the hydroxyl groups on cellulose [36]. Pohl et al. reported that the chemistry of the silanes can be rather complicated, depending on many factors such as the solvent, temperature, pH, concentration of silanes, etc. [37]. Salon et al. concluded that reaction time for the hydrolysis of silane and the following adsorption of silanol groups onto the cellulose surface should be carefully regulated to reduce the degree of self-condensation [38]. Xu et al. grafted nanocrystalline cellulose (CNC) with poly (3-hydroxybutyrate-co-3-hydroxyhexanoate (PHBH) using (3-aminopropyl) triethoxysilane (APES) as a coupling agent, resulting a grafting degree of ~25 wt%. The fracture morphologies of the freeze-fractured surfaces (SEM images) (Fig. 2) showed no or very little agglomeration of PHBH/CNC-g-PHBH blend, when CNC-g-PHBH content was 1.0 wt%. However, agglomeration was observed as the content of CNC increased. The Young's modulus of composites increased by 15% by the addition of 1.0 wt% CNC-g-PHBH [39].

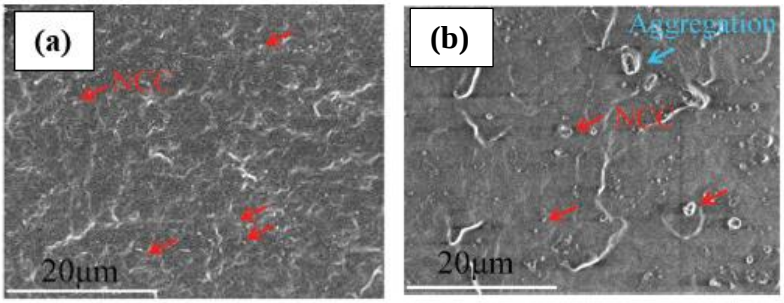

Fig 1.2: SEM micrographs of freeze-fractured surfaces of (a) CNC-g-PHBH (1.0 wt%) blend and (b) CNC-g-PHBH (2.0 wt%) blend. Adapted from Ref [34].

Taipina et al. used a silane with isocyanate groups (isocyanatepropyltriethoxysilane) to modify the surface characteristics of cellulose nanocrystals (CNC). The aim of this study was to produce an oligomeric network of polysilsesquioxane, which can result an efficient nanocrystal surface covering. The modified CNCs showed less polar surface characteristics facilitating compatibility with the hydrophobic polymer matrices. The microscopic images of the modified CNC showed better dispersion in toluene than the pristine ones, which can be a result of the reduction in hydrophilic character of CNC [40]. Salon et al. found out that after solvent evaporation, the residual silanol groups may not only undergo further condensation reaction with the hydroxyl groups present in the cellulose surface, but also lead to self-condensation to form polysiloxane network on the solid surface. This phenomenon can severely affect cellulose grafting, since in this system most of the silane linkages are engaged in siloxane bridges. Only the remaining small proportion of silane groups is available to undergo the reaction with the hydroxyl groups on the cellulose surface to yield chemical bonding between the silane coupling agents and cellulose substrate [41]. Qian et al. introduced silane compatibilized (triethoxyvinylsilane, A-151) bamboo cellulose nano whiskers (BCNW) in poly(lactic acid) (PLA) matrix. The elongation at break of the composites remarkably increased from 12.3±1.7% (untreated) to 213.8±21.6% (silane treated).

But there is no clear evidence of the improvement in dispersion of nano whiskers in the polymer matrix [42]. As silanes are typically used at small addition levels to promote interfacial compatibility because of their high cost and high efficiency, the use of large doses of silane required for good dispersion is not commercially feasible.

Other Chemical Treatments

Substitution of the hydroxyl groups of cellulose with anionic moieties from acid is another common practice of the surface modification of nanocellulose. Dhar et al. produced four varieties of CNC via hydrolysis using different acids with tailored physical, thermal, structural, and surface characteristics. Here four different types of acids are used: sulfuric acid, hydrochloric acid, phosphoric acid, and nitric acid. All fabricated CNCs show cellulose I crystal structure with different degrees of substitution of the surface hydroxyl groups. CNC-PO_4 and CNC-Cl exhibited hydrophobic behaviour, which facilitated their enhanced dispersion in PLA matrix. The morphological analysis of the CNCs was done by FESEM (Fig. 3) and AFM. The variable aspect ratio of different acid functionalized CNCs affects the mechanical reinforcing efficiency and the crystallization behaviour of the fabricated nanocomposites. The CNC-PO_4 with higher aspect ratio and long needle-like morphology, improved the elastic modulus and elongation behaviour of composites [43].

CNCs can also be modified by aliphatic and aromatic isocyanates. Morelli et al. fabricated nanocomposites of poly (butylene adipate-coterephthalate) (PBAT) with 5-10 wt% CNC content via solvent casting technique. In case of the CNCs reacted with aromatic isocyanate (phenyl butyl isocyanate), the PBAT chains were more anchored due to a possible π-π interaction between the polymer aromatic rings and the phenyl rings grafted onto CNCs as shown in the schematic. This

rigid percolated network enhanced the elastic modulus and yield stress up to 120% and 40% respectively, of the composites in comparison to pure PBAT [44].

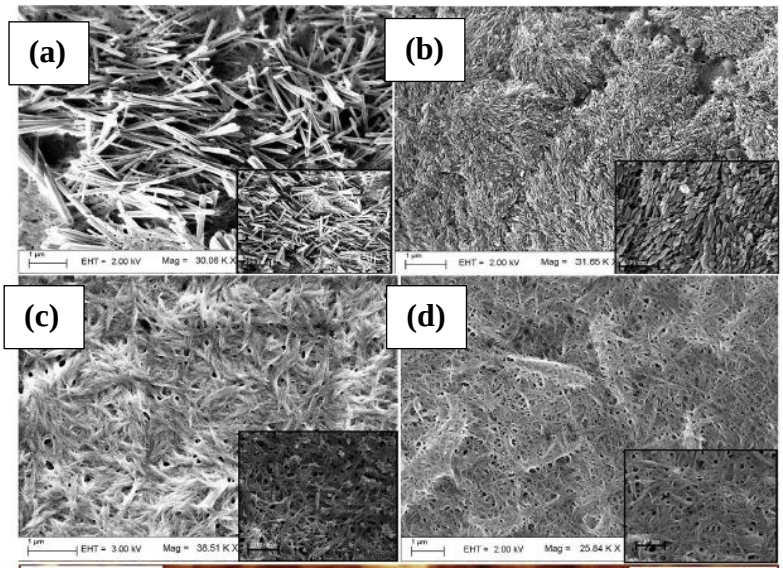

Fig 1.3. FESEM micrographs of CNCs modified with different acids: (a) sulfuric acid, (b) hydrochloric acid, (c) phosphoric acid and (d) nitric acid. Adapted from Ref [38].

Acetylation is another popular method of the surface modification of cellulose nanomaterials. Peng et al. synthesized epoxy nanocomposites reinforced with acetyl, hexanoyl and dodecanoyl modified CNCs. Electron microscopy (Fig. 4) showed that the acetyl grafted CNC (CNC_a) and hexanoyl grafted CNC (CNC_h) had good dispersion in cured epoxy. CNC reinforced epoxy exhibited highest increase in tensile modulus, tensile strength and work of fracture [45].

Shojaeiarani et al. used masterbatch preparation techniques (film casting, spin coating) [46, 47, 48] for the esterification of cellulose nanocrystals (CNCs). Though TEM images did not exhibit significant difference between the esterified and unmodified CNCs, but there was a reduction in dimensional aspect ratio in case of the modified CNCs. These modified CNCs are used as a

reinforcement for poly (lactic acid) (PLA) matrix. The thermal stability and tensile strength of the resultant composites are also enhanced. The spin-coated nanocomposites exhibited higher storage modulus than the film casted samples in the glassy state.

The main drawbacks of the chemical-aided dispersion techniques are: use of toxic and sometimes expensive chemicals, longer reaction time, critical control of reaction conditions and disposal of chemicals etc.

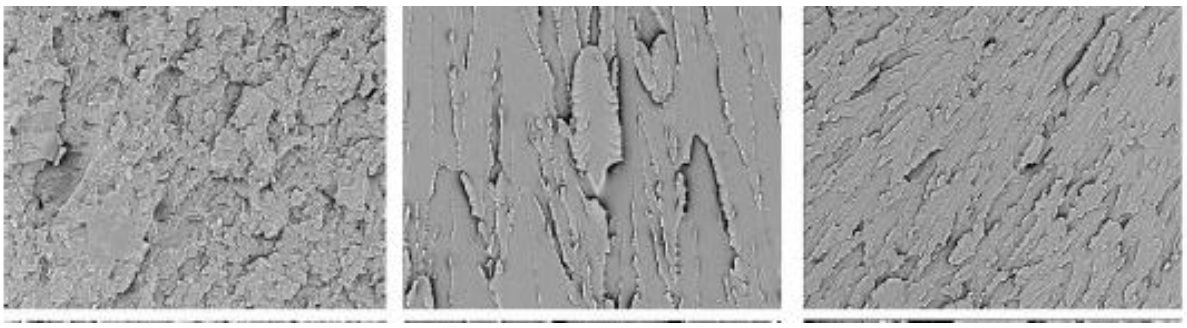

Fig 1.4. Fracture surface of broken tensile specimens of (a) CNC_d, (b) CNC_h and (c) CNC_a. Adapted from Ref [40].

Physical-aided Dispersion of Cellulose Nanomaterials

The chemical treatments are very useful to increase the interfacial compatibility between matrix (especially hydrophobic) and CNMs. In most of the cases, there is a significant increase in thermal stability and tensile properties of the composites. But there is no proper visual or quantitative evidence of the improvement of dispersion state of CNMs. Besides facilitating interfacial interaction, well aligned and oriented CNMs help to enhance the physical properties of the composites. Moreover, in most of the cases, the chemicals used in the surface treatments of CNMs are toxic in nature and some are very expensive. Also, these chemical reactions are very

sensitive to the reaction conditions such as temperature, pH, moisture, pressure etc. Thus, finding a green alternative is critical.

Besides forming covalent bonding via chemical modifications, the dispersion state of CNMs can also be improved by physical means such as plasma, electric discharge, magnetic attraction, ultrasonication, drawing etc.

Plasma induced Surface Modification

Plasma induced surface modification is a simple, replicable and efficient method in which a nanometric layer is deposited on the surface of nanoparticles, thus significantly tuning their surface chemistry [49]. Plasma treatment is widely studied to improve surface properties of cellulose films or sheets [50-55]. The plasma treatment of cellulose powders or fibers is difficult task because of suction, spreading or limited contact. But submerged liquid plasma (SLP) is a promising route to modify powder or nanomaterials when they are dispersed in liquid [50]. In plasma induced polymerization, free radicals are generated through electric discharge. Though this technique was previously used for the polymer surface modification, but recently this is applied to modify surface chemistry of nanoparticles [51].

Alanis et al. proposed a green alternative to functionalize CNC by means of plasma surface modification utilizing monomers of different nature- caprolactone, styrene and farnesene. The TEM images exhibited the typical rod-like structure of the modified CNCs, which confirmed that the modification did not affect the natural anisotropic behaviour of the crystals. Moreover, the coating of polycaprolactone (CNC_{Ca}) provided a lower C/O ratio than the other monomers, due to the polyester structure of polycaprolactone [52]. Vizireanu et al. used a combination of SLP and ultrasonication treatment to modify micro crystalline cellulose (MCC). SEM images (Fig. 5)

showed an enhanced defibrillation, with a small increase in aspect ratio (3-7) of MCC compared to pristine MCC. SEM images of fractured composites emphasized better polymer/cellulose interface in case of the plasma treated MCC containing composites resulting in more effective stress transfer [53]. A study by Panaitescu et al. demonstrated application of plasma torch and filamentary jet plasma, which helped surface chemistry modification of the nanocellulose fibers dispersed in a liquid phase. The plasma treatment was able to remove bonded water and low molecular weight impurities in NC. The plasma treatment facilitated a more homogeneous dispersion of CNCs due to formation of small length nanofibers in higher proportion. Both oxygen and nitrogen functionalization improved adhesion of components in nanocomposites [54]. In another study of Panaitescu et al., Poly (3-hydroxybutyrate) was modified by bacterial nanocellulose fibers (BC) using melt compounding and plasma treatment or zinc oxide (ZnO) nanoparticle plasma coating for anti-bacterial activities [55].

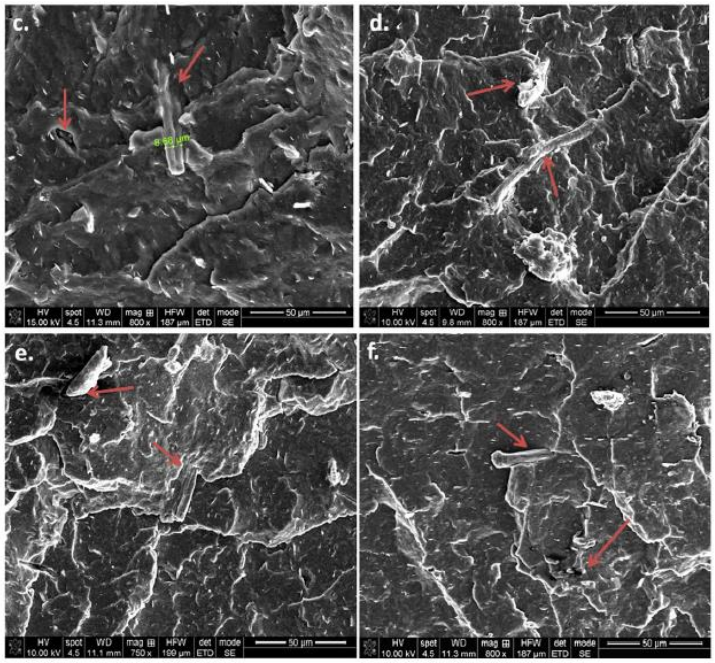

Fig 1.5. SEM images of fractured samples (a) PHB-MCC Ar, (b) PHB-MCC Ar/N_2, (c) PHB-MCC Ar/O_2, (d) PHB-MCC Ar/CAN. Adapted from Ref [53].

All types of plasma treatments showed an increase in thermal stability of the modified CNCs. In case of ABS matrix nanocomposites, the TGA thermographs showed a decrease in weight loss (%) of the modified CNC's at 250 ℃ (onset degradation temperature of cellulose), because of a substantial polymer coating on the surface of nanocrystals [52]. For PHB/MCC composites also, TGA studies confirmed that after 1 h plasma exposure, both the maximum degradation temperature (T_{max}) and onset temperature of thermal degradation (T_{on}) were decreased [53]. For BC nanofibers, irrespective of the amount of fibers, plasma treatment preserved the thermal stability, crystallinity and melting behaviour of PHB-BC nanocomposites [55]. The viscoelasticity of the materials was also analysed by DMA which exhibited a decrease in the integral area of the loss factor (tan delta) indicating more elastic behaviour of ABS/CNC composites compared to ABS. On the other hand, the storage modulus exhibited an increasing

trend compared to the reference material, suggesting an enhanced stiffness of the composite material [52]. The storage modulus of PHB containing 2 wt% BC increased by 19% at room temperature and 43% at 100 ℃ [55]. The higher aspect ratio and the increased surface area of the plasma treated cellulose nanomaterials could be beneficial to improve mechanical properties of the polymer composites reinforced with nanoparticles. Incorporation of CNC_{Ca} in ABS matrix showed an increment of 114% in the impact strength of composites compared to only 34% increase of the unmodified CNC loaded composites [52]. The PHB/MCC composites exhibited 40% increase in Young's modulus values compared to the composites with untreated MCC [53]. Small amount of plasma functionalized NC increased the tensile strength of the composites up to 10-15% compared to the composites formed with untreated NC [54]. In case of PHB-BC composites, the tensile strength also increased by 21%. In addition, the plasma treatment inhibited the growth of bacteria (*Staphylococcus aureus*, *Escherichia coli*) by 44% and 63%, respectively. In case of ZnO plasma coating, a strong chemical bond was formed between PHB surface and metal oxide nanoparticles [55].

Plasma induced surface modification techniques significantly contributed towards novel dispersion methods of CNMs. It is a quick, easy, safe, reliable and replicable method to surface functionalize CNMs and thereby improve dispersion in the polymer matrices. To date, there are many studies on the modification of the surface properties of polymer matrices, but there are very few efforts attributed to the modification of nanoparticles by plasma treatment. Recently, plasma has gained significant attention for the surface functionalization of CNMs. The extent of dispersion of plasma modified CNMs in polymer matrices and subsequent increase in mechanical properties of composites must be studied more elaborately.

Ultrasonication

Ultrasonication is another reliable mechanical method to disperse CNCs in liquids. Ultrasonication improves CNCs' dispersion state in the aqueous suspensions by breaking agglomerates. Efficiency of the ultrasonication is strongly dependent on the power level of the probe, which must be higher than the total energy to favour the dispersion.

Beugel et. al observed a decrease in the average hydrodynamic diameter for CNCs, to a limiting value of ~75 nm. The CNC aqueous suspensions showed a decrease in intrinsic viscosity after strong ultrasonication, and an increase in maximum packing concentration. This phenomenon indicated an increased agglomerate break-up, releasing both ions and water in suspension. The ionic strength increase can produce a thinner electrostatic double layer surrounding the cellulose nanocrystals, reducing their apparent concentration [56]. Cao et al. studied the relationship between the cellulose nanocrystal (CNC) dispersion and strength. They examined whether the ultrasonication reduced agglomeration and improved mechanical performance. For the CNCs in DI water, the critical concentration above which the agglomeration started was 1.35 vol%. When the CNCs were placed in a simulated cement pore solution, the critical concentration reduced to 0.18 vol%. After ultrasonication, the dispersion of CNCs improved the strength of the cement pastes by 50%, compared to cement pastes with raw CNCs (only 20-30% increase). It indicated that the dispersion of CNCs is the key to improve the flexural strength of cement pastes with higher CNC concentration [57]. In an article of Li et al., aqueous NCF water suspension was mixed with an aqueous PVA solution (10 wt%) and dispersed via ultrasonication treatment. The mixtures were degassed in a dessicator for film formation. The composite films were fabricated using variable NCF content (0, 2, 4, 8, 12 wt%). The films became increasingly opaque with the increase in NCF

content. The SEM cross-sectional image of the PVA/NCF (4 wt%) composite film showed uniform dispersion of NCF in the PVA matrix.

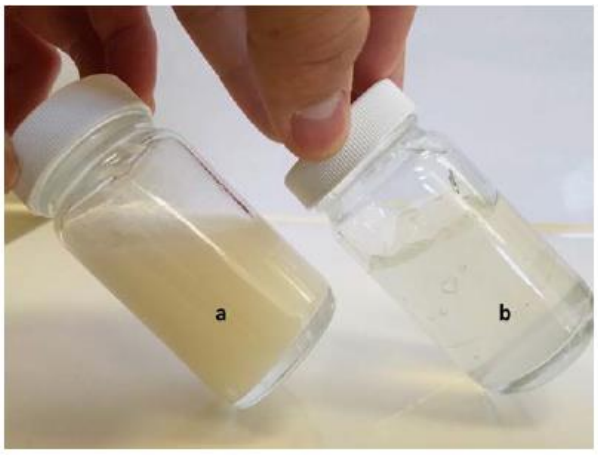

Fig 1.6. Change in transparency of CNF samples (a) before and (b) after ultrasonication. Adapted from Ref [59].

At 4 wt% NCF content, the tensile strength and Young's modulus values of the composites were increased by 1.86 and 1.63 times respectively, compared to the neat PVA. However, both tensile strength and Young's modulus values of the composites were decreased, when the NCF content was increased beyond 4 wt%. This is attributed to the increased aggregation of NCFs in PVA, which triggered local concentration of stress, leading to tensile failure [58]. Sinclair et. al extracted cellulose nanofibrils (CNF) from biomass residue. A clear change in transparency was observed (Fig. 6) in the aqueous suspension of CNF after ultrasonication [59]. Szymańska-Chargot et. al reported the effect of ultrasonication on the physicochemical properties of apple based nanocellulose fibrils (ACNF)/calcium carbonate (PCC) nanocomposites. The effects of different ultrasonication conditions were studied to evaluate time (0-60 min) and power's (0-400 W) influence on the composite properties. The samples were found to be pseudoplastic fluids, in all

cases, with low viscosity. After 60 min of ultrasonication, the mean hydrodynamic diameter of particle dispersions decreased the most and the dispersion was also most homogeneous (Fig. 7) [60]. Syafri et al. fabricated a biocomposite comprising of the nanocellulose from water hyacinth (*Eichhornia crassipes*) and bengkuang starch using solution casting method. The biocomposite gel ultrasonicated for 60 min, showed highest thermal stability and low moisture absorption. The soil burial test proved that this biocomposite sample's biodegradation rate is much slower than the other ones. The morphological evaluation showed that the 60 min vibrated samples had a coarse surface and low porosity [61].

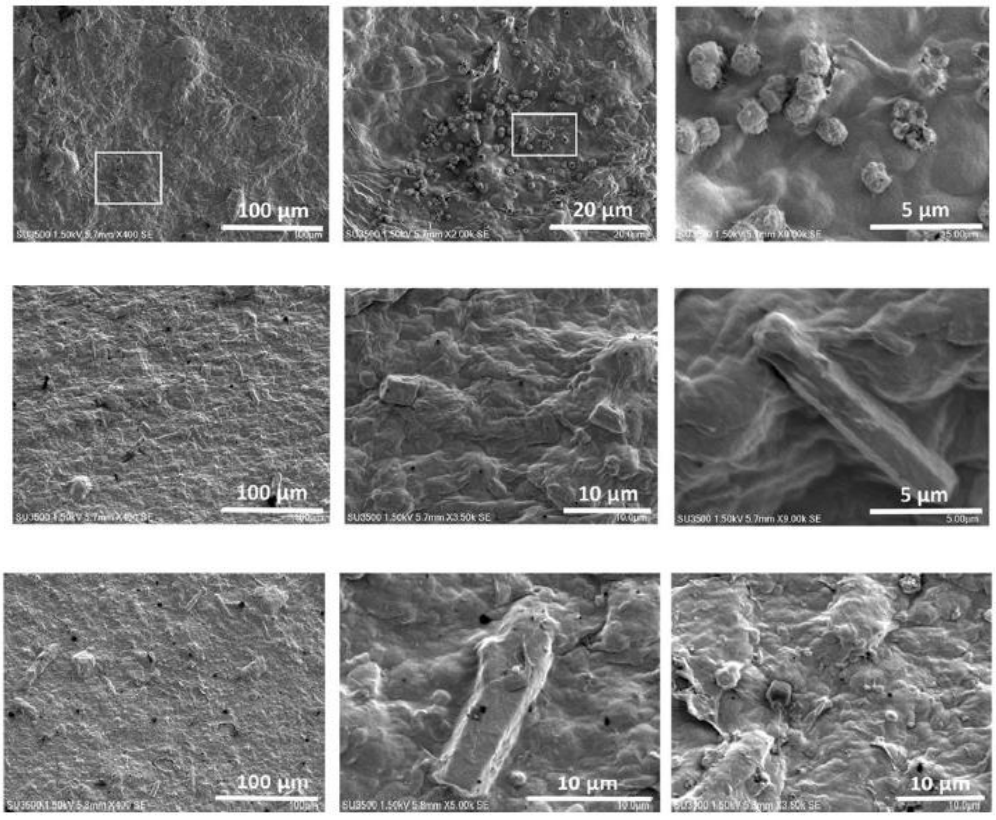

Fig 7. SEM images of ACNF/PCC nanopapers before (a) and after (b)-(c) ultrasonication. The images (b), (c) represent images of composites after use of 80% ultrasonicator power and 30 and 60 min treatment, respectively. Adapted from Ref [60].

Septevani et al. enhanced the thermal insulation and mechanical properties of a rigid polyurethane foam (RPUF) by incorporating CNC through an optimized solvent free ultrasonication method. The lowest initial thermal conductivity and best retention of thermal conductivity with ageing were obtained at 0.4 wt% of CNC, with an ultrasonication period of 40 min at an amplitude of 80%. There was a 5% reduction in the initial thermal conductivity of the resultant RPUF, surpassing the effect of the other unmodified nano-nucleating agents (almost double). This happened due to the enhanced compatibility of CNC with the polymer foam matrix [62]. Shojaeiarani et al. studied the effect of ultrasonication amplitude and time on cellulose nanocrystals (CNC) morphology and the dispersion in a water-soluble polymer. The results showed that the measured particle size of CNCs sonicated for longer time (10 min) and higher amplitude (90 µm) was significantly lower than the other samples. Additionally, higher amplitude (90 µm) helped to reduce the length of CNCs by 17% in comparison to lower amplitude (60 µm) samples sonicated for equal time. With the increase of sonication time and amplitude, the crystallinity index of CNC was decreased by 12% as the ultrasound energy destroyed the crystalline structure of CNCs [63].

Ultrasonication is highly effective for low concentration of CNMs. But in case of higher concentration, ultrasonication may fail to improve the CNM dispersion state. Ultrasonication must be studied in further detail to improve its efficiency for the higher concentration of CNMs.

Magnetic Force induced Alignment

CNCs exhibit lyotropic liquid crystalline phase behavior, i.e. they self-assemble into a cholesteric phase in aqueous medium above the critical concentration. This cholesteric polydomain structure of CNC can be preserved during drying in the presence of a magnetic field [64]. The

diamagnetic susceptibility of CNMs in the direction of the CNM axis is higher than that in the perpendicular axis. In the presence of a magnetic field, the CNMs align perpendicular to the field. Unlike the other methods, an externally applied magnetic field may render itself suitable for industrial scale production [65].

Li et al. fabricated a unidirectional reinforced nanocomposite paper from cellulose nano whiskers and wood pulp under an externally applied magnetic field. In this article, a 1.2 Tesla magnetic field was applied in order to align the nano whiskers. Under the influence of a magnetic field, the slender nano whiskers became aligned perpendicular to the magnetic field due to their anisotropic diamagnetic susceptibility. As a result, the storage modulus along the perpendicular direction of the composite became much higher than that parallel to the field. The storage modulus increased from 652 MPa to 4.88 GPa [65]. De France et al. investigated the effects of comparatively weak magnetic fields (0-1.2 T) and CNC concentration (1.65-8.25 wt%) on the kinetics and degree of CNC ordering. CNCs form chiral nematic liquid crystals above a critical concentration (C^*). In a 1.2 T magnetic field for CNC suspensions above C^*, partial alignment achieved in 2 min and nearly perfect alignment in under 200 min. At 0.56 T the ordering rate was 36% slower. Outside the magnetic field, the order parameter came down to 52% after 5 h, indicating significant effects of weak magnetic field on CNC alignment. Under C^*, no magnetic alignment was seen [66]. Pullawan et al. investigated the effect of magnetic field on the alignment of cellulose nanowhiskers (CNWs) all-cellulose nanocomposites. Tunicate derived CNWs were incorporated in a cellulose matrix system and magnetic field (1.2 T) was applied during solvent casting to improve their alignment.

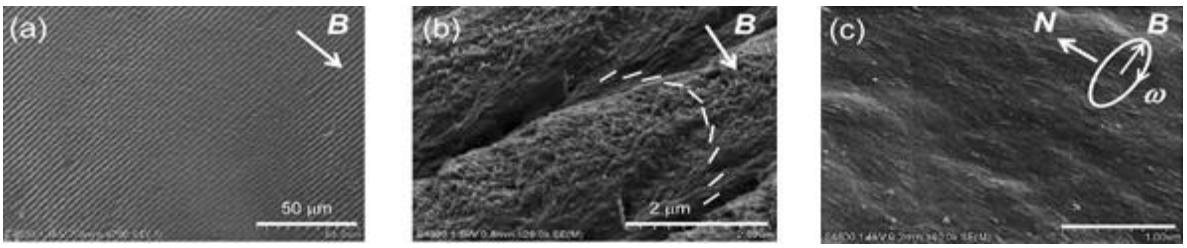

Fig 1.8. FESEM micrographs of fracture surfaces of polymer nanocomposites (a) lower magnification image, (b) enlarged view and (c) higher magnification image under the influence of an external magnetic field. Adapted from Ref [68].

CNWs were found to orient themselves in the direction of the magnetic field and eventually increased stiffness and strength of the composites (Fig. 9). Low volume fraction of CNWs permitted more degree of freedom and increased the mechanical properties of the composites. Polarized light microscopy proved that the composites had a domain structure, with some domains showing pronounced orientation [67].

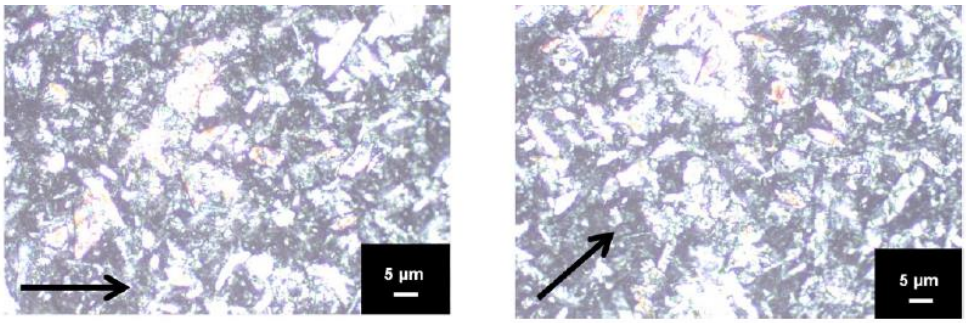

Fig 1.9. Polarized light microscopy images of (a) 5 v/v% CNW reinforced composite within the magnetic field, (b) 5 v/v% CNW reinforced composite rotated by 45º to the polarization axis. Adapted from Ref [67].

Tatsumi et al. produced anisotropic polymer composites synthesized by immobilized cellulose nanocrystal suspension (CNC) oriented under a magnetic field. CNC suspensions (~6 wt%) in 2-hydroxyethyl methacrylate (HEMA) were separated into an upper isotropic phase and a lower anisotropic (chiral nematic) phase. A static or rotational magnetic field was applied to the

system. The structural characterizations (X-ray, optical and scanning electron microscopy) indicated that CNCs of anisotropic phase were oriented distinctively along the applied magnetic field (Fig. 8), while the isotropic ones did not show any specific orientation. In dynamic mechanical experiments (tensile or compressive mode) a clear mechanical anisotropy of polymer composites was observed. A higher modulus (in compression) was also detected for the composites [68].

Magnetic force is an age-old method to disperse CNMs. It is a safe, reliable, and industrially scalable technique to disperse CNMs in polymer matrix. The only drawback of this method is that it is only effective at low concentration of CNMs. To make it operative at higher concentration, the behavior of CNMs under magnetic force must be studied in further details.

Electric Discharge

Although electric field application was widely used to orient nanoscale particles, only a few studies were dedicated to cellulose nanoparticles dispersion. Alignment induced by an electric field is a well-known phenomenon in the cases of liquid crystalline materials, crystalline phases in polymer blends and gels, particles in suspensions and colloids. Recently, there are some investigations on the influence of an external electric field to align cellulose at macroscopic and colloidal levels. Cellulose must be dispersed in an organic apolar solvent during the application of the electric field [70].

Kadimi et al. studied the effect of electric field on the alignment of nano fibrillated cellulose (NFC) in silicone oil. The magnitude, frequency and duration of an AC electric field affected the orientation of NFCs of different surface charge density and aspect ratio. Electric field alignment occurred in two steps. First, NFC made a gyratoty motion influenced by the dielectrophoretic force

(DEP). Second, NFCs interacted with itself to form chains parallel to the electric field lines. When the duration of the electric field was increased, NFC chains became thicker and longer. The optimal parameters of alignment were found to be 5000 Vpp/mm and 10 kHz for the duration of 20 min [69]. Habibi et al. demonstrated that when an alternating voltage is applied to a cellulose nanocrystal suspension (CNC), a highly homogeneous orientation of CNCs is obtained. The parameters of applied electric field such as strength and frequency and CNC aspect ratios affect the orientation and CNC assembly. The orientation of CNCs (Fig. 10) becomes more homogeneous with electric field higher than 2000 V/cm with a frequency range of 10^4-10^6 Hz [70]. Ten et al. explained how cellulose nanowhiskers (CNWs) in a poly(3-hydroxybutyrate-co-3-hydroxyvalerate) (PHBV) matrix were aligned by an external electric field. During solvent evaporation, a DC electric field of 56.25 kV/m was applied. Dynamic mechanical analysis results showed that CNW concentration had a strong influence on the degree of CNW alignment. The electric field remained effective up to 4 wt% CNW concentration. Samples with higher concentration of CNW showed virtually isotropic behaviour. This indicated significant restraints on CNW mobility attributed to CNW/CNW or CNW/polymer interaction [71].

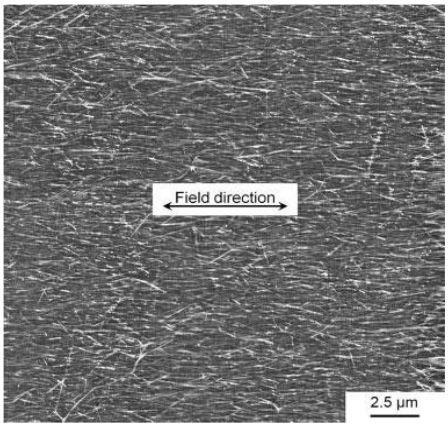

Fig 1.10. AFM image of electric field oriented CNC films. Adapted from Ref [70].

Electric discharge is an established technique to disperse inorganic nanoparticles, but recently it applied to align CNMs. The electric field parameters and nature of the field significantly influence the alignment of CNMs in a polymer matrix. Also, CNM aspect ratios and concentration affect their orientation behaviour under the electric field. These aforesaid parameters must be studied elaborately to make this method more effective and industrially scalable.

Electrospinning

Electrospinning is one of the most powerful methods to produce fibers from micro to nano range and fabricate polymer nanocomposites. This method has advantages such as high quality, low cost, wide material suitability and consistent nanofiber quality. Lee et al. described the reaction mechanism of a classic electrospinning setup. A charged droplet of polymer solution is held at the tip of a fine capillary. During jet initiation, an electric field is applied to the polymer droplet which helps to overcome the surface tension and elongate the polymer droplet to form a conical shape named Taylor cone. When a critical electric field intensity is achieved, the electric forces overcome the surface tension and results in a forcible ejection of polymer jet. Therefore, there are complex electro-hydrodynamic and rheological interactions acting on each other [72].

Cai et al. fabricated uniaxially aligned cellulose nanofibers (CNFs) by electrospinning of the cellulose acetate derived from bamboo cellulose (B-CA) and used those CNFs as reinforcements to make optically transparent composite films. The B-CA concentration and electrospinning parameters (e.g. spinning distance and collection speed) were investigated for their effects on the fiber morphology and orientation (Fig. 11). The improvement in interfacial interactions facilitated the effective stress transfer from polymer matrix to fibers, which in turn enhanced the overall stiffness and mechanical strength of the composite films. The resultant composite films also showed high visible light transmittance even with a high fiber content [73]. He et al. fabricated electrospun nanocomposite nanofibers using uniaxially aligned cellulose nanofibers with cellulose nanocrystals as a reinforcement (CNF/CNC).

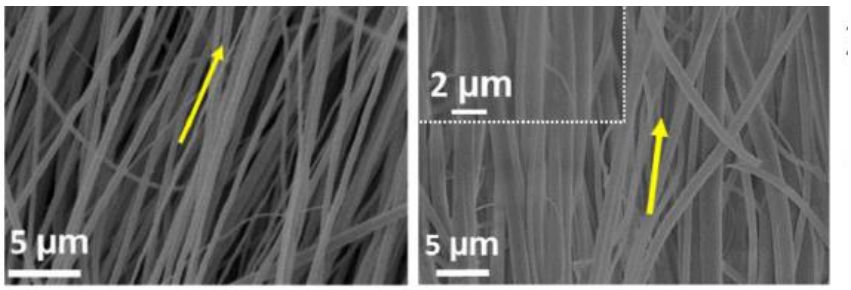

Fig. 1.11: SEM images of (a) aligned B-CA nanofibers and (b) CNFs after regeneration. Adapted from Ref [73].

The micrographs showed (Fig. 12) that most CNFs were uniaxially aligned and CNCs were well dispersed in the non-woven and achieved considerable orientation in the long axis direction. This unique hierarchical microstructure of the composites resulted in remarkable enhancement of the physical properties of the composites. By incorporating 20% (w/w) CNCs, the tensile strength and elastic modulus along the fibre axis direction increased by 101.7% and 171.6%, respectively [74]. Liao et al. fabricated optically transparent epoxy resin nanocomposite films reinforced with

electrospun cellulose nanofibrous mats by solution impregnation method. SEM micrographs showed indistinct epoxy/fibre interfaces, epoxy beads adhered on the fibre surfaces and torn fibre remnants were on the fractured composite film surfaces. So, the epoxy resin and cellulose fibres formed good interfacial adherence through hydrogen bonding. The mechanical strength and Young's modulus also increased by 71 and 61%, respectively [75]. Song et al. investigated the effect of electrospinning on the liquid crystal orientation of CNCs and fibre alignment under high voltage electric field. The composite nanofibers selectively reflected frequent and continuous birefringence, regarded as nematic phases of CNCs, induced by uniaxial stretching under the high voltage electric field. The synergistic effect of the rigidness of the nanocrystals and stretching orientation of the nematic phases provided higher tensile strength and strain to the aligned nanofibrous mats compared to the randomly oriented or core-sheath nanofibrous mats at the same loading of CNC [76].

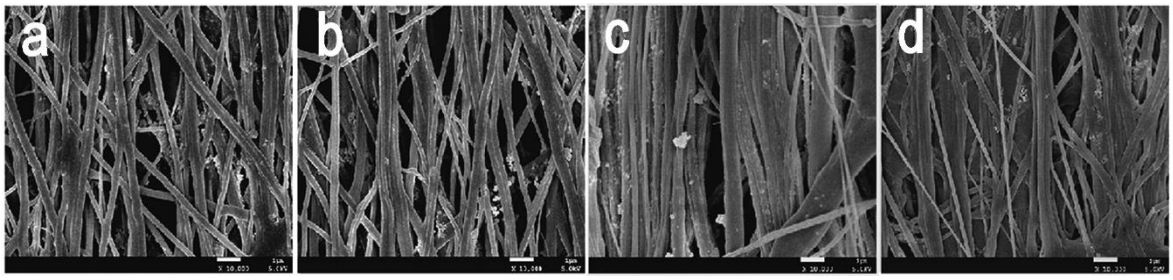

Fig. 1.12: SEM images of CNF/CNC nanocomposite nanofibers: (a) 0% CNC, (b) 5% CNC, (c) 12.5% CNC and (d) 20% CNC. Adapted from Ref [74].

The uniaxial stretching under high voltage electric field of CNMs during electrospinning, facilitates their orientation and thereby enhances the physical properties of the resultant composites. There are several studies on uniaxial alignment of nanofibrous polymer mats during electrospinning, but little attention is attributed to the alignment of reinforcements (CNMs).

Therefore, there is a great scope to investigate the effect of electrospinning process parameters on the CNM alignment and the overall effect on nanocomposite properties.

Drawing

Drawing is an established technique to align the fibers or nanoparticles in the drawing axis direction. There are different types of drawing (hot/cold) depending on the material and process conditions. In a drawing method, there exists a difference in speed which produces sufficient shear force to forcibly align the fibers or nanoparticles along the drawing direction.

Lee et al. fabricated high-performance CNC/PVOH composite fibers via coaxial coagulation spinning, followed by hot-drawing. Drawing condensed the fiber and increased the alignment of both CNC and polymer in the fiber direction as indicated by the X-ray diffraction patterns. The individual CNCs remained well dispersed in the composite at loadings up to 40 wt%. At 40 wt% CNC loading, the tensile strength and stiffness reached up to 880 MPa and 29.9 GPa, respectively [77]. Wang et al. established an effective drawing procedure that induced a high degree of orientation of CNCs in a matrix of carboxymethylcellulose (CMC) at a high level of reinforcement (50 vol%). Scanning electron microscopy (SEM) and two-dimensional X-ray diffraction (Fig. 13) quantify the alignment of CNCs. The improvement in alignment showed a synergistic increase in the stiffness, strength and toughness at the same composition. The composites showed stiffness greater than 10 GPa and tensile strength of 125 MPa at 90% R.H. [78]. Singh et al. studied the effects of drawing conditions (temperature, speed and draw ratio) on the composite tapes of plasticized polylactic acid (PLA)/CNF (1 wt%) prepared using uniaxial solid-state drawing. Microscopy studies confirmed the orientation of the macromolecular chains perpendicular to the draw direction, indicating the formation of ‘shish-kebab’ morphology.

Improved mechanical properties and toughness up to 60 times compared to the undrawn composites was observed. The drawing also improved thermomechanical properties. The storage modulus increased, and the tan delta peak shifted towards higher temperature, broadened and decreased in height with increasing draw ratio and drawing speed [79]. Wang et al. established an effective fabrication method for producing high performance nanofibers from ultralong bacterial

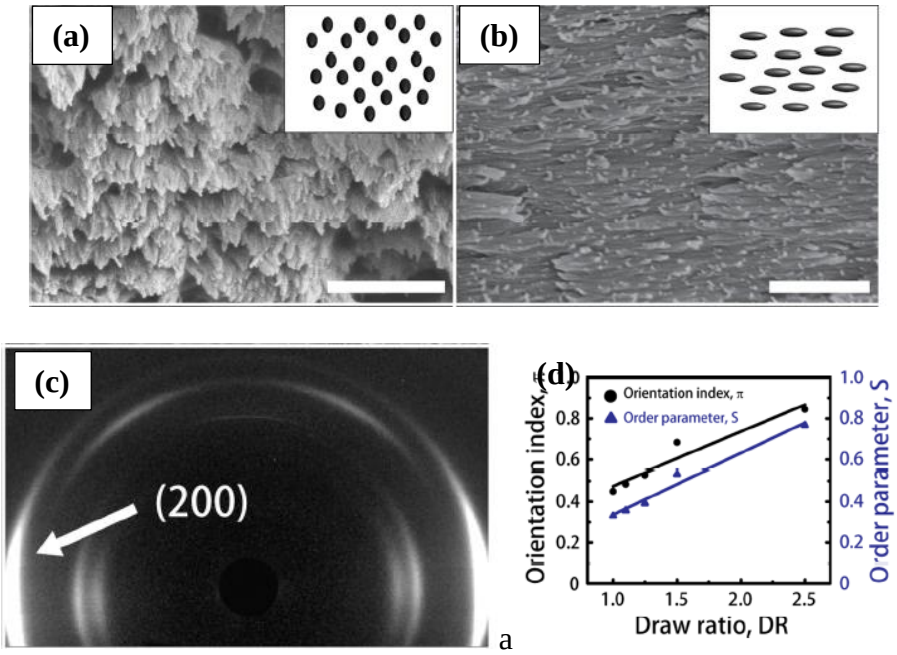

Fig. 1.13: SEM images of a fractured cross section of a drawn and strongly aligned film, DR = 2.5, acquired (a) perpendicular to and (b) within the drawing direction (scale bars are 500 nm), 2D WAXD data to characterize the extent of alignment, (c) DR = 2.5. (d) Orientation index, π, and order parameter, S, as a function of DR, establishing a direct link between drawing and orientation of the reinforcements. Adapted from Ref [78].

nanocellulose fibers (BC fibers) via wet-drawing and wet-twisting process. The as-prepared BC fibers without wet-drawing, showed rough and undulated surfaces, which was composed of randomly oriented nanofiber bundles. But, the surface roughness was significantly reduced in case of 30% wet-drawing strain fibers. The glossy surface was attributed to the closely packed

nanofibers with reduced porosity and orientation along the fiber axis direction. The resulting macrofibers yielded tensile strength as high as 826 MPa and Young's modulus of 65.7 GPa. The specific tensile strength of the macrofibers (598 MPa g^{-1} cm^3) was even higher than novel lightweight steel (227 MPa g^{-1} cm^3) [80]. Sehaqui et al. reported a preparation route of nanocomposite made of nanofibrillated cellulose (TEMPO-NFC)/hydroxyethyl cellulose (HEC) by cold drawing. The AFM images (Fig. 14) clearly showed the preferential orientation of fibrils parallel to the direction of drawing. At high draw ratio, the degree of orientation became as high as 82 and 89% in-the-plane and cross-sectional planes, respectively. The mechanical properties improved, tensile strength increased to 430 MPa and modulus to 33 GPa [81].

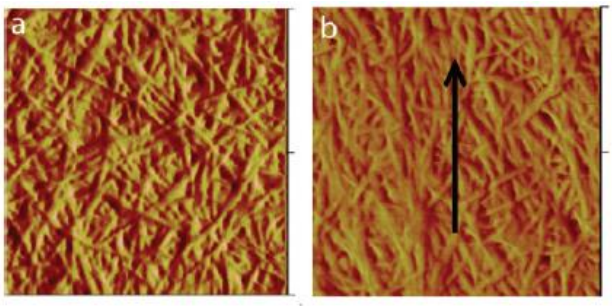

Fig. 14: AFM micrographs of surfaces of (a) a reference undrawn TEMPO-NFC nanopaper sample (DR = 1), (b) a drawn TEMPO-NFC nanopaper at DR = 1.4. Adapted from Ref [81].

Drawing can significantly improve alignment of CNMs in polymer matrices and thereby enhance the overall physical properties of the composites. The drawing parameters (temperature, speed, draw ratio) affect the extent of drawing and eventually the resultant physical properties of the composites. There are several articles on drawing of CNMs as building blocks, but lesser effort is attributed to the drawing of the CNMs as reinforcements. Therefore, there is a great opportunity

to investigate the effects of drawing on the CNMs as reinforcement materials of the polymer composites.

Quantum Dot Treatment

Enzymes, mainly composed of proteins or catalytic RNA molecules, are powerful biocatalysts and have been widely used in industrial, medical, and biological fields. However, because of significant drawbacks of natural enzymes for practical purposes (high cost for preparation and purification, low operational stability, sensitivity to environmental conditions, difficulties in recycling and reusing), researchers have now shifted their focus to alternatives. Nanozymes are emerging as a new class of nanomaterials with nanoscale sizes (1-100 nm) and enzymatic catalytic properties. These nanoparticles (NPs) have garnered special attention because of their facile synthesis process, simple biofunctionalization, wide range of temperature stability and dimensional and morphological tunability. The decrease in dimensions of NPs increases their enzymatic activities because of the larger surface area available. Quantum dots (QDs) are a member of an extremely small class of nanomaterials (typically 2-10 nm diameter) and used for conventional fluorescence based applications. But their enzymatic activity is yet to be explored and can facilitate significant improvement of sensing applications [82,83]. For the last two decades, researchers presented facile approaches to construct hybrid nanomaterials composed of CNMs/metal quantum dots. There are several research papers on the application of these hybrid nanomaterials (CNC-CdSe/ZnS, CNF/CdTe, CNF/CdS) in bioimaging, biosensing, tissue engineering etc [84,85,86]. Compared to traditional metal-based QDs, carbon quantum dots (CQDs) and graphene quantum dots (GQDs) (Fig. 15) have distinct advantages such as low toxicity, biocompatibility, renewability, low cost and better chemical resistance [83].

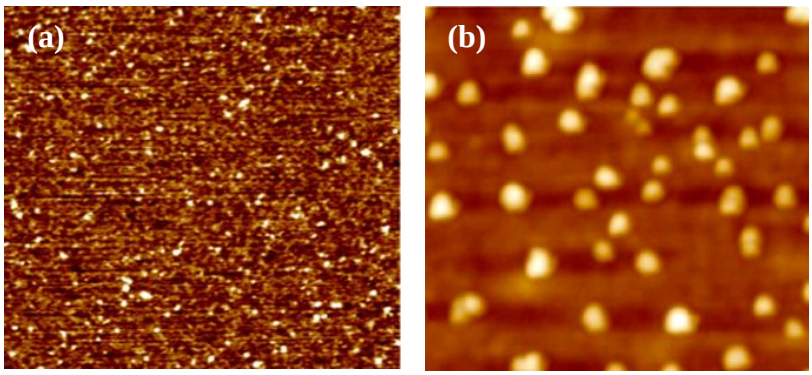

Fig. 15: (a) AFM image of GQDs, (b) AFM image of CQDs. Adapted from Ref [89] and Ref [91], respectively.

GQDs possess one or few layers of graphene and connected chemical groups on edges. They are anisotropic in nature having lateral dimensions larger than their height [87]. Sekiya et al. explained the structural characteristics of GQDs. GQDs are amphiphilic in nature, having hydrophobic character in their basal plane and hydrophilic on the edges as a result of the presence of carboxylic acid groups [88]. CQDs are always spherical and have an obvious crystal lattice. In the article of Zhu et al., many approaches to fabricate GQDs and CQDs are elaborated, most popular of which are ‘top down’ cutting from different carbon sources and ‘bottom up’ synthesis from organic molecules or polymers [87]. Khabibullin et al. fabricated an injectable shear-thinning hydrogel from CNC and GQDs. CNCs and GQDs can exhibit hydrophobic interactions and form hydrogen bonds between the surface hydroxyl groups present in CNC and carboxylic acid groups of GQDs. Moreover, CNCs carry a negative charge on their surface because of the carboxylic groups [89]. Thus, GQDs and CNCs exhibit mutual electrostatic repulsion, which in turn can improve dispersion of CNCs in polymer matrix. Guo et al. and Junka et al. explained the reaction mechanism of CQDs with CNMs. In case of CQDs, there is an electrostatic attraction between the two oppositely charged nanoparticles: positively charged CQDs and negatively charged CNMs.

Generally, the covalent coupling reaction between the CQDs and CNMs are assisted by EDC/NHS chemistry. This reaction is affected by change in pH. At neutral and acidic pH, CQDs are positively charged. But, at alkaline conditions, CQDs become uncharged and result in a reduced electrostatic interaction [90, 91]. Therefore, surface functionalization of CNMs by CQDs/GQDs can be the future path to effectively disperse CNMs in the polymer matrices and eventually improve the physical properties of the polymer nanocomposites.

Conclusion and Future Direction

There exist many challenges in the production of CNM/thermoplastic polymer composites. For example, agglomeration of CNMs during drying, insufficient interfacial compatibility between CNMs and the matrices, and degradation of CNMs during processing. Physical form of CNMs also plays a very significant role in their dispersion. Achieving optimum dispersion of CNMs is very difficult and success depends on multiple efforts attributed to the complexity of the entire process. Both chemical and physical surface treatments have been demonstrated to assist in the dispersion of CNMs in polymer matrix. In case of chemical aided dispersion techniques, polymer grafting, silyation, acid and isocyanate treatment, and acetylation or esterification methods improve mechanical performance of the composites. All these are expected to be industrially scalable techniques. Moreover, silyation is a water/alcohol-based system and esterification can be done in a solvent free reaction medium, which makes them eco-friendly. But there is no visual evidence of improvement in CNM dispersion in any of the aforesaid methods, except polymer grafting. Use of organic solvents makes polymer grafting non eco-friendly. Silanes are expensive chemicals and acid and isocyanate treatments involve use of highly corrosive and toxic chemicals. In case of physical aided dispersion techniques, plasma induced surface modification,

ultrasonication, magnetic force, electric discharge, electrospinning and drawing can visibly improve dispersion or orientation of CNMs in the polymer matrix. Also, mechanical properties of the composites are enhanced in these techniques. Plasma, magnetic force and electric discharge are very quick methods. Electrospinning provides acute control over process parameters which in turn gives consistent product quality. However, ultrasonication and magnetic force are only effective in low concentration of CNMs, till now. Electric discharge and ultrasonication both are energy consuming methods and ultrasonication is a time-consuming. Plasma involves expensive equipment. Electrospinning requires trained personnel for setup. This method also involves use of organic solvents in some cases. In drawing, drawing parameters (draw ratio, speed) and environmental conditions (humidity, temperature) may affect the efficiency of the method. All these physical dispersion techniques are not fully explored to make them industrially scalable. It appears that a combination of chemical and physical treatment can solve this problem at lab scale and at industrial scale. The quantum dots (QDs) are an emerging class of materials which can fine tune the surface properties of CNMs by complex electrostatic interaction and surface chemistry. The comparatively new (discovered in 2004) CQDs and GQDs can be the flagship of the quantum dots treatment, avoiding the toxicity and other limitations of the conventional metal QDs. Both CQDs and GQDs are compatible with CNMs as well as polymer matrix (hydrophobic and hydrophilic), so they can prove to be a successful path to improve both the interfacial interaction between CNMs and polymer and the dispersion state of CNMs.

CHAPTER THREE

SILANE COMPATIBILIZATION TO IMPROVE THE DISPERSION, THERMAL AND MECHANICAL PROPERTIES OF CELLULOSE NANOCRYSTALS IN POLY (ETHYLENE OXIDE)

Contribution of Authors and Co-Authors

Manuscript in Chapter 2

Author: Saptaparni Chanda

Contributions: Conceptualization, Methodology, Formal analysis, Writing – Original draft

Co-Author: Dilpreet S. Bajwa

Contributions: Supervision, Resources, Writing – Review, Editing

Co-Author: Greg Holt

Contributions: Writing- Review, Editing

Co-Author: Nicole Stark

Contributions: Resources

Co-Author: Sreekala Bajwa

Contributions: Writing- Review, Editing

Co-Author: Mohiuddin Quadir

Contributions: Characterizations

Manuscript Information

Saptaparni Chanda, Dilpreet S Bajwa, Greg Holt, Nicole Stark, Sreekala G Bajwa, Mohiuddin Quadir

Nanocomposites

Status of Manuscript:
___ Prepared for submission to a peer-reviewed journal
___ Officially submitted to a peer-reviewed journal
___ Accepted by a peer-reviewed journal
_X_ Published in a peer-reviewed journal

Publisher: Nanocomposites; 7.1: 87-96,
DOI: https://doi.org/10.1080/20550324.2021.1942641

Abstract

Cellulose nanocrystal (CNC) has potential to be used as a reinforcement in polymeric nanocomposites because of their inherent biodegradability, universal accessibility, and superior mechanical properties. The most crucial challenge faced in the nanocomposite production is dispersing the nanoparticles effectively in the polymer matrix, so that the exceptional mechanical properties of the nanoparticles can be transferred to the macroscale properties to the bulk nanocomposites. In this research, a safe, effective and ecofriendly modification was used to functionalize the surface hydroxyl groups of CNC via silane treatment. These modified CNCs were used as reinforcements to prepare poly (ethylene oxide) (PEO)/CNC nanocomposites. The composites were prepared using solvent casting method. The composite properties were evaluated using Fourier Transform Infrared Spectroscopy (FT-IR), Scanning Electron Microscopy (SEM), Thermo-Gravimetric Analysis (TGA), Differential Scanning Calorimetry (DSC), and Dynamic Mechanical Analysis (DMA). The SEM micrographs demonstrated that the composites incorporated with silane treated CNCs showed improvement in the dispersion behavior of the nanoparticles in the matrix. Oxidative combustion of the composites containing silane treated CNCs promoted char formation and enhanced thermal stability. The composites containing (1:1) silane treated CNCs exhibited the better crystallization ability, highest storage modulus, and lowest tan δ value compared to the other silane treated systems indicating improved dispersion of CNC. The polysiloxane network provided an efficient surface covering of the CNC molecules, imparting reduced polar surface characteristics and enhancing the overall mechanical properties of the composites.

Keywords: Cellulose nanocrystals, Poly (ethylene oxide), Dispersion, Thermal stability, Mechanical properties, Self-condensation reaction

Introduction

Biodegradable and renewable materials have received special attention from both scientific and industrial communities due to their potential to cope with the effects of global warming and pollution. Cellulose is the most abundant bio-based polymer and has been used as a potential biodegradable and renewable material for industrial products. In the last few decades, nanostructured cellulose materials have become a new field of interest because of the specific physical and chemical properties of these materials. Nanocellulose can be distinguished in two main categories: 1) Cellulose nanofibrils (CNF), which is produced mainly by mechanical defibrillation, and 2) Cellulose nanocrystals (CNC), obtained by acid treatment. Both CNFs and CNCs are used for different applications because of their different properties [92]. The development of high performance/ functional composites using nanofillers has become a prominent area of recent research. The selection of nanofillers has raised serious concerns for the environment and there is an immense need to introduce sustainable and bio-degradable nanofillers. Nanocellulose materials have great potential as nanofillers [93]. Amongst the nanocellulose materials, CNCs have gained special attention because of their high crystallinity (54-88%), superior mechanical properties- (tensile strength ~ 7 GPa, elastic moduli ~150 GPa), light weight, transparency, relatively low cost and broad capacity to modify surface properties [11-16].

In nanocomposites, the surface properties of CNCs affect the interfacial adhesion between filler and matrix, which ultimately dictates the overall properties of the composites together with the filler properties, orientation and aspect ratio. The most critical challenge in nanocomposite

processing is to transfer the exceptional mechanical properties of CNCs at single fiber level to the macroscale properties of the bulk nanocomposites. This can only be achieved by enhancing the dispersion of CNCs and optimizing the filler-matrix interface [30-35], which is where the surface modification processes of CNCs come into play. The surface modifications are mainly conducted to introduce surface charges or functional groups, and tune the surface energy characteristics to enhance compatibility to the polymer matrices, while keeping the original morphology of CNCs intact [36]. Surface modifications not only induce surface charges or tune the surface energies of CNCs, but they also confer new properties to CNCs [37]. The surface modification techniques can be divided into two categories: 1) chemical surface modification through different chemical reactions, and 2) physical surface modification, using different physical means such as ultrasonication, electric pulses, or mechanical drawing. There are different types of chemical modifications reported to date such as polymer grafting, acetylation, esterification, acid treatment, isocyanate treatment, silanization. Amongst these methods, silanization has gained popularity because of the improvement in mechanical performance of the composites and use of a water/ alcohol-based system, making this method more ecofriendly.

CNC has been reported [39, 40, 41, 42] to blend with various polymers, such as, poly (3-hydroxybutyrate-co-3-hydroxyhexanoate (PHBH), poly (lactide), poly (vinyl alcohol), poly (propylene) and poly (caprolactone). Xu et. al [39] reported grafting of CNC with PHBH using (3-aminopropyl) triethoxysilane (APES) as a coupling agent. The experimental results showed improvement in dispersion of CNCs in PHBH matrix and enhancement in mechanical properties. In another study of Taipina et. Al [40], a silane with isocyanate groups (isocyanatepropyltriethoxysilane) was used to modify the surface characteristics of CNCs. The

primary goal of this study was to produce an oligomeric network of polysilsesquioxane, which can create an efficient nanocrystal covering. The modified CNCs showed less polar surface characteristics and better dispersion than the pristine ones. Qian et. al [41] used silane compatibilized (triethoxyvinylsilane, A-151) bamboo cellulose nanowhiskers (BCNW) as nanofillers for poly (lactic acid) (PLA) matrix. The mechanical properties of the silane-treated BCNWs were improved compared to the untreated ones. However, there was no clear evidence of improvement of dispersion of BCNWs in the polymer matrix . Yin et. Al [42] functionalized CNC surface using γ-aminopropyltriethoxysilane and used as nanofillers for poly (lactic acid) (PLA) composites. The electron microscope images showed that the dispersion of CNCs in the polymer matrix was improved because of the change in surface characteristics while as a result thermal stability and mechanical properties are also enhanced.

Inspired by these results of silane treatment, a green and a sustainable technology for CNC functionalization was selected to improve the dispersion of CNCs in poly (ethylene oxide) (PEO) matrix and enhance the overall mechanical performance of the composites. Despite the small quantity of hydroxyl groups on the surface of the CNCs, the formation of the siloxane network provides an efficient surface covering of the CNCs (Fig. 1). Moreover, this surface modification technique ends up in giving the CNCs less polar surface characteristics and makes them more compatible to hydrophobic polymer matrices. Overall, the main aim of the research was to develop a safe, effective and ecofriendly surface modification technique of CNCs to make them compatible to hydrophilic as well as hydrphobic matrices and to improve the dispersion behavior of CNCs in the matrix.

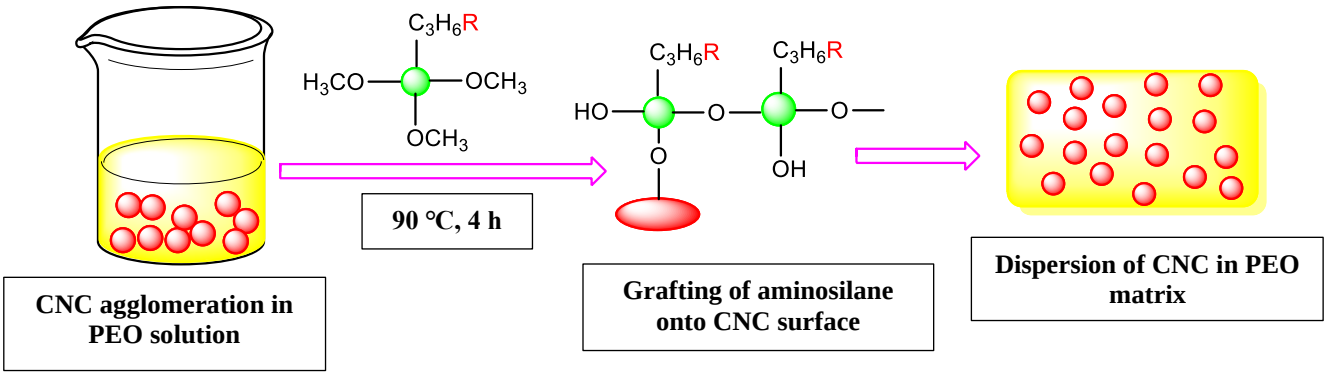

Fig. 2.1: Reaction mechanism of silane grafting onto CNC surface

Experimental Section

Materials

Poly (ethylene oxide) (PEO) (average M_v = 1,000,000) powder, with a melting temperature of 229 ℃, purchased from Sigma Aldrich was used as polymer matrix. The CNC with dimensions of 10-15 nm width and 80-100 nm length and hence aspect ratios of 5-10 were provided by USDA Forest Products Laboratory (Madison, WI, USA). They were extracted by the sulfuric acid hydrolysis process from softwood pulp. The CNCs were desulfated using hydrothermal treatment. The (3-aminopropyl) triethoxysilane (APES) with a purity of 98% was purchased from Sigma Aldrich. The specifications of silane were molecular weight (M_w=221.37 g/mol), boiling point (217 ℃), melting point (93 ℃) and density (0.946 g/mL). Deionized (DI) water purchased from Millipore, USA was used as solvent.

Surface Modification of CNC in PEO Solution

The surface modification of CNCs using APES was done using the procedure as reported in literature [94]. The first step involved dissolving CNCs in deionized water at room temperature under continuous stirring. One gram of dry mass of CNC was dissolved in 100 mL of DI water

separately in four beakers for four formulations. In the second step, 1 g of PEO was dissolved in each beaker at room temperature. In the third step, APES were dissolved in each beaker, in different concentrations. The weight ratios of CNC:APES were 1:1, 1:2.5 and 1:5, respectively in three formulations. In the fourth formulation, no silane was added. The fourth formulation was intended to check the reinforcment effect of CNC to the matrix and to perform the comparative studies of the effect of silane treatment on the dispersion behavior of CNC and mechanical properties of the resultant composites. All the solutions containing silane were kept under continuous stirring for 30 min. The solution without silane was stirred continuously until the CNC and PEO dissolved completely in water. In the fourth step, all the three solutions containing silane, were heated to 90 ℃ for 4 h to trigger silanization in the surface hydroxyl groups of the CNCs. Finally, a control sample solution was also prepared dissolving only 1 g of PEO in 100 mL of DI water, at room temperature. All the characterizations and the property comparison of the resultant composites were done with reference to this control sample of PEO. The formulation of each sample is shown in Table 2.1.

Table 2.1: Formulation of nanocomposite samples

Sample	PEO (%)	CNC (%)	CNC: Silane (Weight ratio)
PEO	1	0	-
1PEO/1CNC	1	1	-
1PEO/1CNC/1Silane	1	1	1:1
1PEO/1CNC/2.5Silane	1	1	1:2.5
1PEO/1CNC/5Silane	1	1	1:5

Nanocomposite Film Preparation

The PEO/CNC nanocomposite films were prepared using the film casting method [95, 96]. All the three formulations containing silane, were cooled to the room temperature. Then 20 mL from each of the five formulations (including the control and the no-silane one) were taken and poured very slowly in Teflon (PTFE) petri-dishes to make films, and to minimize the formation of air bubbles. The solutions were left for 24-48 h until the films were completely solidified. Two films were prepared for each formulation.

Characterization

Fourier Transform Infrared (FTIR) Spectroscopy: The samples were analyzed using FTIR spectroscopy (Nicolet i550, Thermo Fisher Scientific, USA) in an attenuated total reflection (ATR) mode. The final spectrum of each sample was an average of 32 scans at a resolution of 4 cm^{-1}, in the wavenumber range of 400-4000 cm^{-1}.

Scanning Electron Microscopy (SEM): The morphology of the film surface and dispersion of CNC in PEO matrix was analyzed using SEM. Images of surface morphology were taken at three magnifications (20K, 40K and 60K) using field emission scanning electron microscope (Supra 55VP, Zeiss, Thornwood, NY, USA), operating at an accelerating voltage of 1.0 kV, in the Image and Chemical Analysis Laboratory (ICAL) at Montana State University. The samples were coated with a thin film of Iridium for 30 s for conductivity before capturing the images.

Thermogravimetric Analysis (TGA): Thermogravimetric analysis was carried out using a TA Instruments Thermogravimetric Analyzer (TGA Q500, New Castle, USA) in North Dakota State University. The samples were tested in thermal degradation mode, under a flowing nitrogen atmosphere with a flow rate of 60 ml/min, from 25 ℃ to 500 ℃, at a heating rate of 10 ℃/min.

Differential Scanning Calorimetry (DSC): The thermal properties of the samples were measured by using DSC (Q2000, New Castle, USA) under a nitrogen atmosphere in North Dakota State University. The samples of about 4-5 mg were taken and scanned over a temperature range from 20 ℃ to 100 ℃ at a heating rate of 10 ℃/ min.

Dynamic Mechanical Analysis (DMA): Dynamic mechanical analyzer (DMA Q800, New Castle, USA) was used to understand the dynamic storage and loss modulus of the samples. The viscoelastic properties of the samples were also studied through tan δ curve. Selected samples with dimensions of approximately (15mm × 8 mm × 0.6 mm) were tested using the film tension mode at a constant frequency of 1 Hz and a strain amplitude of 15 μm. The test was performed in the temperature range of 30 ℃ to 110 ℃ and the heating rate was set at 5 ℃/ min. For each formulation, two replicates were tested, and the mean values were reported.

Results and Discussion

Spectroscopy Analysis of the Composite Films

The FT-IR spectra of the PEO and all the composites containing CNC (untreated and silane treated) are shown in fig. 2. In the PEO spectra, three -C-O-C- peaks appeared at 1145 cm^{-1}, 1112 cm^{-1} and 1062 cm^{-1}. The characteristic C-H stretching band was also observed between 3000 cm^{-1} and 2800 cm^{-1} [97]. For the PEO-CNC samples, the peaks at 3340 cm^{-1} and 1380 cm^{-1} represented the stretching and bending vibrations of O-H groups, indicating the incorporation of CNC in the matrix [98]. In case of the silane treated CNC composite samples, the characteristic band at 1580 cm^{-1} corresponding to the NH_2 band, shifted to 1560 cm^{-1} because the formation of an amide band [95]. This confirms grafting of silane onto the surface of the CNC.

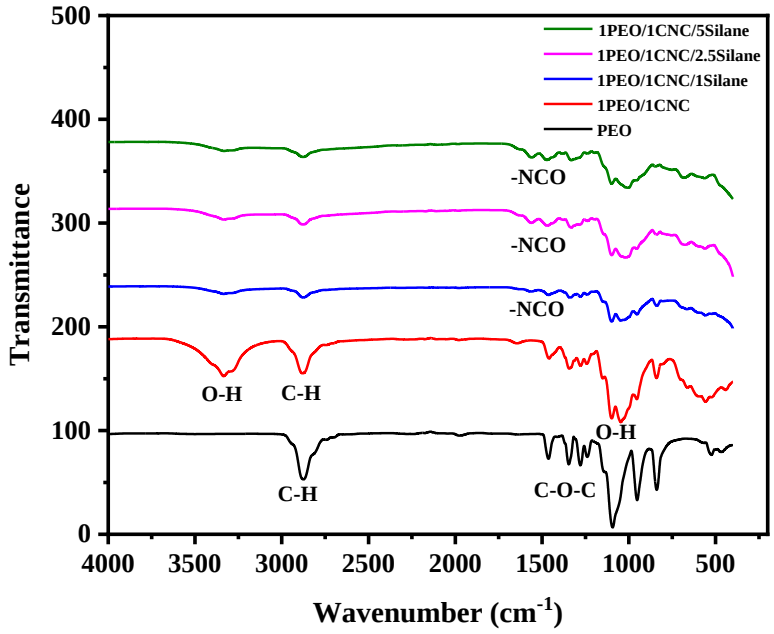

Fig. 2.2: Transmission spectra of PEO, untreated CNC incorporated PEO, (1:1) silane treated, (1:2.5) silane treated and (1:5) silane treated CNC incorporated samples measured using FTIR

Morphological Study of the Composite Films

Fig. 3 shows the SEM images of PEO-CNC composite films, both silane treated and untreated. The untreated CNCs showed a poor dispersion behavior in PEO matrix. The slow evaporation rate of the solvent pushed the nanocrystals to closer proximity and favored the formation of large agglomerates. But, the 1PEO/1CNC/1Silane and 1PEO/1CNC/2.5Silane samples exhibited improved dispersion behavior. In 1PEO/1CNC/1Silane sample, there were still bundles of CNCs clogging together present in the polymer matrix. In case of 1PEO/1CNC/2.5Silane, individual CNC crystals can be observed in some areas and clogging of bundled CNC in other areas. Again, the 1PEO/1CNC/5Silane samples showed very poor dispersion behavior. This may be due to the excess of silane present in the system. The reaction of silane and CNC surface groups reached the saturation point in case of 1PEO/1CNC/2.5Silane, and

started adversely affecting the dispersion behavior of CNC when more silane was added to the system.

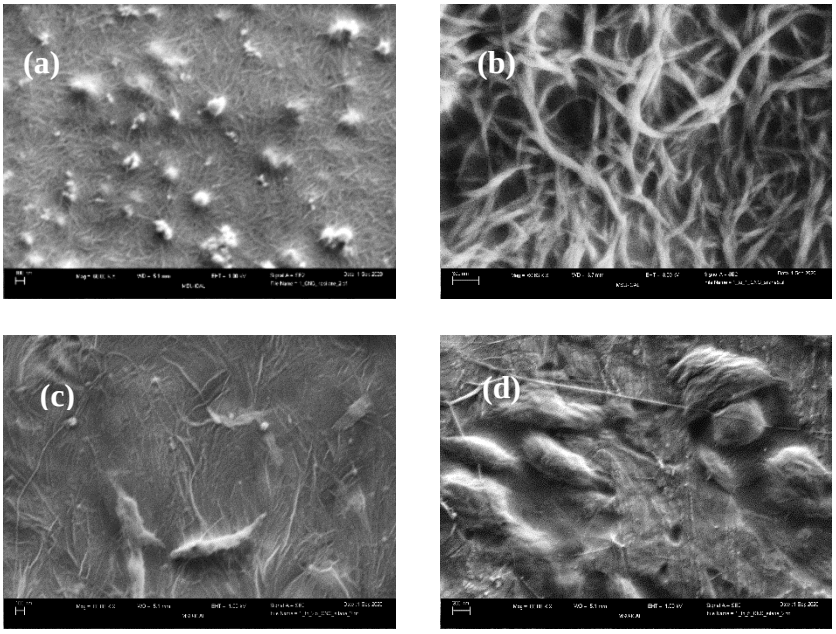

Fig. 2.3: SEM images of PEO-CNC composite films :(a) 1PEO/1CNC, (b) 1PEO/1CNC/1Silane, (c) 1PEO/1CNC/2.5Silane and (d) 1PEO/1CNC/5Silane samples

Thermogravimetric Property Analysis

The effect of CNC incorporation and the silane treatment on the thermal properties of the PEO matrix were examined using thermogravimetric measurement and represented in Fig. 4, Fig. 5 and Table 2. The degradation of PEO started at ~340 ℃ and the polymer was sharply decomposed in a single step leaving almost no residue above 490 ℃. After the incorporation of CNC, the onset point was decreased to ~270 ℃, but the rate of mass loss was also decreased and the residue was still 6.7% above 490 ℃. The surface sulfate groups present in the CNC caused the decrease in the onset degradation temperature because of the catalytic nature of the sulfate esters. In this two-step degradation process, the first step was caused by the degradation of the amorphous

regions of CNC. The second step indicated the degradation of the crystalline part of CNC. Therefore, there is a slight decrease in thermal stability with the incorporation of CNC in the matrix. When the (1:1) silane grafted CNCs were incorporated in the PEO matrix (1PEO/1CNC/1Silane samples), the onset point was improved to ~310 ℃, and the char formation was increased leaving almost 22% residue. As the amount of silane was increased, the amount of residue also increased, reaching 33.6% and 40.4% for 1PEO/1CNC/2.5Silane and 1PEO/1CNC/5Silane samples, respectively. In all the silane treated composite films, the mass loss was much lower than the pristine CNC treated ones. The incorporation of silane treated CNCs increased the thermal stability of the composite films as inferred from the above data. This increase in thermal stability of the nanocomposites can be attributed to the shielding effect of the three dimensional polysiloxane network grafted onto the surface of the modified CNC. Therefore, the degree of grafting of silane onto CNC was calculated using the following equation:

$$\text{Grafting degree} = (W_a - W_0) \times 100 / W_a \qquad (2.1)$$

where W_a is the residue weight of composite after grafting and W_0 is the residue weight of composite before grafting. The degree of grafting was maximum in case of 1PEO/1CNC/5Silane samples, around 70%, followed by the 1PEO/1CNC/2.5Silane and 1PEO/1CNC/1Silane ones.

Table 2: Grafting degree of each formulation from TGA

Sample	Residue wt. (%)	Grafting degree (%)
PEO	2.5	-
1PEO/1CNC	6.7	-
1PEO/1CNC/1Silane	22.1	26.4
1PEO/1CNC/2.5Silane	33.6	49.6
1PEO/1CNC/5Silane	40.4	77.9

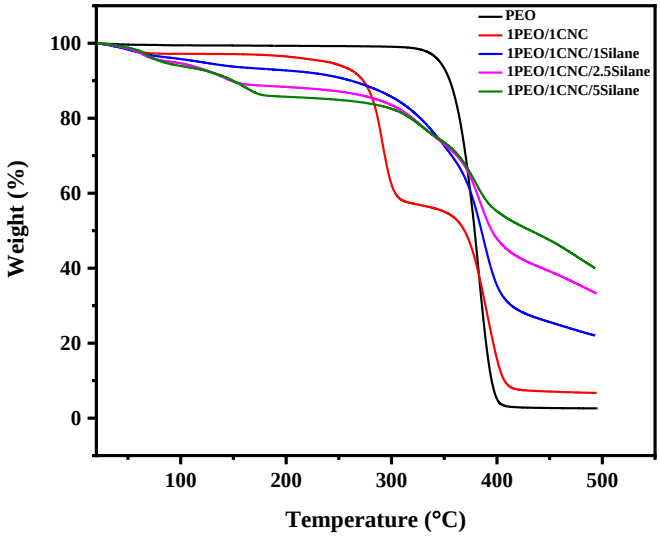

Fig. 2.4: TGA thermogram of PEO, untreated CNC incorporated PEO, (1:1) silane treated, (1:2.5) silane treated and (1:5) silane treated CNC incorporated samples

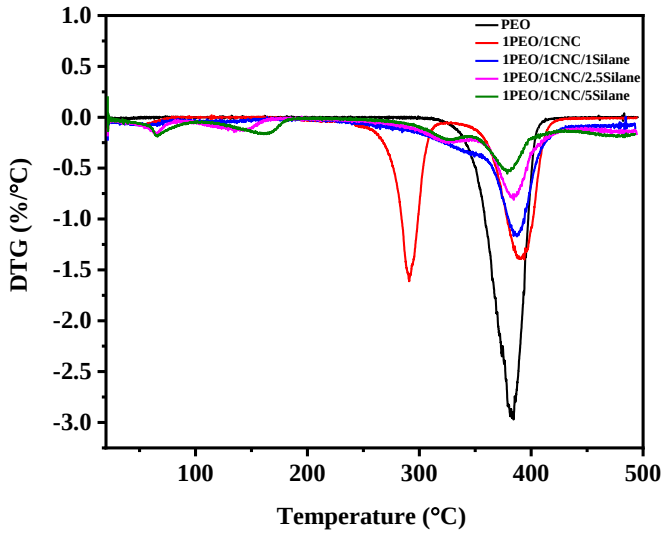

Fig. 2.5: Derivative thermogravimetric (DTG) curves of PEO, untreated CNC incorporated PEO, (1:1) silane treated, (1:2.5) silane treated and (1:5) silane treated CNC incorporated samples

Crystallization Behavior of the Composite Films

The non-isothermal crystallization behavior of the PEO-CNC composites was studied using DSC. The DSC results were shown in Fig. 6 and Table 3. The crystallinity (X_c) was determined by the following equation:

$$X_c\ (\%) = \Delta H_m \times 100/\ \Delta H_m^0 \times (1\text{-}x) \qquad (2.2)$$

where ΔH_m is the melting enthalpy, ΔH_m^0 is the theoretical enthalpy of 100% crystalline PEO (197 J g^{-1}), and x is the weight fraction of filler (CNC).

In case of pure PEO, the crystallinity (%) was 61.7%, but the glass transition temperature (T_g) was not detected, as it was significantly lower (-67 ℃) than room temperature. In contrast to pure PEO, all the CNC incorporated samples, both silane treated and untreated, showed a decrease in crystallinity. The 1PEO/1CNC sample showed a decrease in crystallization temperature (T_c) and melting temperature (T_m) and crystallinity (%) compared to pure PEO, indicating the nucleating effect of CNCs. A heterogeneous nucleation mechanism was induced by the nanofillers which in turn decreased the free energy barrier and accelerated the crystallization process. The PEO polymer chains surrounded the crystal nucleus and created an energy barrier to hinder the macromolecular chains to enter the lattice, favoring the formation of disordered and metastable crystal structures [99]. The confinement effect of nanocrystals hindered the chain diffusion and folding at the crystal growth front and formed thinner spherulites [100]. The 1PEO/1CNC/1Silane samples showed an improvement in crystallization ability (X_c=55.1%) compared to the 1PEO/1CNC and other silane treated samples. Also, the highest crystallization temperature (T_c) (48.1 ℃) was observed in case of 1PEO/1CNC/1Silane samples. In general, the higher the T_c observed upon cooling, the faster the crystallization rate of the polymers. Therefore, the crystallization ability of PEO was the best in the case of (1:1) silane treated CNC incorporation.

The T_c and crystallinity of 1PEO/1CNC/1Silane samples were increased because of the restricted mobility of the polymer chains, indicating a better interfacial interaction between the modified filler (silane treated CNC) and the matrix. Silane acted as a compatibilizer which facilitated the dispersion and penetration of CNCs within the polymer matrix [101].

Table 3: Crystallization behavior of each formulation from DSC

Sample	T_c	T_m	Crystallinity (%) (X_c)
PEO	45.9 ℃	65.8 ℃	61.7
1PEO/1CNC	35.1 ℃	56.9 ℃	26.2
1PEO/1CNC/1Silane	48.1 ℃	60.9 ℃	55.1
1PEO/1CNC/2.5Silane	47.2 ℃	61 ℃	41.5
1PEO/1CNC/5Silane	47.8 ℃	61.2 ℃	24.1

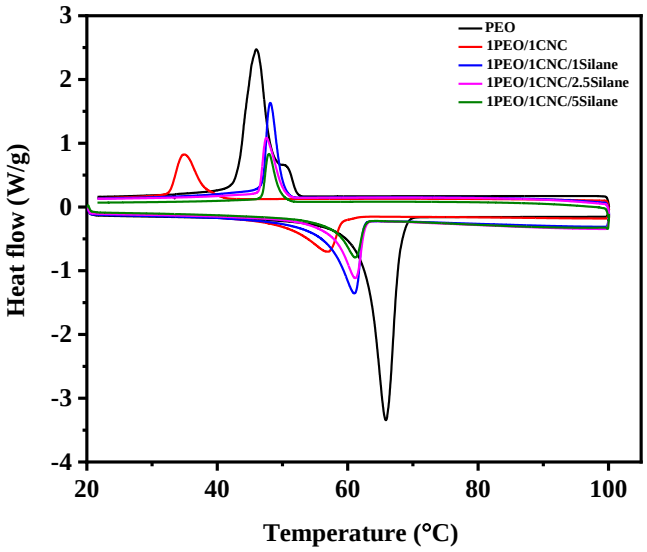

Fig. 2.6: DSC thermograms of PEO, untreated CNC incorporated PEO, (1:1) silane treated, (1:2.5) silane treated and (1:5) silane treated CNC incorporated samples

Dynamic Mechanical Property Analysis of the Composite Films

Dynamic viscoelastic properties such as storage modulus (E'), loss modulus (E") and loss factor (damping parameter, tan δ) were studied through dynamic mechanical analysis. The variation in storage modulus of pure PEO and corresponding composites as a function of composition and temperature while the samples were subjected to elevated temperature at a constant rate is shown in Fig 7 and the values are tabulated in Table 4.

For pure PEO, the storage modulus is approximately 206 MPa. The addition of untreated cellulose nanocrystals (1PEO/1CNC) led to a significant increase in storage modulus (3034 MPa), which further increased when silane treated CNCs (1PEO/1CNC/1Silane) were incorporated in the matrix (3147 MPa). However, as the concentration of silane is increased from (1:1) to (1:2.5), the storage modulus sharply decreases (2258 MPa) due to the plasticizing effect of silane. Over the temperature range in this study, the formulation 1PEO/1CNC/1Silane exhibited the highest storage modulus value. This indicates that the grafted CNCs can form strong interaction networks that can facilitate stress transfer better than the ungrafted CNCs. The 1PEO/1CNC/5Silane formulation could not be tested for storage modulus as it was too brittle to withstand any amount of tensile force.

Table 4: Dynamic mechanical properties of each formulation from DMA

Sample	Peak tan δ	Storage modulus (MPa)	
		45 ℃	85 ℃
PEO	0.3264	206	-
1PEO/1CNC	0.0758	3034	1814
1PEO/1CNC/1Silane	0.0911	3147	1087
1PEO/1CNC/2.5Silane	0.0935	2258	251
1PEO/1CNC/5Silane	-	-	-

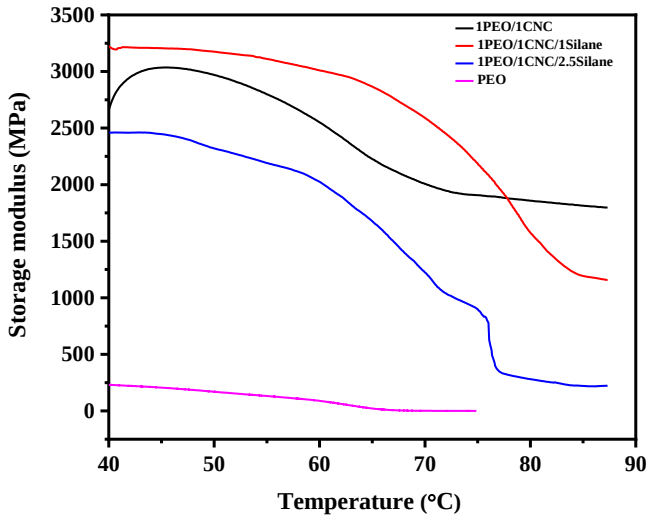

Fig. 2.7: Representative curve of storage modulus as a function of temperature of PEO, untreated CNC incorporated PEO, (1:1) silane treated and (1:2.5) silane treated CNC incorporated samples

As observed from the graph, the 1PEO/1CNC/1Silane samples, exhibited higher modulus than the other samples. When the amount of silane was increased in the reaction system, the storage modulus gradually decreased. This may be due to the formation of increased self-condensation reaction to form polysiloxane network on the CNC surface. Since in the other systems most of the silane linkages were engaged in the formation of siloxane bridges, this phenomenon severely influenced the grafting of CNCs and in turn the mechanical properties of the samples [102].

The tan δ is the ratio of the loss modulus to storage modulus indicating the damping characteristics of polymers. A low tan δ intensity indicates that the material is more elastic than viscous [103]. According to that, all the nanocomposite samples indicated a more elastic response, as shown in fig. 8. However, with the incorporation of silane in the composites, the tan δ values increased, exhibiting more viscous behavior compared to the no silane containing samples. As the concentration of silane was increased, the tan δ values gradually increased. The nanocomposite

samples exhibiting higher peaks in tan δ curves and lower storage modulus, indicated more viscoelastic behavior.

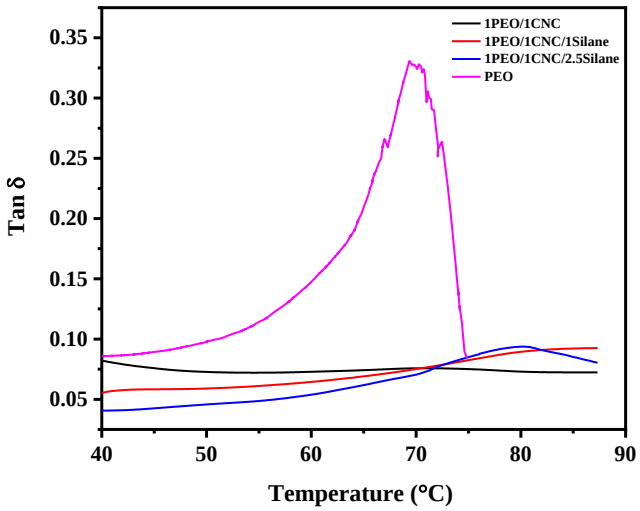

Fig. 2.8: Tan δ curves as a function of temperature for PEO, untreated CNC incorporated PEO, (1:1) silane treated and (1:2.5) silane treated CNC incorporated samples

The relatively simple Cox-Krenchel model was used to calculate the moduli of the composites and their results were compared with the experimental values [104]. The rule of mixture type relationship for the randomly oriented short fiber composites is:

$$E = \eta_0 \eta_L E_f v_f + (1-v_f) E_m \quad (2.3)$$

where E is the elastic modulus of the composite, E_f and E_m are fiber and matrix moduli, respectively, v_f is the fiber volume fraction, η_0 is fiber orientation factor and η_L is fiber length efficiency factor. Neglecting transverse deformations, η_0 for random 3-D fiber orientation = 1/5, η_L was assumed as 1, fiber volume fraction was of 50%. The modulus of PEO (E_m) was 206 MPa based on the experimental results. The modulus of CNC varies considerably between 50-200 GPa, based on the methods used to measure the tensile properties, types of cellulose (cellulose I or II)

and the ratio between two celluloses. In the current study, a value of 145 GPa for CNC (E_f) was used for theoretical modeling [103].

Therefore, the theoretical modulus of composite was

$$E = 1/5\times 1 \times 145 \times 0.5 + 0.5 \times 0.206 = 14.6 \text{ GPa}$$

The experimental modulus was only 3 GPa. This indicated that the CNC was highly agglomerated in the PEO matrix because of the high viscosity of the polymer solution and weaker hydrogen bonding with the nanocrystals. Moreover, the mechanical dispersion step used to mix PEO and CNC could influence the size of CNC. The low aspect ratio of CNC (5-10) also plays a pivotal role in reducing the length efficiency factor from 1(100%) about 0.2 (20%) [104, 105]. Table 5 represents the storage modulus values of other CNC composites with similar filler loadings. From the following data, it is clearly evident that silane treatment of CNC significantly improved the mechanical properties of the composites.

Table 5: Storage modulus of other CNC composites with similar filler loadings

Composite	Storage modulus (MPa)	Ref.
PEO/CNC	820	[104]
PHBH/CNC	1385	[100]
PLA/CNC	1992	[99]
PLA/CNC	2642	[103]
PLA/CNC	2490	[105]

Conclusion

The dispersion of nanofillers in the polymer matrix is the most crucial challenge in the process of nanocomposite production. In this study, PEO was successfully grafted onto the surface of CNC via aminosilane in a typical silane treatment. The grafting mechanism was carefully studied and confirmed by the FT-IR spectra. The scanning electron micrographs showed

improvement in dispersion behavior of the silane treated CNCs in the matrix as compared to the untreated ones. Incorporation of silane treated CNC increased the amount of char formation, compared to the untreated CNC composites and control samples. The (1:1) silane treated CNC incorporated samples showed the highest degree of crystallization (X_c= 55.1%) and the highest crystallization temperature (T_c= 48.1℃), compared to the other silane treated samples. The addition of (1:1) silane treated CNC led to a significant increase in the storage modulus of the nanocomposites. However, a further increase in concentration of silane resulted in a decrease in storage modulus, increase in tan δ and lowering of onset degradation temperature. This indicated an optimal concentration of silane in the composite samples, as a result of an increase in the self-condensation reaction of the silane linkages to form the polysiloxane network. As a result, only a small amount of silane linkages were available to react with the surface hydroxyl groups of CNC. It can be concluded from this research, that the (1:1) silane treated CNC incorporated composites exhibited the best overall performance in terms of thermal and physical and mechanical properties. Thus, this surface silane treatment of CNC can prove to be a successful path to disperse CNCs in polymer matrices, and also enhanced compatibility between the matrix and the fillers, reducing the polar characteristics of the fillers.

CHAPTER FOUR

NANO BORON OXIDE AND NANO ZINC OXIDE INCORPORATION TO CELLULOSE NANOCRYSTALS TO IMPROVE THE THERMAL, MECHANICAL AND FLAMMABILITY PROPERTIES OF HIGH-DENSITY POLY (ETHYLENE) POLYMER

Contribution of Authors and Co-Authors

Manuscript in Chapter 3

Author: Saptaparni Chanda

Contributions: Conceptualization, Methodology, Formal analysis, Writing – Original draft

Co-Author: Dilpreet S. Bajwa

Contributions: Supervision, Resources, Writing – Review, Editing

Co-Author: Nicole Stark

Contributions: Resources

Co-Author: Sreekala Bajwa

Contributions: Writing- Review, Editing

Manuscript Information

Saptaparni Chanda, Dilpreet S Bajwa, Nicole Stark, Sreekala G Bajwa

Nanocomposites

Status of Manuscript:
__X__ Prepared for submission to a peer-reviewed journal
____ Officially submitted to a peer-reviewed journal
____ Accepted by a peer-reviewed journal
____ Published in a peer-reviewed journal

Abstract

Recent developments in nanotechnology have captured the attention of polymer composites industry. To produce functional composites, bio-based sustainable nanofillers like cellulose nanocrystal (CNC) and its derivatives are being exploited. Nanoscale fire retardant (FR) additives are added to improve the thermal properties of petroleum-based composites. Nano metal oxides can reduce the flammability of polymers by modifying their degradation pathways. Zinc and boron-based compounds are well known for their superior flame retardancy, low toxicity and eco-friendly nature. In this research, safe, effective and eco-friendly hybrid systems of nano ZnO/CNC and nano B_2O_3/CNC were prepared and incorporated in high density poly (ethylene) (HDPE) matrix to improve their physico-mechanical and FR properties. Nano ZnO nanoparticles were prepared using zinc acetate and sodium hydroxide in aqueous dispersion and were coated onto CNC particles in different concentrations. Nano B_2O_3 was produced by ultrasonication of B_2O_3 powder and was coated onto CNC particles in different concentrations. These hybrid systems were incorporated in HDPE matrix separately to produce composites via melt blending extrusion process. The composite properties were evaluated using Fourier Transform Infrared Spectroscopy (FT-IR), Scanning Electron Microscopy (SEM), Energy Dispersive X-ray analysis (EDX), Thermo-Gravimetric Analysis (TGA), Differential Scanning Calorimetry (DSC), Dynamic Mechanical Analysis (DMA), tensile testing, horizontal burning test and microcalorimetry test. The composites containing ZnO coated CNC showed better mechanical and thermal properties compared to the B_2O_3 coated CNC composites. Fire retardant efficiency was also better in case of ZnO coated composites. Overall, 50% increase in elastic modulus and 14% reduction in peak heat release rate compared to neat HDPE were observed in case of ZnO coated composites. The SEM

micrographs and EDX images demonstrated some agglomeration and irregular distribution of the inorganic oxides in the polymer matrix. The results indicate that effective dispersion techniques can further enhance the thermos-mechanical properties of HDPE based polymer composite.

Keywords: Cellulose nanocrystals, High density poly(ethylene), Zinc oxide, Boron oxide, Hybrid system, Mechanical property, Thermal property, Dispersion

Introduction

The growth of fossil-fuel derived polymeric materials in every sector of modern life also brings additional hazard with it: hydrocarbon based polymeric materials are inherently highly flammable and release toxic gases during combustion. Loss of property and lives has become a continuous reminder of the need to find a suitable solution to limit flammability of materials. In the U.S., annually there are 2.4 are reported, resulting in 7.8 billion dollars of property loss, 29,000 civilian injuries, 101,000 firefighter injuries, and 6000 civilian fatalities [106, 107]. The combustion of polymers is an endothermic pyrolysis to flammable and toxic gases, which ignite in contact with air and lead to exothermic processes of flame propagation and heat release. The modes of action of flame retardancy are mainly in the condensed phase and vapor phase [108]. Different types of flame retardants (FRs) are used to cope the flammability of polymers which generally act chemically and/or physically in the condensed or vapor phase to interfere with the combustion process during heating, pyrolysis, ignition or flame spread [109].

The compounds mainly responsible for improving fire retardancy are minerals, halogenated monomers, phosphorous containing, silicon containing, and nano metric compounds [110]. Mineral flame retardants such as Alumina trihydrate (ATH) dominates the market because of its low cost, low decomposition temperature and high-water loss (34.5%) and high efficiency

in decreasing fire hazard. ATH is blended with the resin prior extrusion at relatively high levels, often presenting problems of poor compatibility, leaching, and reduced mechanical properties. Magnesium hydroxide follows ATH with decomposition temperature (T_{dec}) of 300 °C, and widely used in thermoplastic applications. The metal hydroxides require loading level of 60% or more which leads to deleterious effect on viscosity and mechanical properties. The most widely used fire retardant additives for thermoplastics and thermoset resins are halogenated compounds [111]. They act in the vapor phase to interrupt the exothermic processes and suppress combustion. They are also considered persistent organic pollutants that are not easily broken down or oxidized [112, 113]. Phosphorus containing flame retardants also promote char formation in condensed phase and are widely used in flexible polymers. Combinations like halogen-antimony, bromine-ammonium, bromine-chlorine, bromine-phosphorous are reported to provide synergistic effects in flame suppression etc. [114,115,116]. Unfortunately, use of these aforesaid materials as flame retardants is prohibited because of their negative impact on human health and environment [117].

Nanotechnology have helped to improve the fire behavior of polymers through the modification of the degradation pathway of the polymeric matrix as well as the modification of their rheological behavior. Recently combinations of inorganic clays, nano clays and metal hydroxides, carbon nanotubes (CNT), polyhedral silsesquioxanes (POSS) have helped to improve fire performance [114,118,116]. Layered silicates and double hydroxides having clay like structures are reported to increase fire resistance [119]. Montmorillonite based polymer matrices have shown a substantial improvement in fire performance by reducing heat release rate (HRR) [120].

Cellulose nanocrystal (CNC), extracted from the most abundant natural polymer on the earth, cellulose, is one of the most exploited nanofillers in the recent nanotechnology industry because of its superior mechanical properties, good thermal stability, and tunable surface chemistry [121]. Cellulose forms charred structures upon degradation. Low heating rate and low temperature exposure causes degradation reaction and rearrangement of cellulose structure facilitating char formation [122]. Inorganic oxides are very popular as flame retardants because of their low toxicity and low smoke evolution. ZnO coated cellulose fabrics have shown exceptional flame retardancy [116]. Textiles and upholstery cotton (cellulose) materials are now being treated with nano-sized inorganic particles to impart fire resistance [121,122]. Recently nano ZnO formulation with polycarboxylic acid was added as flame retardant for cotton and its blend. In the last ten years, ZnO, micro ZnO, nano ZnO have gained a lot of attention as fire retardant material for different synthetic polymeric based materials, cellulosic cotton, and other lingo-cellulosic fibers. Boron-based compounds are a rapidly developing new class of fire-retardant materials. Under fire exposure, boric acid provides a glass-like coating on the exposed surface inhibiting the flow of oxygen to the exposed polymer surface, promoting polymer dehydration and char formation [123]. Boron is also used to reduce flame spread rate, but it can also stimulate smoldering. However, boric acid is used synergistically with boron to suppress smoldering [124]. The low toxicity, eco-friendliness, preservative effectiveness, neutral pH are some of the beneficial effects of boron-based compounds [125].

Though there are several articles on the use of organo-modified montmorillonite, nano organo-clay and metal oxide nanoparticles in thermoplastics to improve the thermal stability and fire performance, there is currently limited knowledge on how nano-sized metal oxide or boron

oxide coated CNC will function in commodity polymers. In the current study, CNC and nano inorganic oxide hybrid system was used as filler for polyethylene-based composites. The composites were produced via melt blending extrusion and injection molding process. The CNC/inorganic oxide hybrid system is expected to improve the thermal stability of the composites by lowering the flame spread rate and limiting the oxygen supply by charring, shielding or insulating the exposed polymer surface while improving the mechanical properties of the composites. The main aim of the current research is to develop a safe, effective and eco-friendly hybrid system of inorganic oxide/CNC to improve the thermal, physical and mechanical properties of polyethylene-based composites.

Experimental Section

Materials

High density poly (ethylene) (HDPE) powder with a melt index of 3.5 g/10 min, and a melting temperature of 126 ℃, purchased from Nova Chemicals was used as polymer matrix. The CNC with dimensions of 10-15 nm width and 80-100 nm length and hence aspect ratios of 5-10 were provided by USDA Forest Products Laboratory (Madison, WI, USA). They were extracted by the sulfuric acid hydrolysis process from softwood pulp. The CNCs were desulfated using hydrothermal treatment. The (3-aminopropyl) triethoxysilane (APES) with a purity of 98% , zinc acetate dehydrate, sodium hydroxide, boron oxide powder, oleic acid were purchased from Sigma Aldrich. The specifications of silane were molecular weight (M_w=221.37 g/mol), boiling point (217 ℃), melting point (93 ℃) and density (0.946 g/mL). Zinc acetate dehydrate and sodium hydroxide were the ingredients for producing Zinc oxide (ZnO). Laboratory grade methanol of Thermo Fisher Scientific was purchased from the chemistry store of MSU and used as a solvent for ZnO

production. Boron oxide powder and oleic acid are used to produce nano boron oxide. Deionized (DI) water purchased from Millipore, USA was used as solvent.

Synthesis of ZnO coated Silane Functionalized CNC

Zinc acetate dehydrate (0.02 mol) was dissolved in 50 mL of methanol and heated at 50 ^{o}C under vigorous stirring for 0.5 h to make a precursor solution A. Then, 0.04 mol of sodium hydroxide was dissolved in 50 mL of methanol and heated at 50 ^{o}C along while vigorously stirred for 1 h, to make precursor B. To make ZnO nano-sol, solution B was added into solution A, drop-wise under constant stirring for 0.5 h at 50 ^{o}C. The mixture was stirred for another 2 h and cooled at room temperature to obtain transparent ZnO sol. This ZnO sol was freeze-dried and added to aqueous silane functionalized CNC [] dispersions at different weight ratios (1:1, 1:2, 2:1). Another sample was also prepared adding freeze-dried ZnO to pristine CNC aqueous dispersion in a weight ratio of 1:1 to understand the effect of ZnO incorporation into the composites. After sonication, the blends were freeze-dried for use in polymer composites.

Synthesis of B_2O_3 coated Silane Functionalized CNC

Boron oxide (B_2O_3) granules (0.100 g or 1.43 mmol) were ground to a coarse powder using an agate mortar and pestle. This powder was transferred to a 50 mL centrifuge tube and 5 mL (35 mmol) of oleic acid was added. The reaction mixture was then probe sonicated at 50 unit amplitude for 3 hours while placed in an ice bath. Following this, the colloidal product obtained was centrifuged at 9,000 rpm for 15 minutes and the supernatant oleic acid was discarded. The solid product was washed with 5 mL of anhydrous hexane and vacuum dried in an oven to produce a fluffy, white powder. This B_2O_3 powder was added to aqueous silane functionalized CNC dispersions [] at different weight ratios (1:1, 1:2, 2:1). Another sample was also prepared

by adding B_2O_3 powder to pristine CNC aqueous dispersion in a weight ratio of 1:1 to understand the effect of B_2O_3 incorporation into the composites. After sonication, the blends were freeze-dried for use in polymer composites.

Design and Manufacture of Polymer Composites using Inorganic Oxide Coated CNC as Filler Material

HDPE served as the matrix resin to manufacture composite samples. Four ZnO-CNC formulations synthesized in the previous step were used to manufacture HDPE masterbatches. Freeze dried ZnO-CNC was melt-blended with resin. Each master batch was further used to manufacture test planks representing 1:1, 1:2 and 2:1 ZnO-CNC ratios. The design of experiment included four types of ZnO-CNC complexes (silanated and non-silanated), pristine CNC incorporated and control (only HDPE) with 5 replications. Composite samples were prepared by melt compounding in a Thermo Fisher Scientific HAAKE Minilab II dual screw extruder. Samples were extruded at 100 rpm and 145 °C for 5 minutes. After mixing, composites were injection molded using a Thermo Fisher Scientific Minijet Pro injection molder. Samples were molded into either a DMA sample mold (Thermo Fisher Scientific, Waltham, MA USA, Part # 557-2295) with dimensions of 60 mm × 10 mm × 1 mm or a tensile test dog bone mold (Thermo Fisher Scientific, Waltham, MA USA) of the geometry described in ASTM D1708.

Table 3.1. Formulations of composite samples

Sample code	Resin (HDPE) (wt%)	CNC (Weight ratio)	ZnO (Weight ratio)
Neat HDPE	100	-	-
C1Z0	99	1	0
C1Z1	99	1	1
CS1Z1	99	1	1
CS1Z2	99	1	2
CS2Z1	99	2	1
C1B0	99	1	0
C1B1	99	1	1
CS1B1	99	1	1
CS1B2	99	1	2
CS2B1	99	2	1

Characterization

Fourier Transform Infrared (FTIR) Spectroscopy: The chemical structure and functional groups of the samples were analyzed using FTIR spectroscopy (Nicolet i550, Thermo Fisher Scientific, USA) in an attenuated total reflection (ATR) mode. The final spectrum of each sample was an average of 32 scans at a resolution of 4 cm^{-1}, in the wavenumber range of 400-4000 cm^{-1}.

Scanning Electron Microscopy (SEM): The composites were cryo-fractured in the liquid nitrogen atmosphere and the morphology of the cross-section of the composites was analyzed using SEM. Images of cross-section morphology were taken at different magnifications using field emission scanning electron microscope (Supra 55VP, Zeiss, Thornwood, NY, USA), operating at an accelerating voltage of 15.0 kV, in the Image and Chemical Analysis Laboratory (ICAL) at Montana State University. The samples were coated with a thin film of Iridium for 60 s for conductivity before capturing the images.

Thermogravimetric Analysis (TGA): Thermogravimetric analysis was carried out to analyze the thermal stability of the composites using a TA Instruments Thermogravimetric Analyzer (TGA Q5000, New Castle, USA) at Montana State University. The samples were tested in thermal degradation mode, under a flowing nitrogen atmosphere with a flow rate of 60 ml/min, from 30 ℃ to 600 ℃, at a heating rate of 10 ℃/min.

Differential Scanning Calorimetry (DSC): The crystallization ability of the composites was studied using DSC. The melt peak and fusion enthalpy of the samples were measured by using a TA Instruments DSC (Q2500, New Castle, USA) under a nitrogen atmosphere at Montana State University. The samples of about 4-5 mg were taken and scanned over a temperature range from 30 ℃ to 400 ℃ at a heating rate of 10 ℃/ min.

Dynamic Mechanical Analysis (DMA): The viscoelastic properties of the composites were analyzed by using a TA Instruments Dynamic mechanical analyzer (Q800), using a three-point bending fixture. The composites were heated from 30 ℃ to 110 ℃, with a frequency of 1 Hz, amplitude of 20 μm and a force track of 125%. Two replicates were tested for each formulation and the mean values were reported.

Tensile Testing: The tensile properties of the composites were measured using an MTS C43 load frame with 5 mm/min speed and a 35 mm gauge length from clamp to clamp. Five replicates were tested for each formulation and the mean values were reported.

Horizontal Burning Test: Horizontal burning test was carried out to get a preliminary idea of the flammability behavior of the composites. The test was conducted on a rectangular bar specimen with dimensions of 60 mm x 10 mm x 1mm according to the ASTM D635-14 standard. The samples were fixed to the mount and their longitudinal axis was kept in the horizontal way

during the test. A butane lighter was used, and the flame was applied to the free end of the sample at a 45° angle. For each formulation, two replicates were tested, and the mean values were reported.

Microcalorimetry Test: The heat release properties of the composites were evaluated using microcalorimetry test. The static and dynamic combustion parameters of the composites were measured using a Microscale Combustion Calorimeter (MCC-2) by Deatak (University of Texas, Austin), following ASTM D7309 standard. Samples weighing 2-3 grams were combusted by rapid-controlled pyrolysis under an atmosphere of 80%-20% nitrogen to oxygen gas ratio. The combustor temperature was set to 900 °C with a heating rate of 1 °C/min. For each formulation, three replicates were tested, and the mean values were reported.

Results and Discussion

Spectroscopy Analysis of the Composites

The FT-IR spectra of Neat HDPE and all the composites containing ZnO and/or B_2O_3 are shown in Fig. 3.1. The neat HDPE spectra showed characteristic asymmetric and symmetric stretching band of -C-H respectively, at 2917 cm^{-1} and 2852 cm^{-1}. The bending vibration mode of CH_3 and CH_2 rocking vibration mode were also observed at 1472 cm^{-1} and 720 cm^{-1}, respectively [126]. In case of CNC incorporated composites, the -C-H stretching band of cellulose overlapped with the -C-H stretching of PE and increased the intensity. The bending vibration of -O-H groups of CNC also overlapped with the bending band of CH_3 [98], showing successful incorporation of CNC in the system. The lower intensities of some composite formulations (CS1B2 and CS1Z2) can be the result of agglomeration CNC/inorganic oxide complex [127], similar to the other studies.

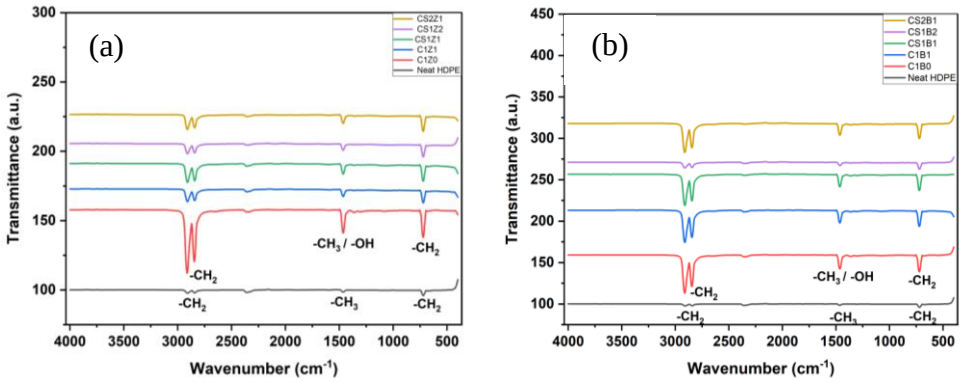

Fig 3.1: Transmission spectra of (a) ZnO coated CNC composites and (b) B_2O_3 coated CNC composites

Morphological Study of the Composites

Fig. 3.2 shows the SEM micrographs of the cryo-fractured cross-sections of the ZnO and B_2O_3 treated composites. The micrographs showed some aggregates which may be the result of CNC/inorganic nano oxide agglomeration. The presence of ZnO and B_2O_3 was confirmed by energy dispersive X-ray (EDX) analysis and the images showed an irregular distribution of inorganic oxide nanoparticles.

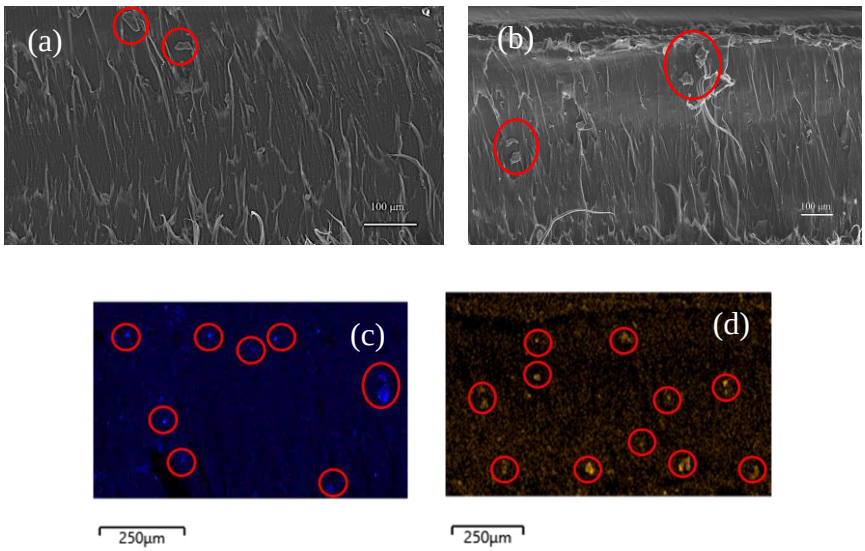

Fig. 3.2: SEM images of HDPE composites cross-sections: (a) CNC-ZnO, (b) CNC- B_2O_3 (agglomerations shown in red circles) (c) elemental mapping of Zn, and (d) elemental mapping of B (shown in red circles)

Thermogravimetric Property Analysis of the Composites

The effect of ZnO and B_2O_3 incorporation on the thermal properties of the HDPE composites were investigated using thermogravimetric measurement and represented in Table 3.2 and Table 3.3. The TGA curves demonstrated a single step degradation for all formulations. The thermal stability of the samples was analyzed by comparing the T_{onset}, T_{50}, T_{endset} values. T_{onset} represents the initial degradation temperature at which the composites start degrading, T_{50} is the temperature at 50% weight loss and T_{endset} is the temperature at the end of degradation. The C1Z0 composite, which only had pristine CNCs as filler material, showed no change in T_{onset} because of the catalytic nature of the surface sulfate groups present in CNC. The C1Z1 formulation exhibited a significantly higher thermal stability (T_{onset}= 431.85 °C) than neat HDPE sample (T_{onset}= 404.05 °C). This can be attributed to the shielding effect of nano ZnO which prevented pyrolysis and thermal decomposition of cellulose molecules [126].

Table 3.2: Thermal properties of each formulation (CNC/ZnO) from TGA

Sample name	T_{onset} (℃)	T_{50} (℃)	T_{endset} (℃)
Neat HDPE	404.05	460.24	481.70
C1Z0	405.23	462.82	481.80
C1Z1	431.85	466.80	483.06
CS1Z1	416.37	463.01	482.15
CS1Z2	396.29	460.75	482.58
CS2Z1	406.74	459.19	480.11

The CS1Z1 formulation, which has silanized CNCs as reinforcement, showed a decrease in the thermal stability. The possible reason is the plasticizing effect of the silane molecules.

Table 3.3: Thermal properties of each formulation (CNC/ B_2O_3) from TGA

Sample name	T_{onset} (℃)	T_{50} (℃)	T_{endset} (℃)
Neat HDPE	404.05	460.24	481.70
C1B0	405.23	462.82	481.80
C1B1	412.73	444.77	464.55
CS1B1	412.52	449.76	468.59
CS1B2	397.41	446.11	468.05
CS2B1	404.63	450.83	472.34

Higher concentration of ZnO provoked an intensive degradation of polymer chains which intensified at higher temperatures. Overall, the C1Z1 formulation exhibited higher thermal stability compared to the other formulations, suggesting a synergistic action and formation of a relatively strong network between the composite components resulting the shielding effect of CNC/ZnO complex. A similar trend was observed in the case of B_2O_3 coated CNC composites, though the thermal stability was not as high as ZnO coated composites. The reason can be the presence of oleic acid in B_2O_3 structure to prevent moisture adsorption. The oleic acid acted as a lubricate which facilitated the polymer chain slippage, increased the free volume between the chains and decreased the thermal stability of the system [128, 129].

Crystallization Behavior Analysis of the Composites

The non-isothermal crystallization behavior of the HDPE composites was studied using DSC. The DSC results were shown in Fig. 3.3, Table 3.4 and Table 3.5. The crystallinity (X_c) was determined by the following equation:

$$X_c\ (\%) = \Delta H_m \times 100/\ \Delta H_m^0 \times (1\text{-}x) \qquad (1)$$

where ΔH_m is the melting enthalpy, ΔH_m^0 is the theoretical enthalpy of 100% crystalline HDPE (293 J g^{-1}), and x is the weight fraction of filler (CNC-ZnO or B_2O_3).

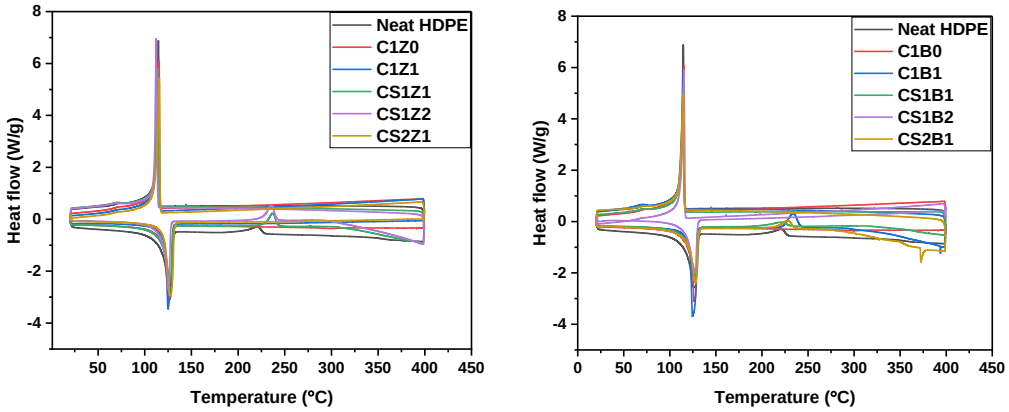

(a) (b)

Fig. 3.3: DSC thermograms of (a) ZnO coated CNC composites and (b) B_2O_3 coated CNC composites

Incorporation of CNC in HDPE matrix did not show any significant change in crystallinity (%), but the C1Z1 composites exhibited a slight increase in crystallinity (%) (X_c= 47.02%), compared to neat HDPE. The CS1Z1 formulations showed a slight decrease in crystallinity (%) (X_c= 41.39%), compared to neat HDPE. A possible reason for this phenomenon is the plasticizing effect of silane molecules due to which degradation of the polymer occurred during high shear and

high temperature extrusion [130]. Any plasticizer increases the softness and flexibility of the polymer, by facilitating easy flow of polymer chains. Due to this reason, the apparent viscosity of the material decreases which degrades the thermos-mechanical properties of the composites [128], which is shown in the DMA analysis.

Table 3.4: Crystallization behavior of each formulation (CNC/ZnO) from DSC

Sample name	T_c (℃)	T_m (℃)	Crystallinity (%) (X_c)
Neat HDPE	114.54	127.53	44.12
C1Z0	115.38	126.31	38.19
C1Z1	115.29	125.03	47.02
CS1Z1	113.99	127.05	41.39
CS1Z2	112.43	125.42	37.71
CS2Z1	115.68	126.76	45.76

Increased loading of nano ZnO further decreased the crystallinity (%) because of shortening of polymer chains due to intense scissoring effect of ZnO. Similar conditions were reported in different literature [129, 130, 131].

Table 3.5: Crystallization behavior of each formulation (CNC/ B_2O_3) from DSC

Sample name	T_c (℃)	T_m (℃)	Crystallinity (%) (X_c)
Neat HDPE	114.54	127.53	44.12
C1B0	115.38	126.31	38.19
C1B1	114.52	124.59	47.51
CS1B1	114.88	128.23	36.85
CS1B2	115.42	127.40	35.38
CS2B1	114.54	127.86	36.53

A similar trend was observed in the case of B_2O_3 coated CNC composites. For both inorganic oxides, the possible change in the aspect ratio of CNC/inorganic oxide complex and aggregate formation during freeze-drying also hindered the stable crystal formation [130]. In the

case of B_2O_3 coated CNC composites, the effect is more prominent as seen from the TGA, DSC and DMA analysis. The oleic acid present in B_2O_3 structure also acted as a lubricant which further decreased the probability of stable crystal formation [128].

Dynamic Mechanical Property Analysis of the Composites

Dynamic viscoelastic properties storage modulus (E'), loss modulus (E") and loss factor (damping parameter, tan δ) were studied through dynamic mechanical analysis. The results are shown in Fig. 3.4 and table 3.6 and 3.7. For pure HDPE, a sharp α-transition peak was observed at around 95.7 ℃ in the storage modulus curve. For a semi-crystalline polymer like HDPE, the primary relaxation process or α-relaxation is associated with long range motion of chain segments [132].

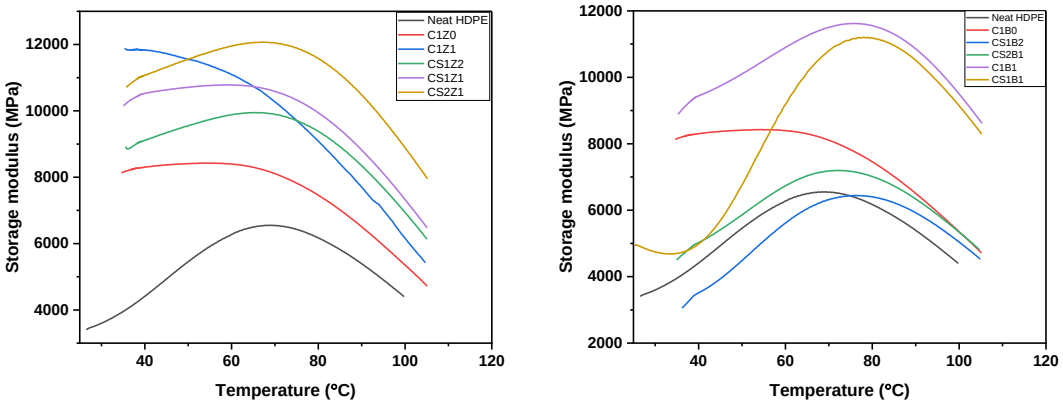

(a) (b)

Fig. 3.4: Representative curves of storage modulus as a function of temperature of (a) ZnO coated CNC composites and (b) B_2O_3 coated CNC composites

The dynamic mechanical properties of the composites are largely dependent on the filler content. Incorporation of CNC increased the storage modulus value (9451.5 MPa) significantly (table 3.6 and Fig. 3.5), compared to neat HDPE. The reason behind this phenomenon is that the incorporation of CNC makes the polymer chains less mobile, increases the flow resistance of HDPE and reduces the slippage between crystallites [130].

Table 3.6: Dynamic mechanical properties and mean comparison (Fisher LSD) of each formulation (CNC/ZnO) (p= 0.05)

Sample code	Mean	Groups	Groups	Groups
CS2Z1	11898	A		
C1Z1	11626	A		
CS1Z2	11205	A	B	
CS1Z1	10600.5	A	B	
C1Z0	9451.5		B	
HDPE	6462			C

Incorporation of nano ZnO further significantly increased the value of storage modulus (11626 MPa), corroborating the observations from TGA and DSC analysis. Incorporation of silanized CNCs (CS1Z1) did not show any significant change in the storage modulus values, indicating the lubricating effect of silane [133], as explained in DSC analysis.

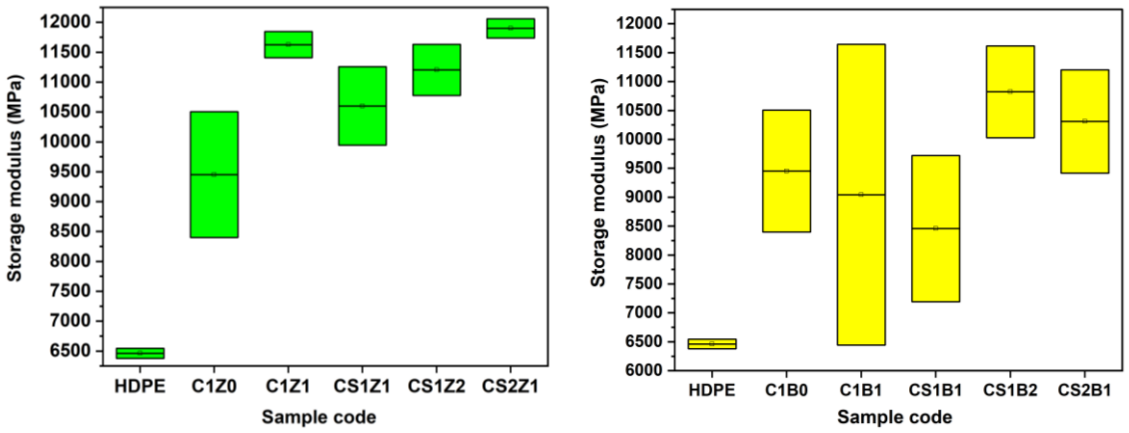

(a) (b)

Fig. 3.5: Representative box plots of statistical analysis of (a) ZnO coated CNC composites and (b) B_2O_3 coated CNC composites

Increased loading of CNC also exhibited a significant increase in the storage modulus value (11898 MPa) compared to formulation with higher amount of ZnO (CS1Z2). ZnO served as an accelerator which enhanced the degradation of HDPE at higher concentrations. Furthermore, the higher concentration of ZnO provokes CNC's ability to absorb ZnO, which in turn increased the possibility of forming large and unstable agglomerates in the polymer matrix [134].

Table 3.7: Dynamic mechanical properties and mean comparison (Fisher LSD) of each formulation (CNC/ B_2O_3) (p= 0.05)

Sample code	Mean	Groups
CS1B2	10822.5	A
CS2B1	10310.5	A
C1B0	9451.5	A
C1B1	9043.5	A
CS1B1	8457	A
HDPE	6462	A

There is no significant mechanical property improvement observed in the case of B_2O_3 coated CNC composites. Overall, there is an 84% increase in storage modulus of ZnO coated composites compared to Neat HDPE.

Tensile Property Analysis of the Composites

The mechanical property analysis such as Young's modulus, elongation at break were investigated to gain an insight into the tensile behavior of the composites, the effect of ZnO and B_2O_3 on the tensile properties and comparison of the tensile properties with neat HDPE. Typically, the addition of CNCs to a polymer matrix would lead to an increase in yield strength and young's modulus value and a decrease in elongation [135].

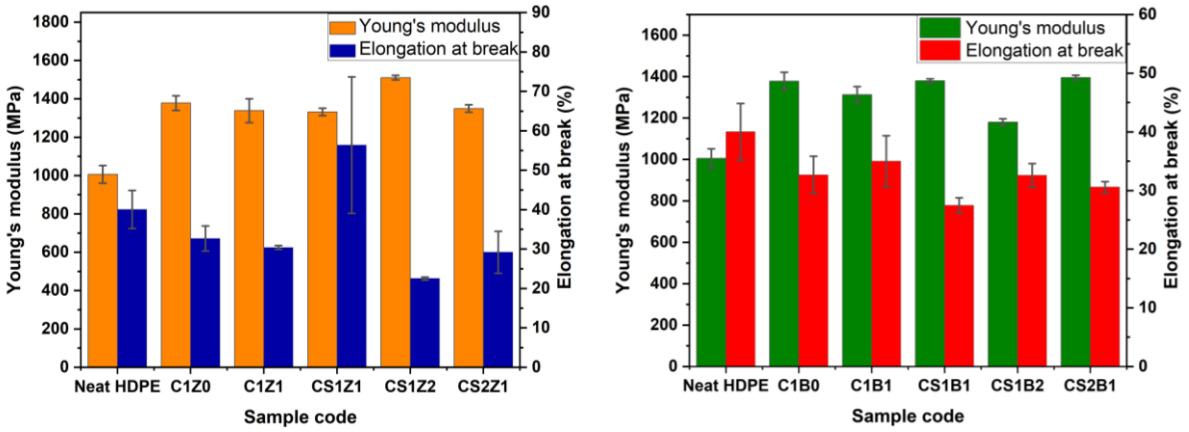

(a) (b)

Fig. 3.6: Bar graphs comparison of tensile properties of (a) ZnO coated CNC composites and (b) B_2O_3 coated CNC composites

Incorporation of ZnO and CNC led to a significant improvement in the elastic modulus of the composites compared to neat HDPE, because of the reinforcement effect of the fillers [136], similar to the other studies. Incorporation of silanized CNC and ZnO in the composites

significantly increased the elastic modulus in comparison with neat HDPE, indicating better interfacial bonding with the HDPE matrix [137]. But there is no significant change in the modulus value was observed in case of silanated CNC incorporated composites when compared to the non-silanated composites (C1Z0 and C1Z1). This phenomenon can be attributed to the plasticizing effect of silane molecules, which increased the flowability of the polymer chains and decreased the viscosity of the polymer melt [130], which resulted in a lower modulus value. On the other hand, the addition of more ZnO further improved mechanical properties. The addition of more ZnO to the system enhanced the reinforcement effect of the fillers which hindered the chain mobility and favored the formation of stable crystals [131].

Table 3.8: Young's modulus and mean comparison (Fisher LSD) of each formulation (CNC/ZnO) (p= 0.05)

Sample code	Mean	Groups	Groups	Groups
CS1Z2	1510.6	A		
C1Z0	1356.816		B	
CS2Z1	1349.574		B	
C1Z1	1338.384		B	
CS1Z1	1331.879		B	
HDPE	1130.032			C

According to the statistical analysis shown in table 8, the silane functionalized formulations showed no significant change in elongation compared to neat HDPE. But C1Z1 formulation showed a significant increase in elongation compared to other formulations. The elongation at break mainly depends on the facilitation of stress transfer from molecular level to the bulk. In case of C1Z1, though there is no significant change observed in modulus value, in case of elongation the filler/polymer interaction is more important. The most probable explanation for this condition is that there can be a change in the aspect ratio of the fillers (CNC/ZnO complex) during the freeze-

drying [138], which hindered better interaction between the polymer matrix and the filler and showed a more ductile behavior by increasing the elongation at break (%).

Table 3.9: Elongation at break (%) and mean comparison (Fisher LSD) of each formulation (CNC/ZnO) (p= 0.05)

Sample code	Mean	Groups	Groups
C1Z1	56.375	A	
C1Z0	34.775	A	B
HDPE	32.875	A	B
CS1Z1	30.375		B
CS1Z2	29.175		B
CS2Z1	22.525		B

Overall, incorporation of ZnO in the system showed almost 50% increase in elastic modulus and decrease in elongation around 37% compared to neat HDPE.

In the case of B_2O_3 coated CNC composites, incorporation of B_2O_3 in the system led to a significant decrease in elastic modulus of the composites whereas incorporation of CNC improved the mechanical properties. During the production of B_2O_3, oleic acid was used as a reaction medium and was capped on the surface of B_2O_3 to avoid moisture adsorption. But due to the large and bulky structure of the oleic acid, it has an adverse effect on the tensile properties of the composites. Oleic acid is a fatty acid and behaves as a lubricant which can increase the free volume between the polymers chains to increase the chain mobility and slippage between the chains [129]. Due to this reason, the B_2O_3 coated CNC composites showed a more ductile behavior and showed no significant improvement in mechanical properties.

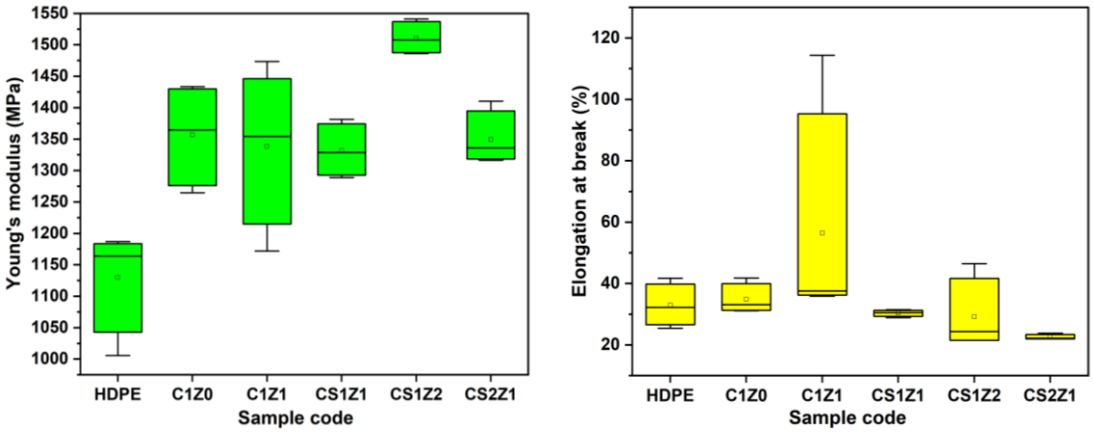

(a) (b)

Fig. 3.7: Representative box plots of statistical analysis of (a) elastic modulus and (b) elongation at break (%) of ZnO coated CNC composites

Table 3.10: Young's modulus and mean comparison (Fisher LSD) of each formulation (CNC/ B_2O_3) (p= 0.05)

Sample code	Mean	Groups	Groups	Groups
CS2B1	1395.351	A		
CS1B1	1380.012	A	B	
C1B0	1378.072	A	B	
C1B1	1313.289		B	
CS1B2	1180.64			C
HDPE	1135.681			C

Table 3.11: Elongation at break (%) and mean comparison (Fisher LSD) of each formulation (CNC/ B_2O_3) (p= 0.05)

Sample code	Mean	Groups
C1B1	35	A
HDPE	32.84	A
C1B0	32.68	A
CS1B2	32.6	A
CS2B1	30.58	A
CS1B1	27.48	A

Overall, incorporation of B_2O_3 in the system showed around 38% increase in elastic modulus which is lower than the ZnO containing composites.

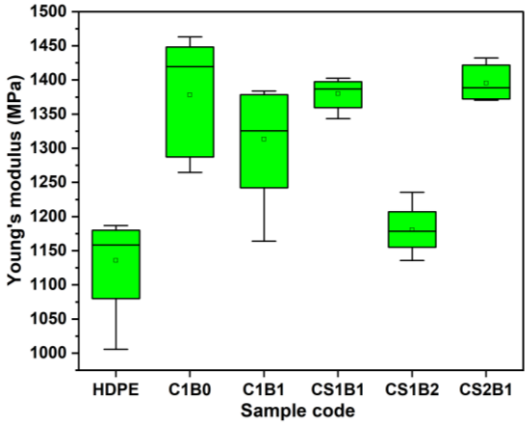

Fig. 3.8: Representative box plots of statistical analysis of B_2O_3 coated CNC composites

Horizontal Burning test Results Analysis

The horizontal burning test was conducted to evaluate the flame spread rate, type of burning, and weight loss (%), to gain a primary idea of the fire-retardant behavior of the composites. The results and the statistical analysis are shown in Fig. 3.9 and table 3.12, 3.13, 3.14 and 3.15.

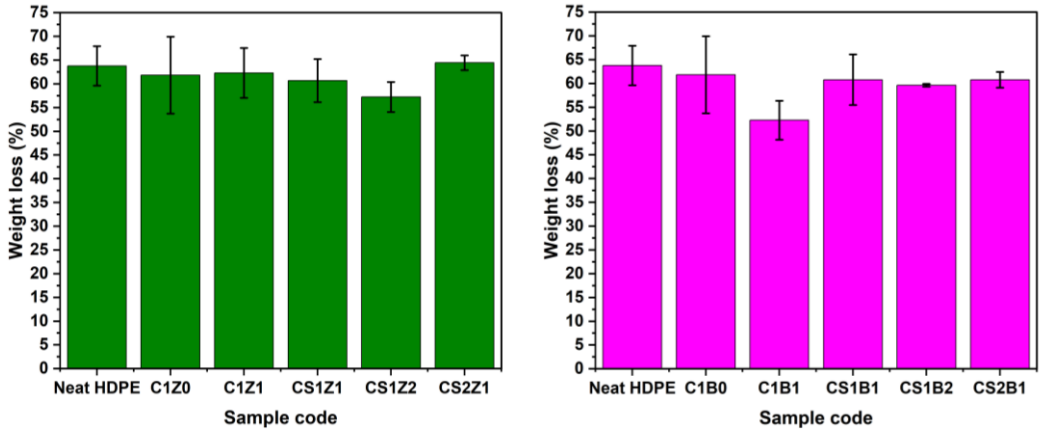

(a) (b)

Fig. 3.9: Weight loss (%) graphs of (a) ZnO coated CNC composites and (b) B_2O_3 coated CNC composites

The addition of ZnO did not significantly impact the flame spread rate of the composites, but the weight loss (%) was reduced compared to neat HDPE.

Table 3.12: Mean comparison (Fisher LSD) of flame spread rate (mm/s) of (CNC/ZnO) composites (p= 0.05)

Sample code	Mean	Groups
C1Z1	1.255	A
HDPE	1.08	A
C1Z0	1.055	A
CS1Z2	1	A
CS1Z1	0.975	A
CS2Z1	0.895	A

Table 3.13: Mean comparison (Fisher LSD) of flame spread rate (mm/s) of (CNC/B_2O_3) composites (p= 0.05)

Sample code	Mean	Groups
CS1B2	1.09	A
HDPE	1.08	A
C1B0	1.055	A
C1B1	1.05	A
CS2B1	1.01	A
CS1B1	0.975	A

The shielding effect of the CNC/ZnO complex on the outer surface of polymer composites reduced oxygen penetration which in turn diminished weight loss. Increased piloted time to ignition is the result of reduced pyrolysis rates of polymer composites [139, 140].

Table 3.14: Mean comparison (Fisher LSD) of weight loss (%) of (CNC/ZnO) composites (p= 0.05)

Sample code	Mean	Groups	
Neat HDPE	80.76674	A	
CS1Z1	65.36049		B
CS2Z1	64.43779		B
C1Z1	62.29243		B
CS1Z2	57.21525		B
C1Z0	53.72583		B

Table 3.15: Mean comparison (Fisher LSD) of weight loss (%) of (CNC/B_2O_3) composites (p= 0.05)

Sample code	Mean	Groups	
Neat HDPE	80.76674	A	
CS1B1	60.7663		B
CS2B1	60.75362		B
CS1B2	59.6047		B
C1B0	53.72583		B
C1B1	52.25841		B

Similarly, incorporation of B_2O_3 in the system did not improve flammability but it helped to lower mass loss. This phenomenon can be attributed to the formation of glassy surface barrier inherent to boron-based compounds, which effectively inhibited weight loss [142]. Overall, there is a 10% reduction in weight loss for ZnO coated composites and 18% reduction for B_2O_3 coated composites compared to neat HDPE.

Microcalorimetry test Results Analysis

The microcalorimetry test was conducted to evaluate the heat release capacity (J/gK), peak heat release rate (W/g) and total heat release (kJ/g) of the composite samples. It was observed in the horizontal burning test that the inorganic oxide coated formulations did not show any significant differences in properties between themselves. So, for the microcalorimetry test the best performing formulation from each type of inorganic oxide was chosen to compare the fire-retardant property of inorganic oxides. The heat release rate (HRR) is one of the most important properties to control fire hazards, as it is the driving force for fire spread. The mass loss rate of a material multiplied by material's heat of combustion is defined as the heat release rate [143]. The results of these tests are shown in Fig. 3.10 and table 3.18.

Table 3.16: Mean comparison (Fisher LSD) of HR capacity (J/gK) of HDPE composites (p= 0.05)

Sample code	Mean	Groups	Groups
HDPE	414.6667	A	
C1B1	405	A	
CS1Z2	355		B

Table 3.17: Mean comparison (Fisher LSD) of peak HRR (W/g) of HDPE composites (p= 0.05)

Sample code	Mean	Groups	Groups
HDPE	413.0333	A	
C1B1	403.1333	A	
CS1Z2	353.1333		B

The nature of the reaction of the polymers and organic fillers is endothermic. The combustion of the flammable volatiles resulted from the decomposition of the resin matrix and the fillers/fire retardants control the amount of heat released from a polymer composite [143].

Table 3.16 & 3.17, and Fig. 3.10 show the statistical analysis of HR capacity, peak HRR, average heat release rate and statistical comparison of peak heat release (PHRR) of neat HDPE, C1B1 and CS1Z2 formulations.

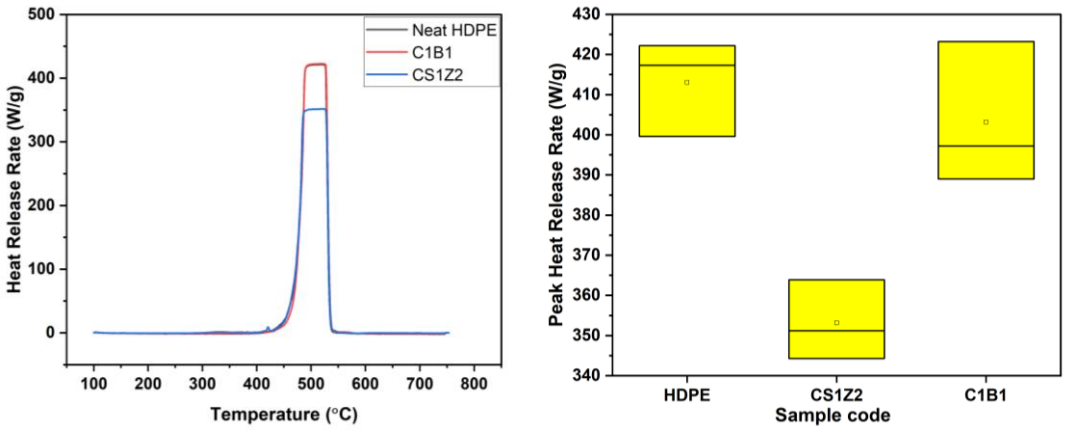

(a) (b)

Fig. 3.10: (a) Heat release rate graph of neat HDPE, C1B1 and CS1Z2 formulations and (b) statistical comparison of peak heat release rate of the three formulations (significance level=0.05)

The initial delay period (till 400 °C) before heat release was present because the temperature of the composite was still below the pyrolysis temperature of the matrix, HDPE. In TGA, it was observed that the decomposition of the system started around 400 °C. There was a rapid increase in HRR following the previous induction period where the combustion of the volatiles began at the interface of the composite/fire. Around 500 °C, the PHRR was achieved and after a short stabilization period the heat release decreased drastically. The shielding effect of the char produced on the exposed polymer surface reduced the penetration of the combustible

volatiles, the low-molecular weight hydrocarbons, and the decomposition rate of the underlying material declined. The decreasing resin content of the composites also decreased the PHRR [144].

Table 3.18: Microcalorimetry test results of neat HDPE and the composite

Sample code	HR capacity (J/gK)	PHRR (W/g)	Total HR (kJ/g)
Neat HDPE	414.67±12.09	413.03±11.88	22.73±0.23
CS1Z2	355±10.14	353.13±9.94	20.33±0.45
C1B1	405±17.77	403.13±17.85	22.2±0.65

The ZnO coated CNC composites showed significantly lower HRR and PHRR compared to the neat HDPE and B_2O_3 coated composites, shown in fig. Nano ZnO contained more -OH groups than bulk ZnO on its surface due to the smaller size (30-150 nm) and higher surface area [145]. Therefore, the ZnO coated composites showed better thermal stability at low add-on%, compared to the neat HDPE. Theoretically, nano B_2O_3 coated composites should also show better thermal stability than HDPE forming a glassy barrier on the exposed composite surface. But the B_2O_3 coated composites did not show any improvement in HRR. During the production of B_2O_3, the surface of the nanoparticles was covered with oleic acid to increase the hydrophobicity of the inorganic oxides. But the lower flash point (189.9 °C) and lubricating effect of oleic acid, decreased the thermal stability of the composite system [146], which in turn could not improve the heat release properties. Overall, there is a 14% reduction in PHRR for ZnO coated composites compared the neat HDPE and B_2O_3 coated composites.

Conclusion

HDPE, a widely used commercial polymer, demonstrates poor thermo-mechanical behavior. This study investigated the role of nano sized ZnO or B_2O_3 coated CNC as functional

additives for improving the fire resistance properties. HDPE composite formulations containing nano ZnO or B_2O_3 and silanated CNC were manufactured using melt blending extrusion process. In this study, the ZnO coated composites showed better mechanical properties compared to the B_2O_3 coated composites. The thermal stability and fire-retardant properties of the ZnO coated composites showed better performance than the B_2O_3 coated composites. Nano ZnO facilitated fire-retardancy by reducing the heat release rate, because of its smaller size and higher surface area, even at a low add-on%. Overall, the ZnO coated composites showed an 84% increase in storage modulus. 50% increase in elastic modulus and 14% reduction in heat release rate compared to neat HDPE. The B_2O_3 coated composites showed no significant improvement in thermal stability or heat release rate due to the lubricating effect of oleic acid. The scanning electron micrographs showed some agglomerations and irregular distribution of the inorganic oxides in the cryo-fractured cross-section of the composites. Therefore, the overall physical, mechanical and thermal properties of the polymer composites can be further improved by improving the dispersion of CNC and inorganic oxides in the matrix.

CHAPTER FIVE

NANO BORON OXIDE AND NANO ZINC OXIDE INCORPORATION TO LIGNIN CONTAINING CELLULOSE NANOCRYSTALS TO IMPROVE THE THERMAL, MECHANICAL AND FLAMMABILITY PROPERTIES OF HIGH-DENSITY POLY (ETHYLENE) POLYMER

Contribution of Authors and Co-Authors

Manuscript in Chapter 5

Author: Saptaparni Chanda

Contributions: Conceptualization, Methodology, Formal analysis, Writing – Original draft

Co-Author: Dilpreet S. Bajwa

Contributions: Supervision, Resources, Writing – Review, Editing

Co-Author: Nicole Stark

Contributions: Resources

Manuscript Information

Saptaparni Chanda, Dilpreet S Bajwa, Nicole Stark, Sreekala G Bajwa

Nanocomposites

Status of Manuscript:
__X__ Prepared for submission to a peer-reviewed journal
____ Officially submitted to a peer-reviewed journal
____ Accepted by a peer-reviewed journal
____ Published in a peer-reviewed journal

Abstract

Functional polymer composites have captured the attention of researchers and industrial sectors. To produce functional composites, bio-based sustainable nanofillers like cellulose nanocrystal (CNC) and its derivatives are being exploited. The central challenge of using hydrophilic CNC as nanofiller for polymer composites is their tendency of self-agglomeration in the hydrophobic matrix. Therefore, lignin containing CNC (LCNC) can be used as nanofiller instead of pristine CNC to improve the interfacial interaction between the filler and matrix. Nanoscale fire retardant (FR) additives are added to improve the thermal properties of petroleum-based composites. Nano metal oxides reduce the flammability of polymers by modifying their degradation pathway. Zinc and boron-based compounds are well known for their superior flame retardancy, low toxicity and eco-friendly nature. In this research, safe, effective and eco-friendly hybrid systems of nano ZnO/LCNC and nano B_2O_3/LCNC were prepared and incorporated in high density polyethylene (HDPE) matrix to improve their physico-mechanical and FR properties. Nano ZnO nanoparticles were prepared using zinc acetate and sodium hydroxide in aqueous dispersion and were coated onto LCNC particles in different concentrations. Nano B_2O_3 was produced by ultrasonication of B_2O_3 powder and was coated onto LCNC particles in different concentrations. These hybrid systems were incorporated in HDPE matrix separately to produce composites via melt blending extrusion process. The composite properties were evaluated using Fourier Transform Infrared Spectroscopy (FT-IR), Scanning Electron Microscopy (SEM), Energy Dispersive X-ray analysis (EDX), Thermo-Gravimetric Analysis (TGA), Differential Scanning Calorimetry (DSC), Dynamic Mechanical Analysis (DMA), tensile testing, horizontal burning test and microcalorimetry test. In this study, the inherently lower thermal stability of lignin adversely

affected the thermal properties of the composites. The TGA, horizontal burning test and microcalorimetry test showed the declination of thermal stability and fire-retardant properties of all the composite systems. Though the ZnO coated composites did not show any significant improvement in the fire-retardant properties of the composites, it prevented further declination of thermal stability of the composites compared to neat HDPE. The B_2O_3 coated composites showed a decline in fire properties. The mechanical properties of the composites were improved because of the reinforcement effect of LCNC and inorganic oxides. There is a 30% increase in elastic modulus observed in case of ZnO coated composites, while the B_2O_3 coated composites showed a 27% increase in elastic modulus compared to neat HDPE.The SEM micrographs and EDX images demonstrated some agglomeration and irregular distribution of the inorganic oxides in the polymer matrix. Therefore, the overall physical and thermal properties of the LCNC containing composites did not show any significant improvement compared to neat HDPE. The presence of the bulky lignin structure hindered the interaction between the LCNC and inorganic oxides and declined the overall properties of the composites.

Keywords: Lignin containing cellulose nanocrystals, High density poly(ethylene), Zinc oxide, Boron oxide, Hybrid system, Mechanical property, Thermal property, Dispersion

Introduction

Renewable biobased fillers, polymers and composites derived from natural resources are generating great interest due to depleting fossil fuel resources and the negative environmental impact of fossil fuel-based plastic products [120]. Functional polymer composite materials are one of the flagship products for the researchers and for the industrial sector also. Incorporation of physical cross-link points in the polymer matrix by addition of fillers or nanofillers has shown

promises to improve the viscoelastic and mechanical properties [135]. However, the effectiveness of fillers and nanofillers strongly depends on the quality of the dispersion and distribution in the polymer matrix. Many types of biobased fillers have also been studied regarding modifying the properties of polymers [111]. Among biobased fillers, cellulose nanocrystals (CNCs) are attractive materials to improve the performance of polymers without compromising their sustainability, and inherent properties. CNCs can be obtained by acid hydrolysis of cellulose fibers [112], which is one of the most abundant natural biopolymers on Earth and has been recognized as an excellent reinforcing agent due to its excellent strength, biodegradability, high aspect ratio, and low density [113]. Several studies [114] have shown that both processing and physical properties of a polymer matrix can be modified by incorporation of CNCs. However, CNCs tend to form agglomerates upon incorporation in a polymer matrix due to its hydrophilic nature and potential to form strong intermolecular hydrogen bonds. These properties have prevented the realization of the full potential of CNCs as a reinforcing phase. The presence of CNC aggregates in a composite act as stress concentration points which are detrimental to mechanical properties [115]. Different approaches have been developed to improve the dispersion and interfacial adhesion of CNCs within the polymer matrix including solution mixing, reactive compatibilization, ring opening polymerization, and surface modification of CNCs [37]. Although surface modifications of CNCs can improve compatibility and dispersion with hydrophobic polymers, such harsh chemical treatment often leads to loss in its intrinsic properties and also adds to the overall cost of the material. An alternative approach to improve the dispersion of CNCs in a polymer matrix is through addition of a compatibilizing material such as a surfactant, starch, lignin, etc. Lignin is particularly interesting because it is naturally present in biomass. Lignin is a complex, three-

dimensional aromatic polymer that contributes to the various properties of plant cell walls, including mechanical resistance, hydrophobicity, and dimensional stability [147]. Moreover, lignin can absorb UV light and therefore, transparent coatings with controlled UV-absorbent properties have been developed [148].

There are several studies [149, 150, 151] which reported improved interaction between CNC and hydrophobic polymers in presence of lignin. The use of lignin-coated CNCs (L-CNC), to modify the rheological and thermo-mechanical properties of poly (lactic acid) (PLA) composites was reported Gupta et. al. The lignin coating on CNCs not only improved the dispersion of CNCs but also enhanced their interfacial interaction with the PLA matrix, resulting in a significant improvement in rheological and thermo-mechanical properties. The improvement in mechanical properties can be attributed to a significant increase in the degree of crystallinity of the PLA. Excellent dispersion and compatibility of L-CNCs with PLA allowed generation of a high density of nucleating sites resulting in an increase in the degree of crystallinity of the PLA matrix. Improvement in the storage modulus at higher loading of L-CNCs can be attributed to both high crystallinity and reinforcement by L-CNCs [149]. In another article of Wei et. al, LCNCs were compounded with PLA via melt processing. High Young's modulus and elongation at break values were obtained by addition of 2% LCNCs to PLA. Better interfacial bonding of more hydrophobic LCNCs and hydrophobic PLA matrix was achieved [150]. L-CNC was incorporated by Feng et. al into methacrylate (MA) resin. Mechanical properties increased with the addition of 0.1% and 0.5% L-CNC, and thermal stability was improved at 0.5% L-CNC. Dynamic mechanical analysis demonstrated that incorporation of L-CNC increased the storage modulus in the rubbery plateau [151].

In the current research, LCNCs were coated with ZnO and B_2O_3 as fire-retardant additives and dispersed in the high-density poly (ethylene) (HDPE) matrix using melt blending extrusion process. The thermo-mechanical and fire-retardant properties of the manufactured composites were studied. Overall, the main aim of the research is to improve the dispersion of CNC in the hydrophobic polymer matrix in the presence of lignin and enhancement of the thermal, physical and mechanical properties of the composites.

Experimental Section

Materials

High density poly (ethylene) (HDPE) powder with a melt index of 3.5 g/10 min, and a melting temperature of 126 ℃, purchased from Nova Chemicals was used as polymer matrix. The LCNC containing 2 wt% of lignin with dimensions of 10-15 nm width and 80-100 nm length and hence aspect ratios of 5-10 were provided by USDA Forest Products Laboratory (Madison, WI, USA). Zinc acetate dehydrate and sodium hydroxide were purchased from Sigma Aldrich for producing Zinc oxide (ZnO). Boron oxide powder and oleic acid were also purchased from Sigma Aldrich to produce nano boron oxide. Methanol was purchased from the chemistry store of MSU and used as a solvent for nano ZnO production. Deionized (DI) water purchased from Millipore, USA was used as solvent.

Synthesis of ZnO Coated LCNC

Zinc acetate dehydrate (0.02 mol) was dissolved in 50 mL of methanol and heated at 50 ^{o}C under vigorous stirring for 0.5 h to make a precursor solution A. Then, 0.04 mol of sodium hydroxide was dissolved in 50 mL of methanol and heated at 50 ^{o}C along while vigorously stirred

for 1 h, to make precursor B. To make ZnO nano-sol, solution B was added into solution A, drop-wise under constant stirring for 0.5 h at 50 ^{o}C. The mixture was stirred for another 2 h and cooled at room temperature to obtain transparent ZnO sol. This ZnO sol was freeze-dried and added to aqueous LCNC dispersions at different weight ratios (1:1, 1:2, 2:1). After sonication, the blends were freeze-dried for use in polymer composites.

Synthesis of B_2O_3 Coated LCNC

Boron oxide (B_2O_3) granules (0.100 g or 1.43 mmol) were grounded to a coarse powder using an agate mortar and pestle. This powder was transferred to a 50 mL centrifuge tube and 5 mL (35 mmol) of oleic acid was added. The reaction mixture was then probe sonicated at 50 unit amplitude for 3 hours while placed in an ice bath. Following this, the colloidal product obtained was centrifuged at 9,000 rpm for 15 minutes and the supernatant oleic acid was discarded. The solid product was washed with 5 mL of anhydrous hexane and vacuum dried in an oven to produce a fluffy, white powder. This B_2O_3 powder was added to aqueous LCNC dispersions at different weight ratios (1:1, 1:2, 2:1). After sonication, the blends were freeze-dried for use in polymer composites.

Design and Manufacture of Polymer Composites using Inorganic Oxide Coated LCNC as Filler Material

HDPE served as the matrix resin to manufacture composite samples. Three ZnO-LCNC formulations synthesized in the previous step were used to manufacture HDPE masterbatches. Freeze dried ZnO-LCNC was melt-blended with resin. Each master batch was further used to manufacture test planks representing 1:1, 1:2 and 2:1 ZnO-LCNC ratios. The design of experiment included three types of ZnO-LCNC complexes, pristine LCNC incorporated and control (only

HDPE) with 5 replications. Composite samples were prepared by melt compounding in a Thermo Fisher Scientific HAAKE Minilab II dual screw extruder. Samples were extruded at 100 rpm and 145 °C for 5 minutes. After mixing, composites were injection molded using a Thermo Fisher Scientific Minijet Pro injection molder. Samples were molded into either a DMA sample mold (Thermo Fisher Scientific, Waltham, MA USA, Part # 557-2295) with dimensions of 60 mm × 10 mm × 1 mm or a tensile test dog bone mold (Thermo Fisher Scientific, Waltham, MA USA) of the geometry described in ASTM D1708.

Table 4.1. Formulations of composite samples

Sample code	Resin (HDPE) (wt%)	LCNC (Weight ratio)	ZnO/ B_2O_3 (Weight ratio)
Neat HDPE	100	-	-
LC1Z0	99	1	0
LC1Z1	99	1	1
LC1Z2	99	1	2
LC2Z1	99	2	1
LC1B0	99	1	0
LC1B1	99	1	1
LC1B2	99	1	2
LC2B1	99	2	1

Characterization

Fourier Transform Infrared Spectroscopy: The samples were analyzed to study their chemical structure using a FTIR spectroscopy (Nicolet i550, Thermo Fisher Scientific, USA) in an attenuated total reflection (ATR) mode. The final spectrum of each sample was an average of 32 scans at a resolution of 4 cm^{-1}, in the wavenumber range of 400-4000 cm^{-1}.

Scanning Electron Microscopy: The composites were cryo-fractured in the liquid nitrogen atmosphere and the morphology of the cross-section of the composites was analyzed using field emission scanning electron microscopy (FESEM). Images of cross-section morphology were taken

at different magnifications using field emission scanning electron microscope (Supra 55VP, Zeiss, Thornwood, NY, USA), operating at an accelerating voltage of 15.0 kV, in the Image and Chemical Analysis Laboratory (ICAL) at Montana State University. The samples were coated with a thin film of Iridium for 60 s for conductivity before capturing the images.

Thermogravimetric Analysis: Thermogravimetric analysis (TGA) was carried out to analyze the thermal stability of the composites using a TA Instruments Thermogravimetric Analyzer (TGA Q5000, New Castle, USA) at Montana State University. The samples were tested in thermal degradation mode, under a flowing nitrogen atmosphere with a flow rate of 60 ml/min, from 30 ℃ to 600 ℃, at a heating rate of 10 ℃/min.

Differential Scanning Calorimetry: The crystallization ability of the composites was studied using DSC. The melt peak, crystallization peak and fusion enthalpy of the samples were measured by using a TA Instruments DSC (Q2500, New Castle, USA) under a nitrogen atmosphere at Montana State University. The samples of about 4-5 mg were taken and scanned over a temperature range from 30 ℃ to 400 ℃ at a heating rate of 10 ℃/ min.

Dynamic Mechanical Analysis: The viscoelastic properties of the composites was studied using a TA Instruments Dynamic mechanical analyzer (Q800) was used to measure the dynamic storage and loss modulus of the samples, using a three-point bending fixture. The composites were heated from 30 °C to 110 °C, with a frequency of 1 Hz, amplitude of 20 μm and a force track of 125%. Two replicates were tested for each formulation and the mean values were reported.

Tensile testing: The tensile properties of the composites were measured using an MTS C43 load frame with 5 mm/min speed and a 35 mm gauge length from clamp to clamp. Five replicates were tested for each formulation and the mean values were reported.

Horizontal Burning test: The horizontal burning test was carried out to get a preliminary idea of the fire-retardant behavior of the composites. The test was conducted on a rectangular bar specimen with dimensions of 60 mm x 10 mm x 1mm according to the ASTM D635-14 standard. The samples were fixed to the mount and their longitudinal axis was kept in the horizontal way during the test. A butane lighter was used, and the flame was applied to the free end of the sample at a 45° angle. For each formulation, two replicates were tested, and the mean values were reported.

Microcalorimetry test: Microcalorimetry test of the composites was carried out to evaluate the heat release properties which is essential for the fire-retardant behavior of composites. The static and dynamic combustion parameters of the composites were measured using a Microscale Combustion Calorimeter (MCC-2) by Deatak (University of Texas, Austin) following ASTM D7309 standard. Sample weighing 2-3 grams was combusted by rapid-controlled pyrolysis under an atmosphere of 80%-20% nitrogen to oxygen gas ratio. The combustor temperature was set to 900 °C with a heating rate of 1 °C/min. For each formulation, three replicates were tested, and the mean values were reported.

Results and Discussion

Spectroscopy Analysis of the Composites

The FT-IR spectra of Neat HDPE and all the composites containing ZnO and/or B_2O_3 are shown in Fig. 4.1. The neat HDPE spectra showed characteristic asymmetric and symmetric stretching band of -C-H respectively, at 2917 cm^{-1} and 2852 cm^{-1}. The bending vibration mode of CH_3 and CH_2 rocking vibration mode were also observed at 1472 cm^{-1} and 720 cm^{-1}, respectively [126]. In the case of LCNC incorporated composites, the -C-H vibration peaks of $-CH_2$ and $-CH_3$ groups at 2914 cm^{-1} and 1461 cm^{-1} of lignin overlapped with the -C-H bending vibration peaks of

PE and increased the intensity of the peaks. The -C-H vibration of -CH_3O groups of lignin showed an absorption band at 2844 cm^{-1} which also overlapped with the stretching band of -C-H from HDPE [98], showing the incorporation of lignin in the CNC structure. All the ZnO and B_2O_3 incorporated samples showed slightly higher intensity peaks which can be related to the strong interaction between the oxygen groups and inorganic oxide nanoparticles and hydroxyl groups of LCNC [127].

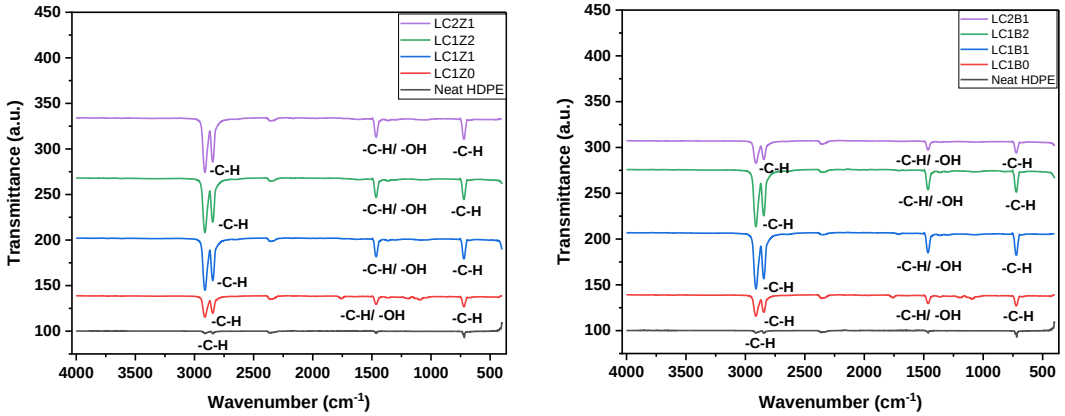

(a) (b)

Fig. 4.1: Transmission spectra of (a) ZnO coated LCNC composites and (b) B_2O_3 coated LCNC composites

Morphology Study of the Composites

Fig. 4.2 shows the SEM micrographs of the cryo-fractured cross-sections of the ZnO and B_2O_3 treated composites. The micrographs showed some aggregation which may be the result of CNC/inorganic nano oxide agglomeration. The presence of ZnO and B_2O_3 was confirmed by energy dispersive X-ray (EDX) analysis and the images showed an irregular distribution of inorganic oxide nanoparticles.

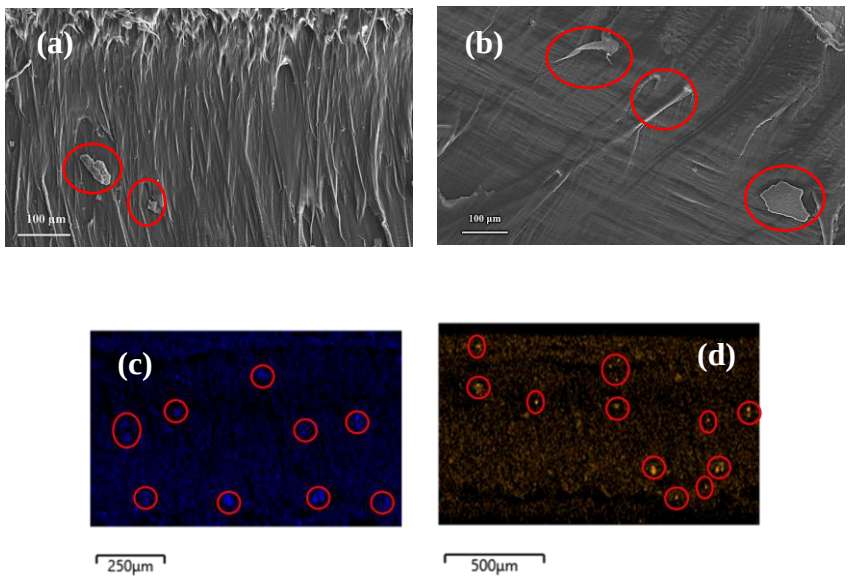

Fig. 4.2: SEM images of HDPE composites cross-sections: (a) LCNC-ZnO, (b) LCNC- B_2O_3 (agglomerations shown in red circles) (c) elemental mapping of Zn, and (d) elemental mapping of B (shown in red circles)

Thermogravimetric Property Analysis of the Composites

The effect of ZnO and B_2O_3 incorporation on the thermal properties of the HDPE composites were investigated using thermogravimetric measurement and represented in Table 4.2 and Table 4.3. The TGA curves demonstrated a single step degradation for all formulations. The thermal stability of the samples was analyzed by comparing the T_{onset}, T_{50}, T_{endset} values. T_{onset} represents the initial degradation temperature at which the composites start degrading, T_{50} is the temperature at 50% weight loss and T_{endset} is the temperature at the end of degradation.

Table 4.2: Thermal properties of each formulation (LCNC/ZnO) from TGA

Sample name	T_{onset} (°C)	T_{50} (°C)	T_{endset} (°C)
Neat HDPE	404.05	460.24	481.70
LC1Z0	405.91	451.09	469.85
LC1Z1	380.85	448.53	466.26
LC1Z2	385.47	450.63	469.12
LC2Z1	398.21	449.23	466.52

The thermal degradation of lignin occurred over a broad range of temperature, from 150 ℃ to 800 ℃, resulting in lignin structure decomposition and leading to the formation of highly stable carbonaceous structure. The thermal stability of lignin is strongly dependent on its chemical structure and specific chemical composition [150]. The presence of lignin generally leads to a decrease of material thermal stability due to catalysis of thermal degradation at lower temperatures. Scissoring effect of ZnO also played a significant role in degrading the thermal properties of the composites [128].

Table 4.3: Thermal properties of each formulation (LCNC/ B_2O_3) from TGA

Sample name	T_{onset} (℃)	T_{50} (℃)	T_{endset} (℃)
Neat HDPE	404.05	460.24	481.70
LC1B0	405.91	451.09	469.85
LC1B1	387.86	451.36	471.56
LC1B2	393.61	450.74	470.41
LC2B1	397.03	455.35	472.91

A similar trend was observed in the case of B_2O_3 coated LCNC composites. The decreasing trend of thermal stability of B_2O_3 coated LCNC composites can be attributed to the inherent lower thermal stability of lignin along with oleic acid present in B_2O_3 structure. To prevent the highly hygroscopic nature and moisture adsorption capability of B_2O_3, oleic acid was introduced on its surface. The moisture contamination can create micro voids in the system which in turn can reduce thermo-mechanical properties of the composites [128]. But the lower flash point of oleic acid (189.9 ℃) [129] and inherent lower thermal stability of lignin adversely affected the overall thermal stability of the composites.

Crystallization Behavior Analysis of the Composites

The non-isothermal crystallization behavior of the HDPE composites was studied using DSC. The DSC results were shown in Fig. 4.3, Table 4.4 and Table 4.5. The crystallinity (X_c) was determined by the following equation:

$$X_c\ (\%) = \Delta H_m \times 100 / \Delta H_m^0 \times (1\text{-}x) \qquad (1)$$

where ΔH_m is the melting enthalpy, ΔH_m^0 is the theoretical enthalpy of 100% crystalline HDPE (293 J g^{-1}), and x is the weight fraction of filler (LCNC-ZnO or B_2O_3).

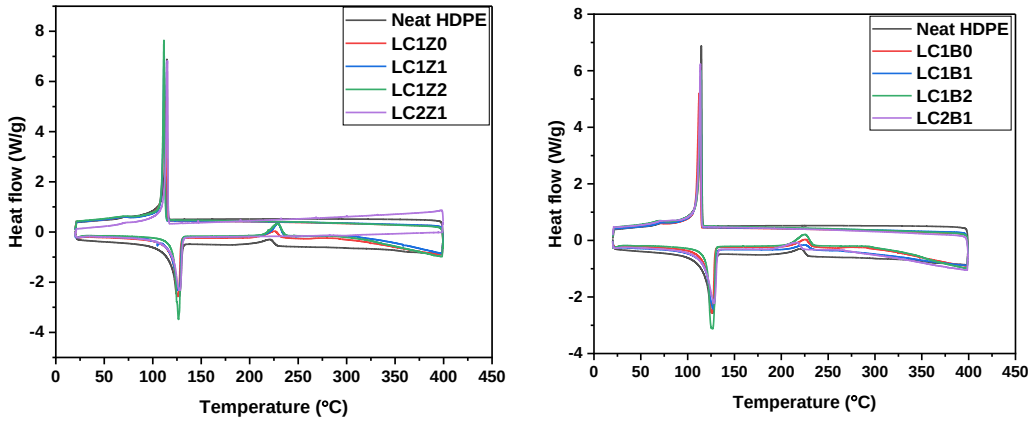

(a) (b)

Fig. 4.3: DSC thermograms of (a) ZnO coated LCNC composites and (b) B_2O_3 coated LCNC composites

Incorporation of LCNC to the system decreased the crystallinity (%) (X_c = 36.45%) compared to neat HDPE. This reason behind this observation may be the formation of less stable random crystals in the presence of LCNCs. Addition of ZnO to the system did not show any significant change in crystallization behavior.

Table 4.4: Crystallization behavior of each formulation (LCNC/ZnO) from DSC

Sample name	T_c (℃)	T_m (℃)	Crystallinity (X_c) (%)
Neat HDPE	114.54	127.53	44.12
LC1Z0	112.40	125.64	36.45
LC1Z1	111.73	126.61	36.49
LC1Z2	111.56	126.54	43.58
LC2Z1	115.15	127.73	36.75

The decrease in X_c of all the composites compared to neat HDPE can be attributed to the decrease in aspect ratios of fillers during freeze drying, which led to agglomeration, similar to the literature [152]. The SEM micrographs also showed evidence of large agglomerates in the system. These agglomerates hindered the formation of stable crystals and thus the crystallinity (%) decreased [130].

Table 4.5: Crystallization behavior of each formulation (LCNC/ B_2O_3) from DSC

Sample name	T_c (℃)	T_m (℃)	Crystallinity (X_c) (%)
Neat HDPE	114.54	127.53	44.12
LC1B0	112.40	126.64	36.45
LC1B1	113.99	127.31	38.47
LC1B2	114.45	126.54	36.69
LC2B1	113.65	128.09	37.65

A similar trend was observed in the case of B_2O_3 coated LCNC composites. In case of B_2O_3 coated LCNC composites, the large and bulky structure of oleic acid present in the B_2O_3, along with LCNC formed agglomerates in the matrix, which hindered the formation of stable crystals [152], thereby decreasing the crystallinity.

Dynamic Mechanical Property Analysis of the Composites

Dynamic viscoelastic properties, storage modulus (E'), loss modulus (E") and loss factor (damping parameter, tan δ) were studied through dynamic mechanical analysis. The results are

shown in Fig. 4.4 and table 4.6 and 4.7. The dynamic mechanical properties of the composites are largely dependent on the filler content. An α-transition peak was observed in the storage modulus curve of neat HDPE around 69.25 °C. Typically for a semi-crystalline polymer, this α-transition is related to the long-range segmental motion, known as glass transition temperature (Tg) [126]. All the composites showed a higher Tg, around 78°C, compared to neat HDPE. Insertion of the bulky side group of lignin increased Tg of the composite system due to restricted mobility of the polymer chains in the amorphous region due to confinement effect [151]. As the temperature exceeded the transition region, a sharp drop in modulus was observed. The mobility of the HDPE chains in the amorphous region increased leading to decreased modulus [150].

Incorporation of LCNC to the system (LC1Z0) as a filler did not improve the storage modulus of the composites. DSC analysis also showed lower crystallinity (%) of the composites compared to neat HDPE. The scenario is the same for LC1Z1 composites. However, increased loading of ZnO to the system (LC1Z2) improved the dynamic mechanical properties compared to neat HDPE.

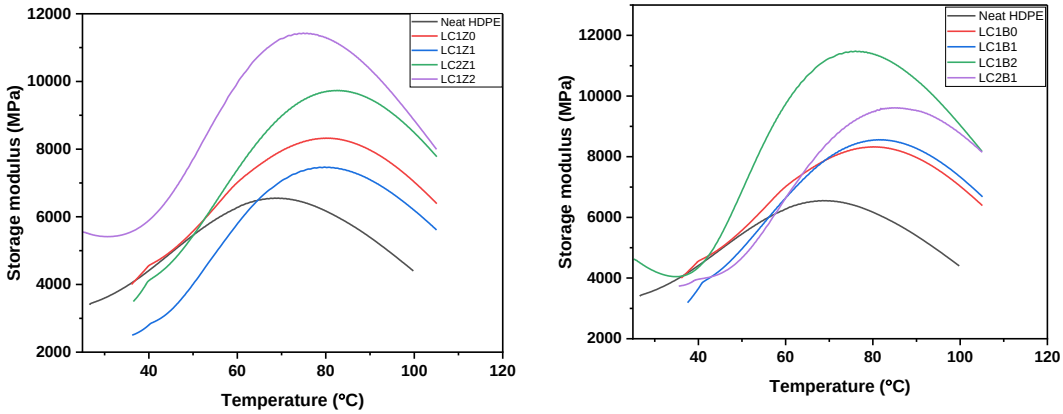

(a) (b)

Fig. 4.4: Representative curves of storage modulus as a function of temperature of (a) ZnO coated LCNC composites and (b) B_2O_3 coated LCNC composites

Table 4.6: Dynamic mechanical properties and mean comparison (Fisher LSD) of each formulation (LCNC/ZnO) (p= 0.05)

Sample code	Mean	Groups	Groups
LC2Z1	10329	A	
LC1Z2	9852.5	A	
LC1Z0	8807.5	A	B
LC1Z1	8629	A	B
HDPE	6462		B

ZnO also facilitated hindering the chain mobility in the amorphous region due to the confinement effect [128] resulting in the increase in storage modulus (9852.5 MPa). Similarly, LC2Z1 also showed increment in storage modulus when compared to HDPE, but the improvement is the same when compared to LC1Z2 formulation. The presence of lignin did not facilitate the dispersion of LCNCs in the system due to the agglomeration during freeze drying [152], which in turn could not improve the mechanical properties of the composites.

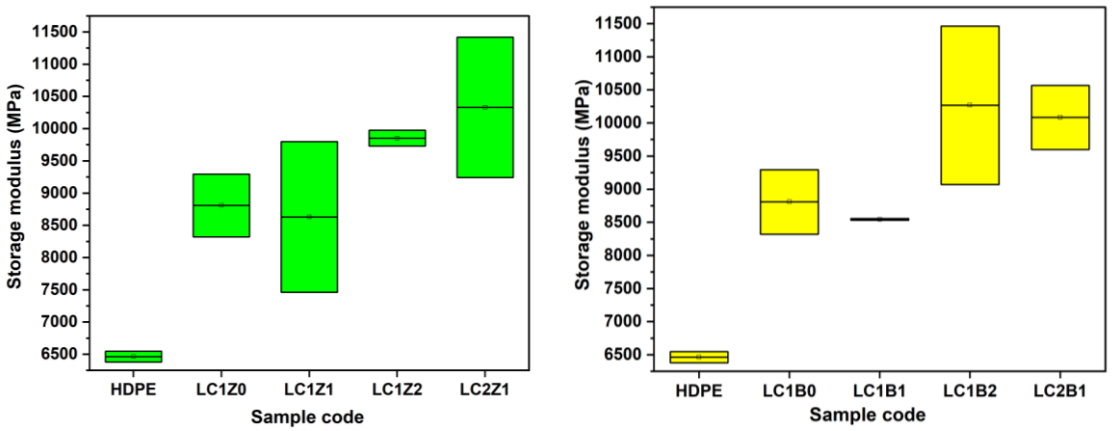

(a) (b)

Fig. 4.5: Representative box plots of statistical analysis of (a) ZnO coated LCNC composites and (b) B_2O_3 coated LCNC composites

Overall, incorporation of ZnO in the system showed almost 54% increase in storage modulus compared to neat HDPE. A similar trend was observed in the case of B_2O_3 coated LCNC composites. In this case, the presence of oleic acid as a bulky side group along with lignin hindered the chain mobility [128, 129] and improved the storage modulus of the composites compared to neat HDPE. There was a 60% increase in storage modulus compared to neat HDPE.

Table 4.7: Dynamic mechanical properties and mean comparison (Fisher LSD) of each formulation (LCNC/ B_2O_3) (p= 0.05)

Sample code	Mean	Groups	Groups
LC1B2	10266.5	A	
LC2B1	9599	A	
LC1B0	8807.5	A	B
LC1B1	8544	A	B
HDPE	6462		B

Tensile Property Analysis of the Composites

The mechanical property analysis such as Young's modulus, elongation at break were investigated to gain an insight into the tensile behavior of the composites, the effect of ZnO and B_2O_3 on the tensile properties and comparison of the tensile properties with neat HDPE. Theoretically, addition of LCNC to a polymer matrix as a filler should increase should improve the tensile properties of the composites [150]. But, like all the nanofillers, there was difficulty while mixing the LCNC with the polymer [150]. Eventually, the increase in the amount of LCNC in the system may adversely affect the mechanical properties of the system.

In the current research, LCNC and the inorganic oxides were incorporated in different ratios to observe and analyze their effect on the mechanical properties of HDPE polymer and the results are shown in Fig. 4.6 and table 4.8, 4.9, 4.10 and 4.11.

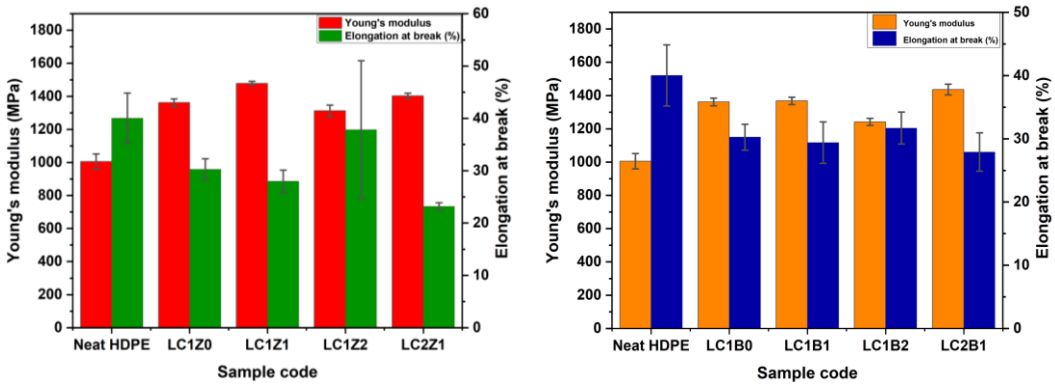

(a) (b)

Fig. 4.6: Graphical representation of the tensile properties of (a) ZnO coated LCNC composites and (b) B_2O_3 coated LCNC composites

All the LCNC incorporated and ZnO coated formulations showed a significant improvement in Young's modulus of the composites, though no significant change was observed in case of elongation at break (%). The filler/polymer interaction is more important in case of low

aspect ratio fillers and polymer compared to the higher aspect ratio fillers [153, 154]. Incorporation of LCNC (LC1Z0) in the composites significantly increased the elastic modulus in comparison with neat HDPE, indicating better interfacial bonding with the HDPE matrix [153]. Incorporation of ZnO in the system further increased the elastic modulus and LC1Z1 formulation showed the highest value of elastic modulus compared to the other systems. But, no additional improvement in the elastic modulus was observed in case of higher amount of ZnO or LCNC incorporation. The plausible explanation of this phenomena is the agglomeration of the reinforcements (LCNC/ZnO complex) during freeze-drying.

Table 4.8: Young's modulus and mean comparison (Fisher LSD) of each formulation (LCNC/ ZnO) (p= 0.05)

Sample code	Mean	Groups	Groups	Groups	Groups
LC1Z1	1478.158	A			
LC2Z1	1402.547		B		
LC1Z0	1361.9		B	C	
LC1Z2	1312.79			C	
HDPE	1135.681				D

Also, there can be a decrease in aspect ratios of the fillers during freeze-drying which can change their shape to flakes instead of rod-like shapes due to the agglomeration [154], as shown in the SEM micrographs of the cross-sections of the composites. These agglomerations in the composites were responsible for the more ductile behavior of the composites and no significant change in the elongation at break (%). Overall, there is around 30% increase in the elastic modulus of the composites compared to neat HDPE.

Table 4.9: Elongation at break (%) and mean comparison (Fisher LSD) of each formulation (LCNC/ ZnO) (p= 0.05)

Sample code	Mean	Groups
LC1Z2	37.82	A
HDPE	32.84	A
LC1Z1	27.98	A
LC1Z0	25.6	A
LC2Z1	23.16	A

Similarly, in the case of LC1B0, the elastic modulus showed a significant improvement compared to neat HDPE, indicating the reinforcement effect of LCNC [156]. But incorporation of B_2O_3 in the system did not show any significant improvement in elastic modulus compared LC1B0. This phenomenon can be related to the micro void formation in the interface of the filler and the matrix [157].

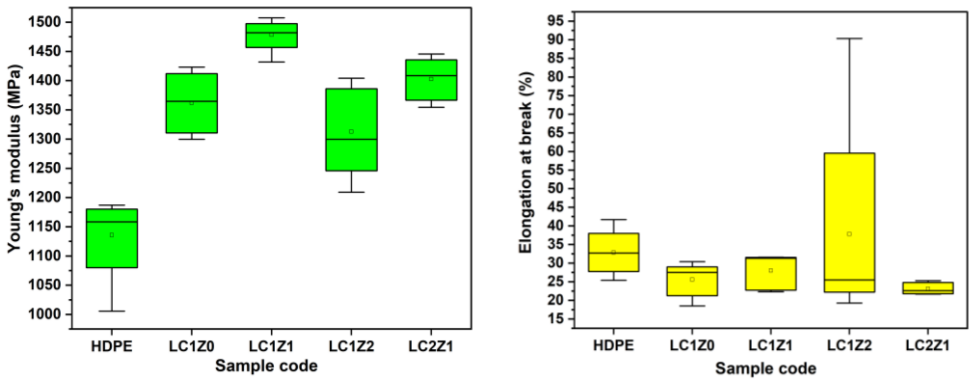

(a) (b)

Fig. 4.7: Representative box plots of statistical analysis of (a) elastic modulus and (b) elongation at break (%) of ZnO coated LCNC composites

During the production of B_2O_3, oleic acid was used as a reaction medium and was capped on the surface of B_2O_3 to increase the hydrophobicity. But due to the large and bulky structure of the oleic acid, it has an adverse effect on the tensile properties of the composites. It hindered the

interaction between LCNC and B_2O_3, because of the bulky structure of both lignin and oleic acid. Due to this reason, agglomerates were formed during freeze drying, as shown in SEM micrographs. This lack of interaction between LCNC and B_2O_3 created micro voids at the interfacial region, affecting the tensile properties of the composites [157, 158].

Table 4.10: Young's modulus and mean comparison (Fisher LSD) of each formulation (LCNC/ B_2O_3) (p= 0.05)

Sample code	Mean	Groups	Groups	Groups	Groups
LC2B1	1436.445	A			
LC1B1	1367.998	A	B		
LC1B0	1307.148		B	C	
LC1B2	1241.494			C	
HDPE	1130.032				D

Table 4.11: Elongation at break (%) and mean comparison (Fisher LSD) of each formulation (LCNC/ B_2O_3) (p= 0.05)

Sample code	Mean	Groups
HDPE	32.875	A
LC1B2	31.7	A
LC1B1	29.425	A
LC2B1	27.95	A
LC1B0	27.375	A

Overall, there is around 27% increase in elastic modulus of the composites compared to neat HDPE.

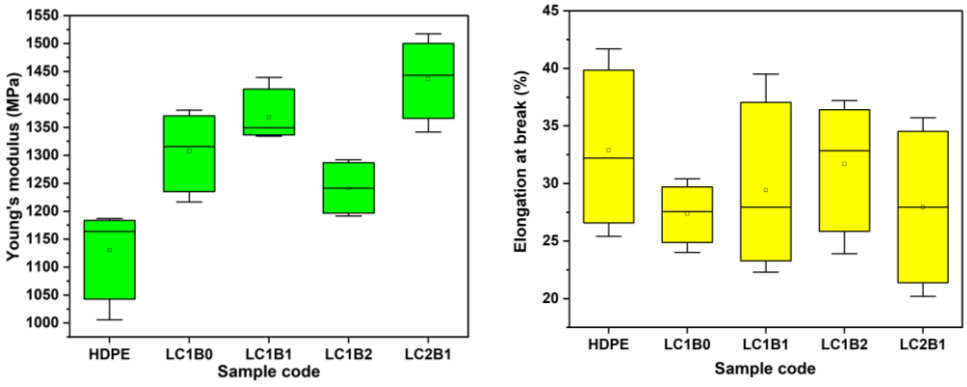

(a) (b)

Fig. 4.8: Representative box plots of statistical analysis of (a) elastic modulus and (b) elongation at break (%) of B_2O_3 coated LCNC composites

Horizontal Burning test Results Analysis of the Composites

The horizontal burning test was conducted to evaluate the flame spread rate, type of burning, and weight loss (%), to gain a primary idea of the fire-retardant behavior of the composites. The thermal degradation of lignin occurred over a broad range of temperature, from 150 ℃ to 800 ℃, resulting in lignin structure decomposition and leading to the formation of highly stable carbonaceous structure. The effectiveness of lignin as a fire retardant is strongly dependent on its chemical structure and specific chemical composition [132].

Table 4.12: Mean comparison (Fisher LSD) of flame spread rate (mm/s) of (LCNC/ZnO) composites (p= 0.05)

Sample code	Mean	Groups
LC1Z1	1.19	A
LC2Z1	1.175	A
HDPE	1.08	A
LC1Z2	1.045	A
LC1Z0	0.915	A

Table 4.13: Mean comparison (Fisher LSD) of flame spread rate (mm/s) of (LCNC/B_2O_3) composites (p= 0.05)

Sample code	Mean	Groups
HDPE	1.08	A
LC2B1	1.075	A
LC1B1	1.02	A
LC1B2	0.99	A
LC1B0	0.915	A

The addition of LCNCs to HDPE did not show any significant change in the flame spread rate in the horizontal burning test along with a small decrease in weight loss (%). The presence of lignin generally leads to a decrease of material thermal stability due to catalysis of thermal degradation at lower temperatures [150]. Also, the poor dispersion and insufficient encapsulation of the agglomerates of freeze dried LCNC/inorganic oxide complex by the polymer melt during extrusion, played a pivotal role in decreasing the thermal stability of the composites [151]. Also, the thermogravimetric analysis results corroborate with these findings.

Table 4.14: Mean comparison (Fisher LSD) of weight loss (%) of (LCNC/ZnO) composites (p= 0.05)

Sample code	Mean	Groups	Groups
Neat HDPE	80.76674	A	
LC1Z0	61.34896		B
LC1Z2	59.68229		B
LC1Z1	52.36875		B
LC2Z1	49.77817		B

Table 4.15: Mean comparison (Fisher LSD) of weight loss (%) of (LCNC/B_2O_3) composites (p= 0.05)

Sample code	Mean	Groups	Groups
Neat HDPE	80.76674	A	
LC1B0	61.34896		B
LC2B1	60.66435		B
LC1B1	56.0413		B
LC1B2	53.72856		B

The char formed during combustion acts as an insulating layer at the surface of the burning material. The inhibition of the mass transfer of the combustible gases results in the dilution of fuel and subsequent termination of the combustion cycle [153, 154]. Because of this reason, there was a slight decrease in weight loss (%) in both cases of inorganic oxide incorporation.

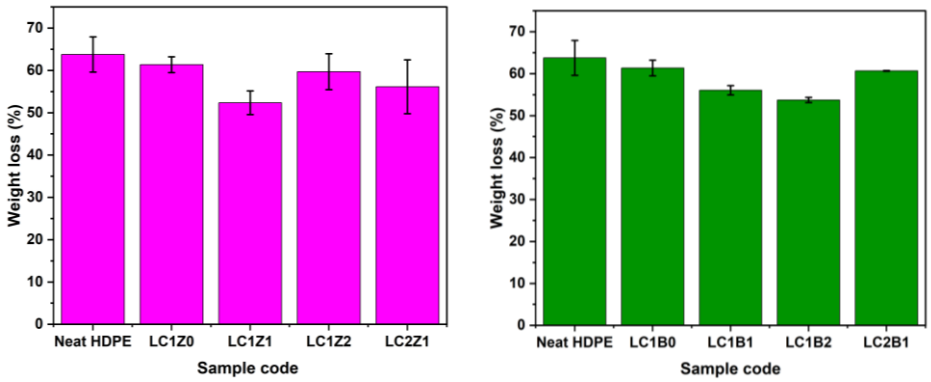

(a) (b)

Fig. 4.9: Weight loss (%) graphs of (a) ZnO coated LCNC composites and (b) B_2O_3 coated LCNC composites

Microcalorimetry test Results Analysis

The microcalorimetry test was conducted to evaluate the heat release capacity (J/gK), peak heat release rate (W/g) and total heat release (kJ/g) of the LCNC composite samples and compare them to neat HDPE. The heat release rate (HRR) is regarded as the driving force for fire spread

and also one of the most important properties to control fire. The HRR is calculated by multiplying the weight loss of a material with the heat of combustion of that material [143]. The results and analysis of these tests are shown in fig. 4.10 and table 4.16, 4.17, 4.18. There was no significant difference in properties observed in the horizontal burning test of the inorganic oxide coated composites. Therefore, the best performing formulation from each type of inorganic oxide was chosen for the microcalorimetry test.

Table 4.16: Mean comparison (Fisher LSD) of HR capacity (J/gK) of HDPE composites (p= 0.05)

Sample code	Mean	Groups	Groups
LC1B2	477.6667	A	
LC1Z1	417		B
HDPE	414.6667		B

Table 4.16 & 4.17, and Fig. 4.10 show the statistical analysis of HR capacity, peak HRR, average heat release rate and statistical comparison of peak heat release (PHRR) of neat HDPE, LC1B2 and LC1Z1 formulations.

During the combustion of the composites, decomposition of the resin matrix is responsible for the release of flammable volatiles. On the other hand, the fillers/fire retardants control the amount of heat released from the polymer composite [143].

Table 4.17: Mean comparison (Fisher LSD) of peak HRR (W/g) of HDPE composites (p= 0.05)

Sample code	Mean	Groups	Groups
LC1B2	475.3667	A	
LC1Z1	415.0333		B
HDPE	413.0333		B

The initial delay period (till 400 °C) before heat release was present because the temperature of the composite was still below the pyrolysis temperature of the matrix, HDPE. In TGA, it was observed that the decomposition of the system started around 400 °C. There was a rapid increase in HRR following the previous induction period where the combustion of the volatiles began at the interface of the composite/fire. Around 500 °C, the PHRR was achieved and after a short stabilization period the heat release decreased drastically. The shielding effect of the char produced on the exposed polymer surface reduced the penetration of the combustible volatiles, the low-molecular weight hydrocarbons, and the decomposition rate of the underlying material declined. The decreasing resin content of the composites also decreased the PHRR [144].

In case of ZnO coated composites, no statistically significant decrease in HRR and PHRR was observed compared to neat HDPE. The presence of lignin decreased the composites' thermal stability due to the catalysis of thermal degradation at lower temperatures [145], as observed in TGA and horizontal burning test analysis. Though the presence of nano ZnO could not decrease the HRR and PHRR compared to neat HDPE, but it shielded the negative effect of lignin and prevented further worsening the situation due to its smaller size (30-150 nm) and higher surface area [146].

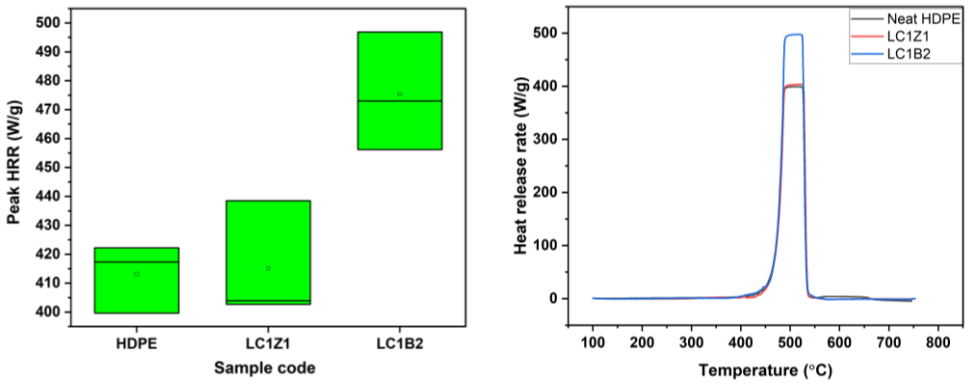

(a) (b)

Fig. 4.10: (a) Statistical comparison of peak heat release rate of the three formulations (significance level=0.05) and (b) heat release rate graph of neat HDPE, LC1Z1 and LC1B2 formulations

In case of B_2O_3 coated composites, a significant increase in PHRR and HRR or a declination of fire-retardant properties compared to HDPE was observed. During the production of B_2O_3, the surface of the nanoparticles was covered with oleic acid to increase the hydrophobicity of the inorganic oxides. But the lower flash point of oleic acid (189.9 °C) and inherent lower thermal stability of lignin adversely affected the overall thermal stability and fire retardancy of the composite system [158].

Table 4.18: Microcalorimetry test results of neat HDPE and the composite

Sample code	HR capacity (J/gK)	PHRR (W/g)	Total HR (kJ/g)
Neat HDPE	414.67±12.09	413.03±11.88	22.73±0.23
LC1Z1	417±19.92	415.03±20.33	22.8±0.79
LC1B2	477.667±20.13	475.37±20.45	25.43±0.06

Also, the large and bulky structures of lignin and oleic acid hindered the interaction between LCNC and B_2O_3 and facilitated the formation of agglomerates of LCNC/B_2O_3 complex during freeze drying, which also affected the dispersion of LCNC and B_2O_3 in the polymer matrix

[129]. The fire-retardant properties of the B_2O_3 coated composites declined due to these two reasons.

Conclusion

High density polyethylene (HDPE) is one of the most widely used commercial polymers. To improve HDPE's poor thermo-mechanical properties, different types of bio-based nanofillers and fire-retardant materials are incorporated. The current study investigated the role of nano sized ZnO or B_2O_3 coated LCNC as functional additives for improving the fire-resistant behavior and mechanical properties of the HDPE based composites. The HDPE composites formulations containing nano ZnO or B_2O_3 and LCNC were manufactured using melt blending extrusion and injection molding process. In this study, the inherently lower thermal stability of lignin adversely affected the thermal properties of the composites. The TGA, horizontal burning test and microcalorimetry test showed the declination of thermal stability and fire-retardant properties of all the composite systems. Though the ZnO coated composites did not show any significant improvement in the fire-retardant properties of the composites, but it prevented further declination of thermal stability of the composites compared to neat HDPE, due to its smaller size and higher surface area. The B_2O_3 coated composites showed a decline in fire properties due to bulky structure of oleic acid capped B_2O_3, lower flash point of oleic acid and lower thermal stability of LCNC. The mechanical properties of the composites were improved because of the reinforcement effect of LCNC and inorganic oxides. There is a 30% increase in elastic modulus observed in case of ZnO coated composites, while the B_2O_3 coated composites showed a 27% increase in elastic modulus compared to neat HDPE. The formation of agglomerates of LCNC/inorganic oxide complex during freeze drying prevented further improvement in mechanical properties of the

composites. The SEM micrographs showed agglomerations and irregular distribution of inorganic oxides in the cryo-fractured cross-sections of the composites. Therefore, the overall physical and thermal properties of the LCNC containing composites did not show any significant improvement compared to neat HDPE. The presence of the bulky lignin structure hindered the interaction between the LCNC and inorganic oxides and declined the overall properties of the composites.

CHAPTER SIX

GRAPHENE QUANTUM DOTS INCORPORATION TO IMPROVE DISPERSION OF CELLULOSE NANOCRYSTALS AND THERMAL, PHYSICAL AND MECHANICAL PROPERTIES OF HIGH-DENSITY POLY(ETHYLENE) POLYMER COMPOSITES

Contribution of Authors and Co-Authors

Manuscript in Chapter 5

Author: Saptaparni Chanda

Contributions: Conceptualization, Methodology, Formal analysis, Writing – Original draft

Co-Author: Dilpreet S. Bajwa

Contributions: Supervision, Resources, Writing – Review, Editing

Co-Author: Cecily Ryan

Contributions: Writing- Review, Editing

Co-Author: Nicole Stark

Contributions: Resources

Manuscript Information

Saptaparni Chanda, Dilpreet S Bajwa, Nicole Stark, Sreekala G Bajwa

Nanocomposites

Status of Manuscript:
__X__ Prepared for submission to a peer-reviewed journal
____ Officially submitted to a peer-reviewed journal
____ Accepted by a peer-reviewed journal
____ Published in a peer-reviewed journal

Abstract

Cellulose nanocrystal (CNC) has potential to be used as a reinforcement in polymeric nanocomposites because of their inherent biodegradability, universal accessibility, and superior mechanical properties. The central challenge regarding the mixing of CNCs with commercial hydrophobic polymers is their poor dispersion in the matrix because of CNC's hydrophilic nature. The surface modification techniques can change or tune the surface characteristics of CNCs to make them more compatible to the hydrophobic matrix. In this research, a safe, effective, and ecofriendly surface modification technique was used to prepare a hybrid system of cellulose nanocrystal (CNC)/graphene quantum dots (GQD). This hybrid system of CNC/GQD was added to high density poly (ethylene) (HDPE) separately to produce composites via melt blending extrusion process. The CNC/GQD inclusion complex properties were evaluated using Zeta potential measurement, Raman spectroscopy, X-Ray Photoelectron Spectroscopy (XPS) and X-Ray Diffraction (XRD) analysis. The composite properties were analysed using Scanning Electron Microscopy (SEM), Thermogravimetric Analysis (TGA), Differential Scanning Calorimetry (DSC), Dynamic Mechanical Analysis (DMA), and tensile testing and electrical impedance spectra analysis. The interaction of CNC and GQD was confirmed by Raman spectroscopy, XPS and XRD analysis. The SEM micrographs of the cross-sections of GQD induced composites showed a uniform fibrillar morphology and no sign of agglomeration. The GQD incorporated composites exhibited better thermal stability and better mechanical properties compared to neat HDPE. The composites showed a purely capacitive response for an AC electrical system. The results indicate the improved dispersion of CNC in the polymer matrix which in turn improved the overall

properties of the composites. The scope of CNC/GQD inclusion complex as an energy storage device can be explored in future.

Keywords: Cellulose nano crystal, High-density poly(ethylene), Graphene quantum dots, Dispersion, CNC/GQD inclusion complex, Thermal stability, Mechanical properties

Introduction

Over the past few years, Biodegradable and renewable materials have received special attention from both scientific and industrial communities due to their potential to cope with the effects of global warming and pollution. Cellulose is the most abundant bio-based polymer and has been used as a potential biodegradable and renewable material for industrial products. In the last few decades, nanostructured cellulose materials have become a new field of interest because of the specific physical and chemical properties of these materials. Amongst the nanocellulose materials, CNCs have gained special attention because of their high crystallinity (54-88%), superior mechanical properties- (tensile strength ~ 7 GPa, elastic moduli ~150 GPa), light weight, transparency, relatively low cost and broad capacity to modify surface properties [11-16].

The most critical challenge in nanocomposite processing is to transfer the exceptional mechanical properties of CNCs at single fiber level to the macroscale properties of the bulk nanocomposites. This can only be achieved by enhancing the dispersion of CNCs and optimizing the filler-matrix interface [17], which is where the surface modification processes come into play. Graphene quantum dots (GQD) is an emerging class of carbon-based materials. Graphene is one layer of sp^2-hybridised carbon atoms arranged in a honeycomb lattice [159], whereas GQDs are chopped fragments of a few graphene sheets (<10 nm lateral dimension) and <10 graphene layers which form final particles [160]. GQDs are used in various applications owing to their higher

photostability, thermal and chemical stability, low cytotoxicity, strong photoluminescence, dispersibility in water, fluorescence, excellent biocompatibility and dimensional and morphological tunability [161, 162]. Due to these excellent properties, GQDs are conventionally used in biomedicine, energy, and sensing photo electronics [163]. But their role as a dispersing agent for other nanomaterials is yet to be explored.

In the past few years, GQD/nanocellulose complex was used in the production of functional hydrogels [164, 165], thin films [166, 167] or composites [168] for different applications. The reaction mechanism between CNC and GQD is very complex in nature. GQDs possess one or few layers of graphene and connected chemical groups on edges. They are anisotropic in nature having lateral dimensions larger than their height [87]. GQDs are amphiphilic in nature, having hydrophobic character in their basal plane and hydrophilic on the edges because of the presence of carboxylic acid groups [88]. CNCs and GQDs can exhibit hydrophobic interactions and form hydrogen bonds between the surface hydroxyl groups present in CNC and carboxylic acid groups of GQDs. Moreover, CNCs carry a negative charge on their surface because of the hydroxyl groups [89]. Thus, GQDs and CNCs exhibit mutual electrostatic repulsion, which in turn can improve dispersion of CNCs in polymer matrix.

Inspired by these findings, an eco-friendly and a sustainable technology for CNC functionalization was selected using GQD to improve the dispersion of CNCs in high density polyethylene (HDPE) matrix and enhance the overall thermo-mechanical performance of the composites. The presence of oxygen containing functional groups on the surface of both CNC and GQD facilitates the formation of CNC/GQD inclusion complex which can be used as reinforcement for HDPE based composites. Overall, the main aim of the research was to develop

a safe, effective and ecofriendly surface modification technique of CNCs to improve their dispersion behavior in the polymer matrix.

Experimental Section

Materials

High density poly (ethylene) (HDPE) powder with a melt index of 3.5 g/10 min, and a melting temperature of 126 ℃, purchased from Nova Chemicals was used as polymer matrix. The CNC with dimensions of 10-15 nm width and 80-100 nm length and hence aspect ratios of 5-10 were provided by USDA Forest Products Laboratory (Madison, WI, USA). They were extracted by the sulfuric acid hydrolysis process from softwood pulp. The CNCs were desulfated using hydrothermal treatment. The aqueous dispersion of graphene quantum dot (GQD) of blue luminescent was purchased from Sigma Aldrich. The concentration of the aqueous dispersion of GQD was 1 mg/mL and the full width half maximum (FWHM) of GQD is 60-80 nm. Deionized (DI) water purchased from Millipore, USA was used as solvent.

Synthesis of CNC/GQD Inclusion Complex

In the first step, CNC was dissolved in deionized water at room temperature under continuous stirring. One gram of dry mass of CNC was dissolved in 100 mL of DI water separately in four beakers for four different formulations. In the second step, GQD sol was added in different concentrations in each beaker except one. The concentrations of GQD were 1%, 1.5% and 2% by the weight of CNC, respectively. In the fourth beaker, no GQD was added. The fourth formulation was used to understand the reinforcement effect of CNC to the matrix and to do the comparative studies of the effect of quantum dot treatment on the dispersion behavior of CNC and mechanical

properties of the resultant composites. All the solutions containing GQD were kept under continuous stirring for 30 min. In the third step, all the three solutions containing GQD, were kept at room temperature for 48 h, to trigger reaction of GQDs with the surface hydroxyl groups of the CNCs. After 48 h, CNC/GQD inclusion complex films were formed. These films were grinded to fine powder using mortar and pestle for addition into polymer composites.

Design and Manufacture of Polymer Composites using GQD Functionalized CNC as Filler Material

HDPE served as the matrix resin to manufacture composite samples. Three GQD/CNC formulations synthesized in the previous step were used to manufacture HDPE masterbatches. Powdered CNC/GQD inclusion complexes were melted blended with resin. Each master batch was further used to manufacture test planks representing 1%, 1.5% and 2% GQDs on the weight of CNC. The design of experiment included three types of GQD/CNC complexes, pristine CNC incorporated and control (only HDPE) with 5 replications. Composite samples were prepared by melt compounding in a Thermo Fisher Scientific HAAKE Minilab II dual screw extruder. Samples were extruded at 100 rpm and 145 °C for 5 minutes. After mixing, composites were injection molded into a Thermo Fisher Scientific Minijet Pro injection molder. Samples were injected into either a DMA sample mold (Thermo Fisher Scientific, Waltham, MA USA, Part # 557-2295) with dimensions of 60 mm × 10 mm × 1 mm or a tensile test dog bone mold (Thermo Fisher Scientific, Waltham, MA USA) of the geometry described in ASTM D1708.

Table 5.1: Formulations of the composite samples

Sample code	Resin (HDPE) (wt%)	CNC (wt%)	GQD (wt%) (by the weight of CNC)
Neat HDPE	100	-	-
C1G0	99	1	-
C1G1	99	1	1
C1G1.5	99	1	1.5
C1G2	99	1	2

Characterization

Zeta Potential Measurement: The electro-kinetic potentials (ζ-potential) of GQDs, CNCs and GQD/CNC were measured using a Zeta-sizer Nano instrument, at 22.7 °C and pH 7.

Raman Spectroscopy: The chemical structure and functional groups of the CNC/GQD inclusion complexes were analyzed using a Horiba LabRam HR Evolution NIR Raman microscope. Raman spectra was acquired with a 50×LWD objective, a stigmatic spectrometer with a grating of 300 gr/mm, and a 532 nm 450 mW laser at 0.01-1% power. The wavenumber range was 900-3000 cm^{-1}, to detect the D (~1350 cm^{-1}) and G (~1583 cm^{-1}) peaks of graphene.

X-Ray Photoelectron Spectroscopy (XPS): XPS analysis was carried out to determine the chemical composition and binding energy of different chemical bonds of CNC/GQD inclusion complexes, using a X-Ray002 400 μm-FG ON with a monochromatic Al Kα source. Measurements were taken at a spot size of 400×400 μm and the incoming photons were set to 200 eV with a step size of 1 eV.

X-Ray Diffraction (XRD) Analysis: XRD analysis was carried out to study the crystallographic structure of the CNC/GQD hybrid system. X-ray diffraction patterns of CNC and CNC/GQD inclusion complexes were obtained from an X-ray powder diffraction spectrometer

with Cu Kα X-ray, wavelength of 1.5418 Å. The stage was set to collect the diffraction pattern from 2θ=5° to 70°.

Scanning Electron Microscopy (SEM): The composites were cryo-fractured in the liquid nitrogen atmosphere and the morphology of the cross-section of the composites was analyzed using SEM. Images of cross-section morphology were taken at different magnifications using field emission scanning electron microscope (Supra 55VP, Zeiss, Thornwood, NY, USA), operating at an accelerating voltage of 5.0 kV, in the Image and Chemical Analysis Laboratory (ICAL) at Montana State University. The samples were coated with a thin film of Iridium for 60 s for conductivity before capturing the images.

Thermogravimetric Analysis (TGA): The thermal stability of the composites was analyzed using TGA. Thermogravimetric analysis was carried out using a TA Instruments Thermogravimetric Analyzer (TGA Q5000, New Castle, USA) at Montana State University. The samples were tested in thermal degradation mode, under a flowing nitrogen atmosphere with a flow rate of 60 ml/min, from 30 ℃ to 600 ℃, at a heating rate of 10 ℃/min.

Differential Scanning Calorimetry (DSC): The DSC analysis was carried out to study the crystallization behavior of the composites. The melt peak and fusion enthalpy of the samples were measured by using a TA Instruments DSC (DSC2A-01552) under a nitrogen atmosphere at Montana State University. The samples of about 4-5 mg were taken and scanned over a temperature range from 30 ℃ to 400 ℃ at a heating rate of 10 ℃/ min.

Dynamic Mechanical Analysis (DMA): The viscoelastic behavior of the composites was studied using DMA. A TA Instruments Dynamic mechanical analyzer (Q800) was used to measure the dynamic storage and loss modulus of the samples, using a three-point bending fixture. The

composites were heated from 30 °C to 110 °C, with a frequency of 1 Hz, amplitude of 20 μm and a force track of 125%. Two replicates were tested for each formulation and the mean values were reported.

Tensile testing: The tensile properties of the composites were measured using an MTS C43 load frame with 5 mm/min speed and a 35 mm gauge length from clamp to clamp. Five replicates were tested for each formulation and the mean values were reported.

Electrical Impedance Spectra Analysis: The electrical behavior of the composite samples was analyzed using a four-point probe set-up and a Hioki 3533-01 LCR meter. The impedance spectra were collected using a voltage of 100 mV, within a frequency range of 4 Hz to 1 MHz. Impedance of each replicate of each formulation was measured at three random points and three replicates were tested for each formulation.

Results and Discussion

Zeta Potential Measurement

The CNCs were negatively charged because of the presence of surface sulfate groups and hydroxyl groups [169] and had a ζ-potential of -46.86±6.49 mV at C_{CNC} = 1mg/mL, 22.7 °C and pH 7. GQDs were also negatively charged because of the deprotonation of the carboxyl groups present in the edge of GQD structure [170] and the ζ-potential was -14.39±1.8 mV at C_{GQD} = 5 mg/mL, 22.7 °C and pH 7. The increase in ζ-potential to -28.39 mV for GQD/CNCs (measured at $C_{GQD/CNC}$ = 1 mg/mL, 22.7 °C and pH 7) compared to CNC because of the hydrogen bond formation between carboxyl and hydroxyl groups of GQD and CNC respectively [171], confirmed the formation of GQD/CNC inclusion complex.

Raman Spectroscopy Analysis of the CNC/GQD Inclusion Complex

Raman spectroscopy was used to investigate the chemical structure of the composites. Typically, Raman spectra of graphitic carbons show two characteristic peaks, D and G peaks. The D peak (1350 cm^{-1}) corresponds to the sp^3 carbon atom or the presence of edge defects or oxygen containing functional groups in the graphene structure. The G peak (1580 cm^{-1}) represents the crystallinity or the relative strength of the sp^2 plane [172]. Raman spectra of all GQD incorporated composites showed both D and G peaks (fig. 5.1), indicating the presence of edge defects or oxygen containing functional groups in the aromatic carbon structure [173]. Generally, the D band and G band integral intensity ratio (I_{DG} ratio) is used to determine the defects in carbon structure. In this case, the I_{DG} ratio increased with the incorporation of more GQD (Table 5.2). This confirmed the presence of more sp^3 domains in the system or in other words more oxygen containing functional groups [174], which facilitated the reaction between surface groups of CNC and GQD.

Additionally, the change in peak position and full width of half maximum (FWHM) or line broadening of the peaks can provide insights of the graphitic structure. In all inclusion complexes, an apparent shift was observed in G peak positions (1554 cm^{-1}). This peak shift can be associated with the increasing interaction between CNC and GQD [173]. Also, the increase in the value of FWHM of G peak indicated broadening of peak or decrease in the size of crystal [], which can be confirmed from XRD analysis.

Moreover, the presence of the surface sulfate groups of CNC was confirmed by the C=S band at 1115 cm^{-1} and -S-H band at 2551 cm^{-1} [175]. After 1700 cm^{-1}, presence of more and more oxygen containing functional groups such as carbonyl (C=O) and carboxylate group (O-C=O) was observed, which is further confirmed in XPS analysis.

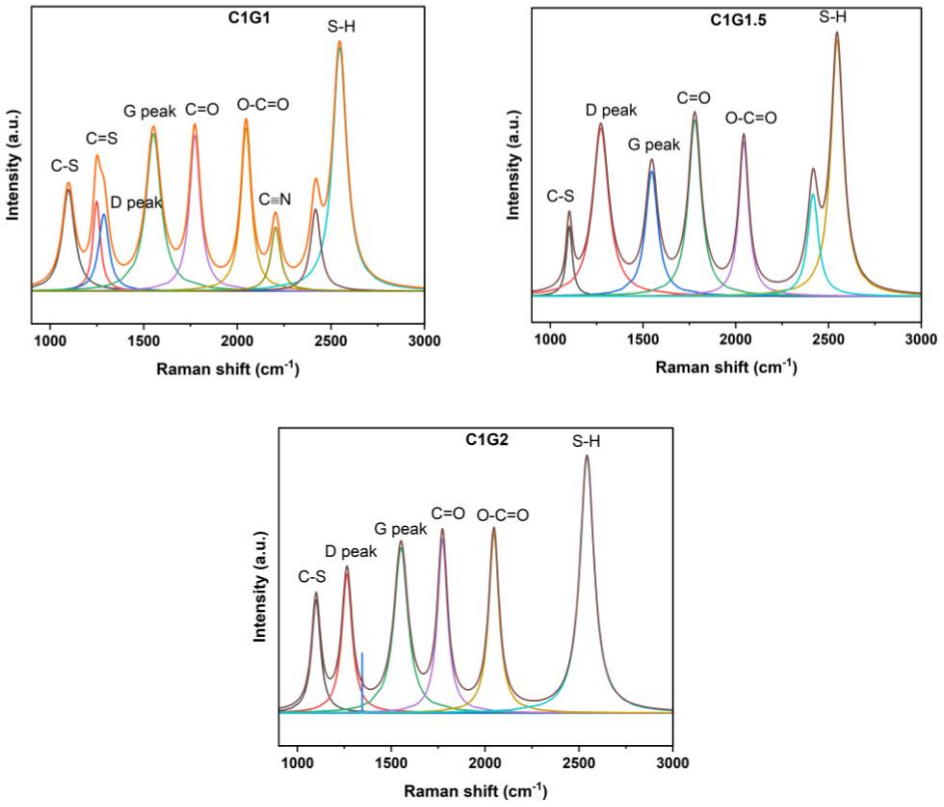

Fig. 5.1: Raman spectra of GQD/CNC inclusion complexes

Table 5.2: Characteristics of D and G bands of CNC/GQD inclusion complexes

Sample code	I_{DG} ratio	FWHM
C1G1	0.68	96
C1G1.5	1.28	89
C1G2	0.74	76

XPS Analysis of CNC/GQD Inclusion Complex

The surface composition of the GQD/CNC inclusion complex was investigated by XPS. The XPS survey spectra of all four CNC/GQD inclusion complexes showed three peaks: C1s peak (~285 eV), O1s peak (~532 eV), N1s peak (400 eV) and S2p peak (~168 eV), with traces of Na and Si, because of impurity present in the system. The atomic percentages of individual elements and O to C ratio are shown in table 5.3 and 5.4. Moreover, the slight shift in the peak positions indicated

the change in elemental and chemical compositions. Also, the FWHM value demonstrated the number of chemical bonds contributing to the peak shape [176], which can be observed from table 5.4.

Table 5.3: Atomic percentages of different elements in CNC/GQD inclusion complex

Sample code	C (atm. %)	O (atm. %)	N (atm. %)	S (atm. %)
C1G1	77.57	19.28	1.345	0.68
C1G1.5	70.47	24.04	1.745	0.41
C1G2	80.85	16.52	1.34	0.58

The lower value of O to C ratio indicated the successful chemical reactions between CNC and GQD [177]. The increase in the value of FWHM confirmed the presence of higher number of chemical bonds in the system, which indicated more intense chemical reaction between CNC and GQD [178].

Table 5.4: O to C ratio and FWHM of CNC/GQD inclusion complex

Sample code	O/C ratio	FWHM
C1G1	0.248	2.16
C1G1.5	0.341	3.53
C1G2	0.205	3.45

The high resolution C1s spectra of C1G1 can be divided into three peaks. A sp^2 hybridized carbon (C-C) at 284.68 eV in the graphene network, sp^3 C (C-O-C) at 286 eV and at 288.48 eV a peak of carboxylate group (O-C=O). The same peaks are observed in the case of C1G1.5 C1s spectra. In the case of C1G2, both sp^2 and sp^3 hybridized carbons were observed along with a carbonyl group (C=O) [179]. All these peaks were also observed in Raman spectroscopy.

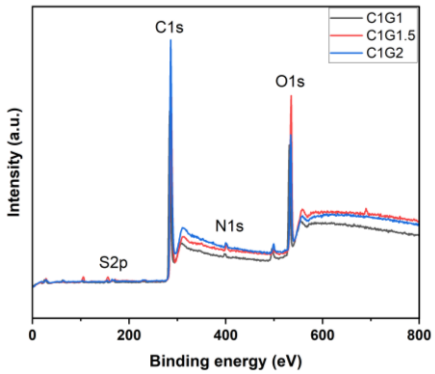

Fig. 5.2: XPS survey spectra of CNC/GQD inclusion complex

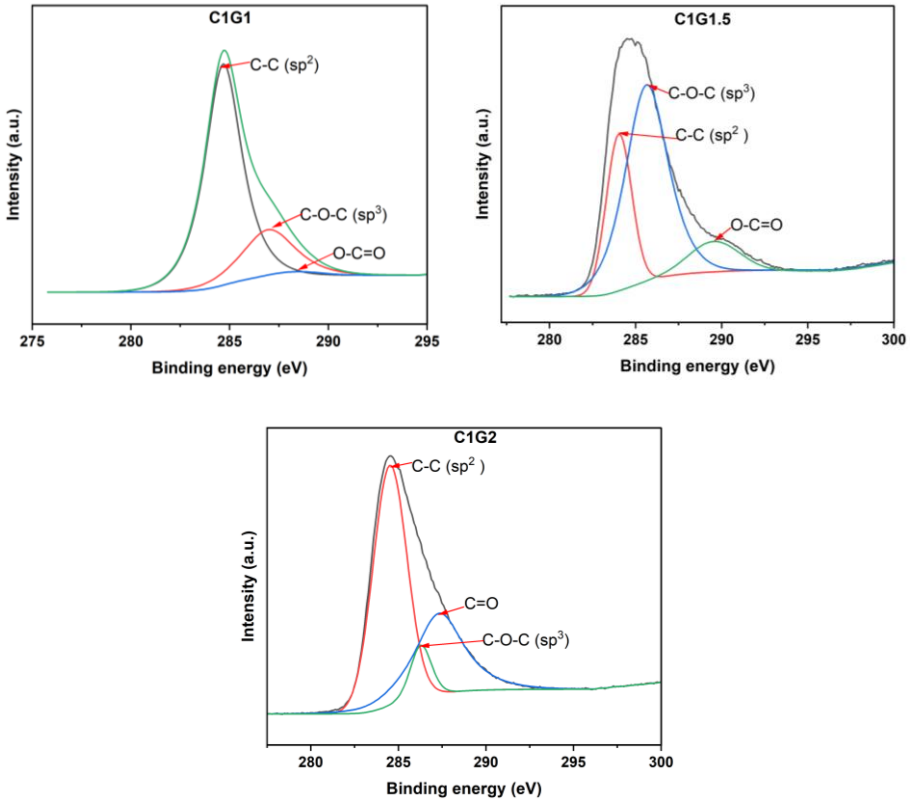

Fig. 5.3: High resolution C1s spectra of CNC/GQD inclusion complexes

But, in each case, the peak centers changed their positions slightly, indicating the covalent reaction between CNC and GQD. The presence of these oxygen containing groups facilitated the excellent dispersion of GQDs in water and acted as potential reaction sites for CNCs [180].

XRD Pattern Analysis of CNC/GQD Inclusion Complex

The crystallographic structure and crystallinity index of the CNC/GQD inclusion complex and pristine CNC were evaluated by XRD pattern analysis.

The interlayer spacing or d-spacing was calculated by using Bragg's equation:

$$n\times\lambda = 2\times d\sin\theta \quad \ldots\ldots(1)$$

where n is diffraction order, for first order n=1, λ is X-Ray wavelength, CuK_α = 1.5418 Å, d is interlayer spacing and θ is Bragg's angle.

The crystallite size was calculated using the Debye-Scherrer equation:

$$D = K\times\lambda / \beta\cos\theta \quad \ldots\ldots.(2)$$

Where D is the crystallite size, K is Scherrer constant, 0.94 for spherical crystallites with cubic symmetry, λ is the same X-Ray wavelength, β is line broadening at full width at half maximum (FWHM) and θ is Bragg's angle.

The XRD spectra of CNC showed three characteristic peaks of cellulose I, identified at 2θ = 16.34°, 22.53° and 34.47° of (110), (200) and (400) lattice planes [181]. According to the calculation of Bragg's equation, the interlayer spacing (d-spacing) of CNC was 0.394 nm. The average crystallize size was calculated using Debye-Scherrer formula and the crystallite size of CNC was 21.78 nm with a crystallinity index of 36.31%.

The XRD spectra of CNC/GQD inclusion complex showed intense and sharper peaks compared to pure CNC, which indicated the successful reaction between CNC and GQD [180]. The

diffraction peak of pure GQD corresponding to (002) plane overlapped with the (200) plane of CNC and the intensity of the peak increased, indicating the presence of a large number of oxygen-containing functional groups in the system [182], also known as size and edge effects of GQDs, which was previously confirmed from Raman spectroscopy and XPS analysis.

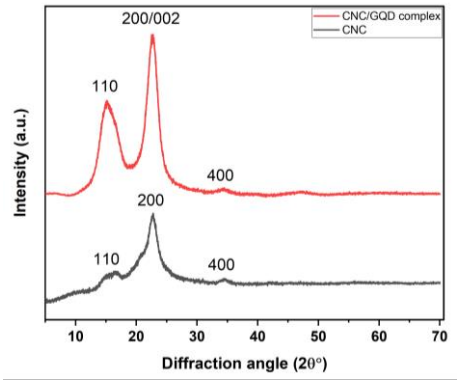

Fig. 5.4: X-Ray diffraction patterns of CNC and CNC/GQD inclusion complex

The average crystallite size of CNC/GQD inclusion complex was 33.30 nm with an average crystallinity index of 78.68%. Larger crystallite size indicated slower nucleation rate and faster growth rate which resulted in a higher degree of crystallinity [183]. Moreover, larger crystallite size and higher crystallinity index of the inclusion complex indicated better thermal stability of the system [], which is further confirmed in TGA analysis of composites.

Morphological Study of the Composites

Fig. 5.5 shows the SEM micrographs of the cryo-fractured composites cross-section. The untreated CNC incorporated composites showed agglomerations in the polymer matrix. On the other hand, the GQD incorporated composites showed an improved dispersion behavior indicated by the lack of agglomeration in the matrix.

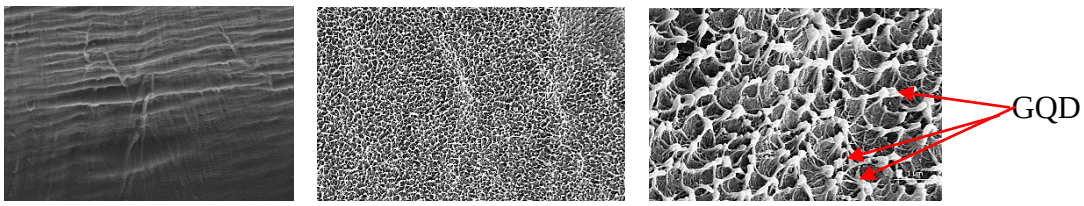

(a) (b) (c)

Fig. 5.5: SEM micrographs of the cryo-fractured cross-sections of (a) HDPE/CNC (2 μm), (b) HDPE/CNC/GQD (2 μm) and (c) HDPE/CNC/GQD (1 μm)

The fibrillar structure of the cross-section of the GQD incorporated composites indicated the separation and distribution of the CNCs throughout the matrix. In other research papers [164-167], the morphology of the produced hydrogels or thin films of CNC/GQD showed a similar fibrillar morphology, as shown here. In the case of composite production, the challenge of dispersion of nanomaterials is more difficult than thin film or hydrogel, as it is impossible to control the flow of the molten polymer and the fillers in the extruder. The recent research papers [168] which used pristine or doped GQD as a reinforcement, presented a similar morphology as the current research. In the present research, the interaction between CNC and GQD overcame the problem of agglomeration and showed synergistic behavior. The hydrogen bond formation between CNC and GQD and their mutual electrostatic repulsion helped to improve their dispersion in the composites [89].

Thermogravimetric Property Analysis

The effect of GQD incorporation on the thermal properties of HDPE was analyzed and the results were showed in Fig. 5.6 and table 5.5. The TGA curves demonstrated a single step degradation for all formulations. The thermal stability of the samples was analyzed by comparing the T_{onset}, T_{50}, T_{endset} values. T_{onset} represents the initial degradation temperature at which the

composites start degrading, T_{50} is the temperature at 50% weight loss and T_{endset} is the temperature at the end of degradation. The C1G0 composite, which only had pristine CNCs as filler material, showed no increase in T_{onset} because of the catalytic nature of the surface sulfate groups present in CNC. The incorporation of GQD exhibited a significantly higher T_{onset}, T_{50}, T_{endset} values compared to the neat HDPE and C1G0. The residual weight (%) of the GQD incorporated composites was also higher.

Table 5.5: Thermal properties of each formulation (CNC/GQD) from TGA

Sample code	T_{onset} (°C)	T_{50} (°C)	T_{endset} (°C)	Residue (wt%)
Neat HDPE	404.05	460.24	481.70	0.38
C1G0	405.23	462.82	481.80	0.49
C1G1	421.98	478.75	498.75	1.99
C1G1.5	424.83	481.12	500.45	2.86
C1G2	426.53	482.26	499.89	2.327

The improved dispersion of the nanofillers and uniformity of the nanocomposite structure are the key factors to improve the fire-resistant behavior of the composites. The incorporation of GQD enhanced the strength of the produced char layer, which in turn formed a protective barrier on the exposed polymer surface [184]. Also, graphene is capable of forming multiple and overlapped char layers which promote “labyrinth effect” or a tortuous path. This tortuous path delayed the exchange of heat/mass transfer in between the condensed and gaseous phases and improved the thermal stability of the composites [185]. Thus, the cycle of mass and heat transfer was interrupted. As a result, the polymer degradation slowed down.

Moreover, the oxygen containing groups of graphene, especially the carboxylate group, facilitated self-decomposition and dehydration at lower temperatures which can lead to adsorption of heat and cooling the polymer substrate. This phenomenon promoted the dilution of oxygen

concentration around the ignition atmosphere [186]. Therefore, the presence of GQD in the composites improved the overall thermal stability of the system.

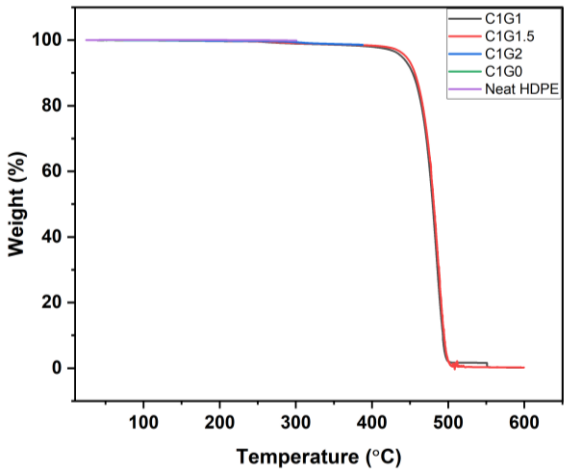

Fig. 5.6: TGA thermograms of Neat HDPE, untreated CNC incorporated HDPE and GQD incorporated composite samples

Crystallization Behavior Analysis of the Composites

The non-isothermal crystallization behavior of the HDPE composites was studied using DSC. The DSC results were shown in Fig. 5.7, and Table 5.6. The crystallinity (X_c) was determined by the following equation:

$$X_c\ (\%) = \Delta H_m \times 100 / \Delta H_m^0 \times (1\text{-}x) \qquad (3)$$

where ΔH_m is the melting enthalpy, ΔH_m^0 is the theoretical enthalpy of 100% crystalline HDPE (293 J g^{-1}), and x is the weight fraction of filler (CNC or CNC/GQD) [111].

Table 5.6: Crystallization behavior of each formulation from DSC

Sample code	T_c (°C)	T_m (°C)	Crystallinity (X_c) (%)
Neat HDPE	114.54	127.53	34.61
C1G0	115.38	126.31	39.42
C1G1	113.42	126.91	42.89
C1G1.5	112.77	126.72	43.73
C1G2	114.35	125.32	44.47

Incorporation of CNC as a filler in the HDPE matrix showed a slight increase in crystallinity (%). The potential reason behind this change is the nucleation effect of CNC which promoted heterogeneous nucleation. A heterogeneous nucleation mechanism was induced by the nanofillers which in turn decreased the free energy barrier and accelerated the crystallization process [110]. The confinement effect of nanocrystals hindered the chain diffusion and folding at the crystal growth front and formed thinner spherulites [112].

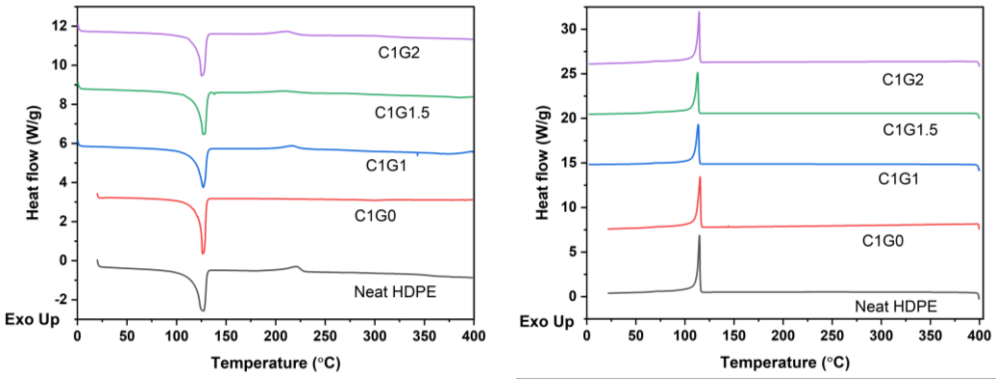

Fig. 5.7: DSC thermograms of composite samples of (a) heating cycle and (b) cooling cycle

The addition of GQD also slightly improved the crystallinity of the system compared to neat HDPE. The introduction of GQDs increased restricted mobility of the polymer chains,

indicating a better interfacial interaction between the filler and the polymer matrix. Here, GQD behaved as a dispersing agent and facilitated the dispersion and penetration of CNCs in the polymer matrix [187].

Dynamic Mechanical Behavior Analysis of the Composites

Dynamic viscoelastic properties such as storage modulus (E'), loss modulus (E") and loss factor (damping parameter, tan δ) were studied through dynamic mechanical analysis. The results were shown in Fig. 5.8 and table 5.7. For pure HDPE, a sharp α-transition peak was observed at around 68.5 ℃ in the storage modulus curve. In a semi-crystalline polymer like HDPE, the primary relaxation process or α-relaxation is associated with long range motion of chain segments, referred to as glass transition temperature (T_g) [130]. The GQD incorporated composites showed higher Tg, around 80°C. The higher Tg indicated the increased intermolecular forces, interchain attraction and cross-linking reaction between CNC and GQD due to the presence of oxygen-containing polar groups. This increased interaction reduced the free volume of the system, thus resulting in higher Tg []. Higher value of Tg also indicated better thermal stability [151], which is previously confirmed in TGA analysis.

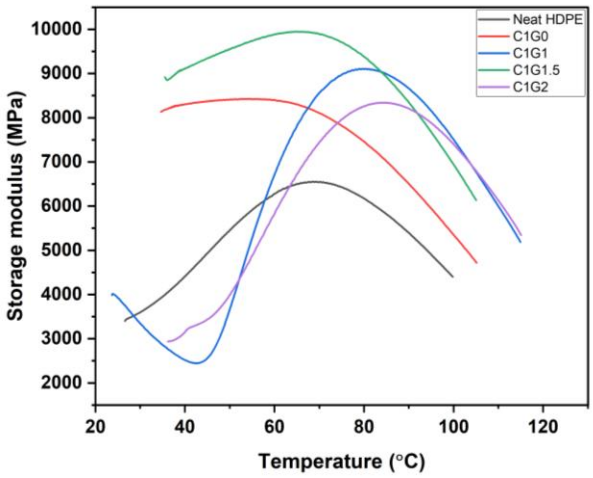

Fig. 5.8: Representative curves of storage modulus as a function of temperature of composite samples

The storage modulus of HDPE is 6462 MPa. The dynamic mechanical properties of the composites are largely dependent on the filler content. Incorporation of CNC increased the storage modulus value (9451.5 MPa) significantly (table 5.7 and Fig. 5.9). Incorporation of CNC makes the polymer chains less mobile, increases the flow resistance of HDPE and reduces the slippage between crystallites [151].

Table 5.7: Dynamic mechanical properties and mean comparison (Fisher LSD) of composites (p= 0.05)

Sample code	Mean	Groups	Groups
C1G1	9487	A	
C1G0	9451.5	A	
C1G2	9442	A	
C1G1.5	9297	A	
Neat HDPE	6462		B

Incorporation of GQD did not show any significant impact on the dynamic mechanical properties of the composites, compared to pristine CNC incorporated composites. Though the

mechanical properties are significantly higher than neat HDPE. Overall, there is a 46% increase in storage modulus for the composites compared to neat HDPE.

The elastic response ability of GQD incorporated composites decreased rapidly with the increase in temperature, after the transition region. At higher temperature, the graphene layers induced more slippage between the chains and enabled higher mobility of polymer chains [187]. On the other hand, the CNCs present in the inclusion complex hindered the chain slippage. Due to these two contradictory phenomena, the overall mechanical properties of the GQD induced composites did not improve.

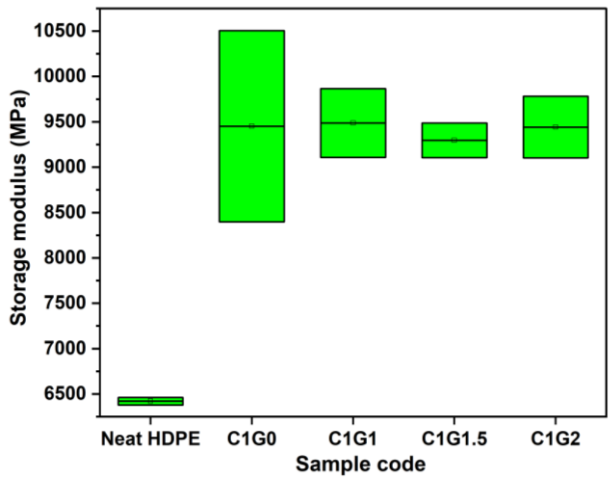

Fig. 5.9: Representative box plots of the statistical analysis of the storage modulus of the composite samples

Tensile Property Analysis of the Composites

The mechanical property analysis such as Young's modulus, elongation at break were investigated to gain an insight into the tensile behavior of the composites, the effect of CNC and GQD on the tensile properties and comparison of the tensile properties with neat HDPE. Theoretically, addition of CNC to a polymer matrix as a filler should improve the tensile properties

of the composites [122]. But, like all the nanofillers, there was difficulty while mixing the CNC with the polymer [150]. CNCs show a self-agglomeration behavior in the polymer matrix [151] which can play an important role for the tensile properties of the composites.

In the current research, CNC and GQD were incorporated in different ratios to observe and analyze their effect on the mechanical properties of HDPE polymer and the results are shown in Fig. 10 and table 5.8 and 5.9.

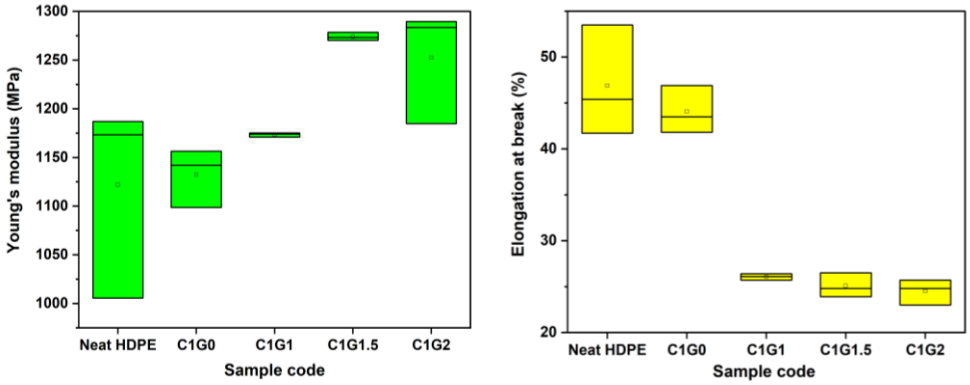

(a) (b)

Fig. 5.10: Representative box plots of statistical analysis of (a) elastic modulus and (b) elongation at break (%) of HDPE composites

In statistical analysis of the tensile properties of the composites, it can be observed that there is no significant difference in the elastic modulus of C1G0 composites and neat HDPE. This phenomenon can be attributed to the self-agglomeration behavior of CNC in the hydrophobic matrix, which reduced the filler/matrix interaction. Also, these agglomerations were responsible for the early failure of the system due to stress concentrations at specific regions [151].

Table 5.8: Young's modulus and mean comparison (Fisher LSD) of each formulation (CNC/GQD) (p= 0.05)

Sample code	Mean	Groups	Groups	Groups
C1G1.5	1273.932	A		
C1G2	1252.492	A	B	
C1G1	1173.307		B	C
C1G0	1132.331			C
Neat HDPE	1121.947			C

On the other hand, the GQD incorporated samples showed a significant improvement in the tensile properties of the composites. The filler/matrix interface, dispersion of the nanofillers and uniformity of the nanocomposite structure played a significant role in improvement of the tensile properties of the composites. Uniform dispersion of fillers leads to an effective stress transfer, producing a stronger composite [188].

Table 5.9: Elongation at break (%) and mean comparison (Fisher LSD) of each formulation (CNC/ GQD) (p= 0.05)

Sample code	Mean	Groups	Groups
Neat HDPE	46.86667	A	
C1G0	44.06667	A	
C1G1	26.06667		B
C1G1.5	25.06667		B
C1G2	24.5		B

In the SEM micrographs, there was no agglomeration present in the system and the composites had a uniform fibrillar structure. The lack of agglomeration and uniform distribution of fillers throughout the matrix helped to improve the elastic modulus of the system as well as decreasing the elongation at break (%) of the system. The incorporation of GQD made the composites more brittle, as the rigid nanofillers restricted planar motion and elongation [189].

Overall, there is 13% increase in elastic modulus and 47% decrease in elongation in case of GQD incorporated composites compared neat HDPE.

Electrical Impedance Spectra Analysis

One of the recent application areas of graphene-based materials is energy storage devices. High surface area, thermal and chemical stability, conductivity, and charge carrier mobility of graphene facilitate accumulation and charge storage, which is the fundamental requirement of energy storage devices. Graphene based materials can be used in the coatings of capacitor plates to produce an electric double layer coating [190]. GQD, a graphene-based material, is a potential candidate for energy storage devices in combination with CNC. The large number of functional groups present on the surface of GQD, such as -COOH, -OH, -NH_2, can perform as active coordination sites for transition metal ions [191]. GQD based energy storage device have electro-chemical double layer and adsorb charges on the surface of the electrodes [192]. On the other hand, CNC is biocompatible, eco-friendly, and thermally stable [193]. These intriguing properties of CNC/GQD composites should be explored in future to unlock their potential to be used as energy storage devices.

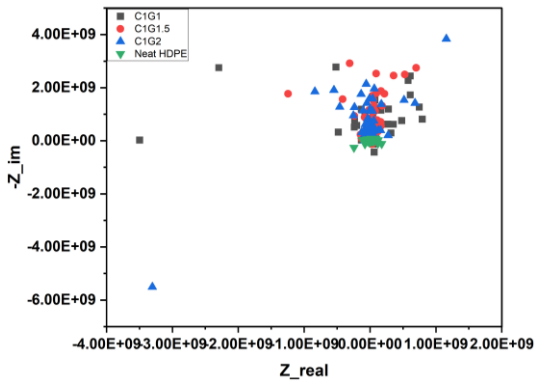

Fig. 5.11: Nyquist plot for electrical impedance spectra of neat HDPE and CNC/GQD composites

All the GQD induced composites and neat HDPE showed a purely capacitive AC electrical behavior. In an AC system for a capacitor, if the frequency is reduced that will lead to higher impedance value (Z). Therefore, at a very high frequency a capacitor has very less or no contribution towards Z, and at low frequency Z value becomes infinite. As a result, the Bode plot of an ideal capacitor shows a constant phase shift of 90° and a linear curve with a negative slope for Z [194]. In the current study, all the GQD induced composites and HDPE showed an average phase shift of 90° and a negative slope linear curve for Z (fig.5.12).

The limited imaginary component of impedance ($-Z_{im}$) was observed for all composites and HDPE in the Nyquist plot. For a purely capacitive behavior, the Nyquist plot showed a straight line for the imaginary component parallel to the ordinate [194], similar to the current study.

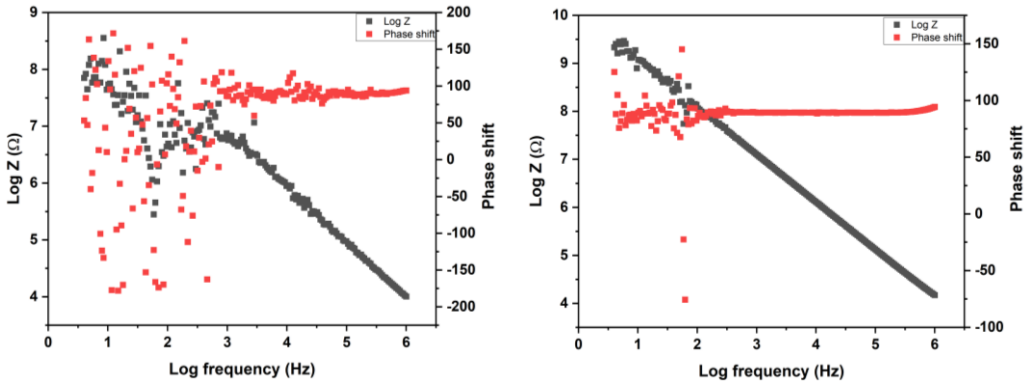

Fig. 5.12: Bode plot for electrical impedance spectra of (a) neat HDPE and (b) CNC/GQD composites

However, the GQD content being too small, no conductive response was observed for the composites. If the GQD content is increased, a continuous network structure will be generated to facilitate the formation of conductive path [195]. The potential of CNC/GQD composites as a capacitor can be explored further in future.

Conclusion

High density polyethylene (HDPE) is one of the most widely used commercial polymers. To improve the poor thermo-mechanical properties of HDPE, different types of bio-based nanofillers are incorporated. The most crucial challenge in nanocomposite production is the dispersion of nanofillers in the polymer matrix. In the current study, the role of GQD as a dispersing agent and its effect on the thermo-mechanical properties of the composites were investigated. In this research, CNC is successfully functionalized with GQD and CNC/GQD inclusion complex was used as filler/reinforcement to produce composites via melt blending extrusion process. The reaction between CNC and GQD was carefully studied and confirmed by

Raman spectroscopy, XPS and XRD analysis. The SEM micrographs of the cryo-fractured cross-sections of the composites showed a uniform dispersion of fillers and a lack of agglomeration in the system. The uniform dispersion of nanofillers and structural uniformity of the composites also helped in improving the thermal stability of the system, confirmed by the TGA analysis. The mechanical properties of the composites were improved due to the reinforcement effect of CNC/GQD inclusion complex. There is a 46% increase in storage modulus, 13% increase in elastic modulus and 47% decrease in elongation was observed in case of the GQD induced composites compared to neat HDPE. The electrical impedance spectra showed a purely capacitive response of GQD induced composites. Application of CNC/GQD inclusion complex as an energy storage device has a great potential and can be explored in future.

REFERENCES CITED

1. Kargarzadeh, Hanieh, et al. "Recent developments on nanocellulose reinforced polymer nanocomposites: A review." *Polymer* 132 (2017): 368-393.

2. Habibi, Youssef. "Key advances in the chemical modification of nanocelluloses." *Chemical Society Reviews* 43.5 (2014): 1519-1542.

3. Iwamoto, S., A. N. Nakagaito, and H. Yano. "Nano-fibrillation of pulp fibers for the processing of transparent nanocomposites." *Applied Physics A* 89.2 (2007): 461-466.

4. MoonRJ, MartiniA. "Cellulosenanomaterialsreview: structure, propertiesandnanocomposites." *ChemicalSocietyReviews* 40 (2011): 3941G3994.

5. Habibi, Youssef, Lucian A. Lucia, and Orlando J. Rojas. "Cellulose nanocrystals: chemistry, self-assembly, and applications." *Chemical reviews* 110.6 (2010): 3479-3500.

6. Angles, M. Neus, and Alain Dufresne. "Plasticized starch/tunicin whiskers nanocomposite materials. 2. Mechanical behavior." *Macromolecules* 34.9 (2001): 2921-2931.

7. Eichhorn, S. J., and G. R. Davies. "Modelling the crystalline deformation of native and regenerated cellulose." *Cellulose* 13.3 (2006): 291-307.

8. Velencoso, Maria M., et al. "Molecular firefighting—how modern phosphorus chemistry can help solve the challenge of flame retardancy." *Angewandte Chemie International Edition* 57.33 (2018): 10450-10467.

9. Davesne, Anne-Lise, et al. "Hexagonal Boron Nitride Platelet-Based Nanocoating for Fire Protection." *ACS Applied Nano Materials* 2.9 (2019): 5450-5459.

10. Lubczak, Renata, et al. "Preparation and characterization of boron-containing polyurethane foams with carbazole." *Polymer Testing* 70 (2018): 403-412.

11. Zarzyka, Iwona. "Foamed polyurethane plastics of reduced flammability." *Journal of Applied Polymer Science* 135.4 (2018): 45748.

12. Dick, C., et al. "The flammability of urethane-modified polyisocyanurates and its relationship to thermal degradation chemistry." *Polymer* 42.3 (2001): 913-923.

13. Bastin, B., R. Paleja, and Jérôme Lefebvre. "Fire behavior of polyurethane foams." *Journal of cellular plastics* 39.4 (2003): 323-340.

14. Price, Dennis, et al. "An investigation into the mechanism of flame retardancy and smoke suppression by melamine in flexible polyurethane foam." *Fire and materials* 26.4-5 (2002): 201-206.

15. Furukawa, Mutsuhisa, and Tetsuo Yokoyama. "Mechanical properties of organic–inorganic polyurethane elastomers. I. Al (OH) 3–polyurethane composites based on PPG." *Journal of applied polymer science* 53.13 (1994): 1723-1729.

16. Bourbigot, Serge, et al. "Recent advances in the use of zinc borates in flame retardancy of EVA." *Polymer degradation and stability* 64.3 (1999): 419-425.

17. Paciorek-Sadowska, Joanna. "Modification of PUR-PIR foams by boroorganic compound prepared on the basis of di (hydroxymethyl) urea." *Journal of Porous Materials* 19.2 (2012): 161-171.

18. Kicko-Walczak, Ewa. "Novel halogen-free flame retardants-flame retardation of unsaturated polyester resins with use of boron compounds." *Polimery* 53.2 (2008): 126-132.

19. Green, Joseph. "Mechanisms for flame retardancy and smoke suppression-a review." *Journal of Fire Sciences* 14.6 (1996): 426-442.

20. LeVan, Susan L., and Hao C. Tran. "The role of boron in flame-retardant treatments." *First International Conference on Wood Protection with Diffusible Preservatives:... Nashville, Tennessee, November 28-30, 1990. Madison, WI: Forest Products Research Society, 1990.: p. 39-41: ill.*. 1990.

21. Ishii, Toshiaki, et al. "Calcium borate flame retardation system for epoxy molding compounds." *Polymer Engineering & Science* 46.6 (2006): 799-806.

22. Lubczak, Renata, et al. "Preparation and characterization of boron-containing polyurethane foams with carbazole." *Polymer Testing* 70 (2018): 403-412.

23. Chmiel, Ewelina, and Jacek Lubczak. "Polyurethane foams with 1, 3, 5-triazine ring, boron and silicon." *Journal of Cellular Plastics* 56.2 (2020): 187-205.

24. Chmiel, Ewelina, Rafał Oliwa, and Jacek Lubczak. "Boron-containing non-flammable polyurethane foams." *Polymer-Plastics Technology and Materials* 58.4 (2019): 394-404.

25. Patil, Deepak M., Ganesh A. Phalak, and Shashank T. Mhakse. "Boron-containing UV-curable oligomer-based linseed oil as flame-retardant coatings: Synthesis and characterization." *Iranian Polymer Journal* 27.10 (2018): 795-806.

26. Morelli, Carolina L., et al. "Supramolecular aromatic interactions to enhance biodegradable film properties through incorporation of functionalized cellulose nanocrystals." *Composites Part A: Applied Science and Manufacturing* 83 (2016): 80-88.

27. Ansari, Farhan, and Lars A. Berglund. "Toward semistructural cellulose nanocomposites: the need for scalable processing and interface tailoring." *Biomacromolecules* 19.7 (2018): 2341-2350.

28. Fu, Lina, Jin Zhang, and Guang Yang. "Present status and applications of bacterial cellulose-based materials for skin tissue repair." *Carbohydrate polymers* 92.2 (2013): 1432-1442.

29. Mohammadkazemi, Faranak, Mehrdad Azin, and Alireza Ashori. "Production of bacterial cellulose using different carbon sources and culture media." *Carbohydrate polymers* 117 (2015): 518-523.

30. Kuo, Chia-Hung, et al. "Utilization of acetate buffer to improve bacterial cellulose production by Gluconacetobacter xylinus." *Food Hydrocolloids* 53 (2016): 98-103.

31. Czaja, Wojciech, Dwight Romanovicz, and R. Malcolm Brown. "Structural investigations of microbial cellulose produced in stationary and agitated culture." *Cellulose* 11.3-4 (2004): 403-411.

32. Nimeskern, Luc, et al. "Mechanical evaluation of bacterial nanocellulose as an implant material for ear cartilage replacement." *Journal of the mechanical behavior of biomedical materials* 22 (2013): 12-21.

33. MoonRJ, MartiniA."Cellulose nanomaterials review:structure, properties and nanocomposites." *Chemical Society Reviews* 40 (2011): 3941-3994.

34. Bauer, Siegfried, et al. "25th anniversary article: A soft future: From robots and sensor skin to energy harvesters." *Advanced Materials* 26.1 (2014): 149-162.

35. Mallick, P.K. “Fiber Reinforced Composites Materials, Manufacturing and design.”

36. Chungm, D. D. L. "Composite Material Science and Application." *Spring Verlag, London* (2010).

37. Kargarzadeh, Hanieh, et al. "Recent developments on nanocellulose reinforced polymer nanocomposites: A review." *Polymer* 132 (2017): 368-393.

38. Wang, Lu, et al. "Spray-dried cellulose nanofibril-reinforced polypropylene composites for extrusion-based additive manufacturing: nonisothermal crystallization kinetics and thermal expansion." *Journal of Composites Science* 2.1 (2018): 7.

39. Paul, Donald R., and Lioyd M. Robeson. "Polymer nanotechnology: nanocomposites." *Polymer* 49.15 (2008): 3187-3204.

40. Yano, Hiroyuki, et al. "Designing cellulose nanofiber surface for high density polyethylene reinforcement." *Cellulose* 25.6 (2018): 3351-3362.

41. Habibi, Youssef, Lucian A. Lucia, and Orlando J. Rojas. "Cellulose nanocrystals: chemistry, self-assembly, and applications." *Chemical reviews* 110.6 (2010): 3479-3500.

42. Moon, Robert J., et al. "Cellulose nanomaterials review: structure, properties and nanocomposites." *Chemical Society Reviews* 40.7 (2011): 3941-3994.

43. Rol, Fleur, et al. "Recent advances in surface-modified cellulose nanofibrils." *Progress in Polymer Science* 88 (2019): 241-264.

44. Islam, Mohammad Tajul, Mohammad Mahbubul Alam, and Marina Zoccola. "Review on modification of nanocellulose for application in composites." *Int J Innov Res Sci Eng Technol* 2.10 (2013): 5444-5451.

45. Missoum, Karim, Mohamed Naceur Belgacem, and Julien Bras. "Nanofibrillated cellulose surface modification: a review." *Materials* 6.5 (2013): 1745-1766.

46. Anirudhan, Thayyath Sreenivasan, and Sylaja Raveendran Rejeena. "Selective adsorption of hemoglobin using polymer-grafted-magnetite nanocellulose composite." *Carbohydrate polymers* 93.2 (2013): 518-527.

47. Wang, Hai-Dong, et al. "Graft modification of crystalline nanocellulose by Cu (0)-mediated SET living radical polymerization." *Journal of Polymer Science Part A: Polymer Chemistry* 53.24 (2015): 2800-2808.

48. Benkaddour, Abdelhaq, et al. "Grafting of polycaprolactone on oxidized nanocelluloses by click chemistry." *Nanomaterials* 3.1 (2013): 141-157.

49. Castellano, M., et al. "Modification of cellulose fibres with organosilanes: Under what conditions does coupling occur?." *Journal of colloid and interface science* 273.2 (2004): 505-511.

50. Pohl, E. R., and F. D. Osterholtz. "Kinetics and mechanism of aqueous hydrolysis and condensation of alkyltrialkoxysilanes." *Molecular Characterization of Composite Interfaces*. Springer, Berlin, Heidelberg, 1985. 157-170.

51. Salon, Marie-Christine B., et al. "Studies of interactions between silane coupling agents and cellulose fibers with liquid and solid-state NMR." *Magnetic Resonance in Chemistry* 45.6 (2007): 473-483.

52. Xu, Pengwu, et al. "Effects of modified nanocrystalline cellulose on the hydrophilicity, crystallization and mechanical behaviors of poly (3-hydroxybutyrate-co-3-hydroxyhexanoate)." *New Journal of Chemistry* 42.14 (2018): 11972-11978.

53. de Oliveira Taipina, Marcia, et al. "Surface modification of cotton nanocrystals with a silane agent." *Cellulose* 20.1 (2013): 217-226.

54. Salon, Marie-Christine B., et al. "Studies of interactions between silane coupling agents and cellulose fibers with liquid and solid-state NMR." *Magnetic Resonance in Chemistry* 45.6 (2007): 473-483.

55. Qian, Shaoping, et al. "Improved properties of PLA biocomposites toughened with bamboo cellulose nanowhiskers through silane modification." *Journal of Materials Science* 53.15 (2018): 10920-10932.

56. Dhar, Prodyut, et al. "Acid functionalized cellulose nanocrystals and its effect on mechanical, thermal, crystallization and surfaces properties of poly (lactic acid) bionanocomposites films: A comprehensive study." *Polymer* 101 (2016): 75-92.

57. Morelli, Carolina L., et al. "Supramolecular aromatic interactions to enhance biodegradable film properties through incorporation of functionalized cellulose nanocrystals." *Composites Part A: Applied Science and Manufacturing* 83 (2016): 80-88.

58. Peng, Shane X., et al. "Enhanced dispersion and properties of a two-component epoxy nanocomposite using surface modified cellulose nanocrystals." *Polymer* 112 (2017): 359-368.

59. Shojaeiarani, Jamileh, Dilpreet S. Bajwa, and Nicole M. Stark. "Green esterification: A new approach to improve thermal and mechanical properties of poly (lactic acid) composites reinforced by cellulose nanocrystals." *Journal of applied polymer science* 135.27 (2018): 46468.

60. Shojaeiarani, Jamileh, Dilpreet S. Bajwa, and Kerry Hartman. "Esterified cellulose nanocrystals as reinforcement in poly (lactic acid) nanocomposites." *Cellulose* 26.4 (2019): 2349-2362.

61. Shojaeiarani, Jamileh, et al. "Rheological properties of cellulose nanocrystals engineered polylactic acid nanocomposites." *Composites Part B: Engineering* 161 (2019): 483-489.

62. Taschuk, Michael T., Matthew M. Hawkeye, and M. J. Brett. "Handbook of Deposition Technologies for Films and Coatings." *Elsevier* 2010 (2010): 621-678.

63. Vander Wielen, L. C., et al. "Surface modification of cellulosic fibers using dielectric-barrier discharge." *Carbohydrate polymers* 65.2 (2006): 179-184.

64. Pertile, Renata AN, et al. "Surface modification of bacterial cellulose by nitrogen-containing plasma for improved interaction with cells." *Carbohydrate Polymers* 82.3 (2010): 692-698.

65. Flynn, C. N., C. P. Byrne, and B. J. Meenan. "Surface modification of cellulose via atmospheric pressure plasma processing in air and ammonia–nitrogen gas." *Surface and Coatings Technology* 233 (2013): 108-118.

66. Bhanthumnavin, W., et al. "Surface modification of bacterial cellulose membrane by oxygen plasma treatment." *Surface and Coatings Technology* 306 (2016): 272-278.

67. Couturaud, Benoit, et al. "Improvement of the interfacial compatibility between cellulose and poly (L-lactide) films by plasma-induced grafting of L-lactide: The evaluation of the adhesive properties using a peel test." *Journal of colloid and interface science* 448 (2015): 427-436.

68. Senthilnathan, Jaganathan, et al. "Submerged liquid plasma for the synchronized reduction and functionalization of graphene oxide." *Scientific reports* 4.1 (2014): 1-7.

69. Ramos-deValle, L. F., M. G. Neira-Velázquez, and E. Hernández-Hernández. "Surface modification of CNFs via plasma polymerization of styrene monomer and its effect on the properties of PS/CNF nanocomposites." *Journal of Applied Polymer Science* 107.3 (2008): 1893-1899.

70. Alanis, Andrés, et al. "Plasma surface-modification of cellulose nanocrystals: a green alternative towards mechanical reinforcement of ABS." *RSC advances* 9.30 (2019): 17417-17424.

71. Vizireanu, Sorin, et al. "Cellulose defibrillation and functionalization by plasma in liquid treatment." *Scientific reports* 8.1 (2018): 1-14.

72. Panaitescu, Denis Mihaela, et al. "Treatment of nanocellulose by submerged liquid plasma for surface functionalization." *Nanomaterials* 8.7 (2018): 467.

73. Panaitescu, Denis Mihaela, et al. "Poly (3-hydroxybutyrate) modified by nanocellulose and plasma treatment for packaging applications." *Polymers* 10.11 (2018): 1249.

74. Beuguel, Quentin, et al. "Ultrasonication of spray-and freeze-dried cellulose nanocrystals in water." *Journal of colloid and interface science* 516 (2018): 23-33.

75. Cao, Yizheng, et al. "The relationship between cellulose nanocrystal dispersion and strength." *Construction and Building Materials* 119 (2016): 71-79.

76. Li, Wei, et al. "Nanocellulose fibrils isolated from BHKP using ultrasonication and their reinforcing properties in transparent poly (vinyl alcohol) films." *Journal of Polymer Research* 20.8 (2013): 210.

77. Sinclair, Alexander, et al. "Cellulose nanofibers produced from various agricultural residues and their reinforcement effects in polymer nanocomposites." *Journal of Applied Polymer Science* 135.21 (2018): 46304.

78. Szymańska-Chargot, M., et al. "Effect of ultrasonication on physicochemical properties of apple based nanocellulose-calcium carbonate composites." *Cellulose* 25.8 (2018): 4603-4621.

79. Syafri, Edi, et al. "Effect of sonication time on the thermal stability, moisture absorption, and biodegradation of water hyacinth (Eichhornia crassipes) nanocellulose-filled bengkuang (Pachyrhizus erosus) starch biocomposites." *Journal of Materials Research and Technology* 8.6 (2019): 6223-6231.

80. Septevani, Athanasia A., et al. "The use of cellulose nanocrystals to enhance the thermal insulation properties and sustainability of rigid polyurethane foam." *Industrial crops and products* 107 (2017): 114-121.

81. Shojaeiarani, Jamileh, Dilpreet Bajwa, and Greg Holt. "Sonication amplitude and processing time influence the cellulose nanocrystals morphology and dispersion." *Nanocomposites* (2020): 1-6.

82. Haywood, A. D., R. W. Ashurst, and V. A. Davis. "Controlling Alignment in Cellulose Nanocrystal Coatings."

83. Li, Dongsheng, et al. "Magnetic alignment of cellulose nanowhiskers in an all-cellulose composite." *Polymer bulletin* 65.6 (2010): 635-642.

84. De France, Kevin J., et al. "Cooperative ordering and kinetics of cellulose nanocrystal alignment in a magnetic field." *Langmuir* 32.30 (2016): 7564-7571.

85. Pullawan, Tanittha, Arthur N. Wilkinson, and Stephen J. Eichhorn. "Influence of magnetic field alignment of cellulose whiskers on the mechanics of all-cellulose nanocomposites." *Biomacromolecules* 13.8 (2012): 2528-2536.

86. Tatsumi, Mio, et al. "Anisotropic polymer composites synthesized by immobilizing cellulose nanocrystal suspensions specifically oriented under magnetic fields." *Biomacromolecules* 15.12 (2014): 4579-4589.

87. Kadimi, Amal, et al. "Electric field alignment of nanofibrillated cellulose (NFC) in silicone oil: Impact on electrical properties." *ACS applied materials & interfaces* 6.12 (2014): 9418-9425.

88. Habibi, Youssef, Thomas Heim, and Roger Douillard. "AC electric field-assisted assembly and alignment of cellulose nanocrystals." *Journal of Polymer Science Part B: Polymer Physics* 46.14 (2008): 1430-1436.

89. Ten, Elena, Long Jiang, and Michael P. Wolcott. "Preparation and properties of aligned poly (3-hydroxybutyrate-co-3-hydroxyvalerate)/cellulose nanowhiskers composites." *Carbohydrate polymers* 92.1 (2013): 206-213.

90. Lee, Jeremy Kong Yoong, et al. "Polymer-based composites by electrospinning: Preparation & functionalization with nanocarbons." *Progress in Polymer Science* (2018).

91. Cai, Jie, et al. "Well-aligned cellulose nanofiber-reinforced polyvinyl alcohol composite film: mechanical and optical properties." *Carbohydrate polymers* 140 (2016): 238-245.

92. He, Xu, et al. "Uniaxially aligned electrospun all-cellulose nanocomposite nanofibers reinforced with cellulose nanocrystals: scaffold for tissue engineering." *Biomacromolecules* 15.2 (2014): 618-627.

93. Liao, Huaqiang, et al. "Aligned electrospun cellulose fibers reinforced epoxy resin composite films with high visible light transmittance." *Cellulose* 19.1 (2012): 111-119.

94. Song, Weiguang, et al. "Fiber alignment and liquid crystal orientation of cellulose nanocrystals in the electrospun nanofibrous mats." *Biomacromolecules* 18.10 (2017): 3273-3279.

95. Lee, Won Jun, et al. "Strong and stiff: high-performance cellulose nanocrystal/poly (vinyl alcohol) composite fibers." *ACS applied materials & interfaces* 8.46 (2016): 31500-31504.

96. Wang, Baochun, et al. "Aligned bioinspired cellulose nanocrystal-based nanocomposites with synergetic mechanical properties and improved hygromechanical performance." *ACS applied materials & interfaces* 7.8 (2015): 4595-4607.

97. Singh, Anshu Anjali, et al. "Aligned plasticized polylactic acid cellulose nanocomposite tapes: Effect of drawing conditions." *Composites Part A: Applied Science and Manufacturing* 104 (2018): 101-107.

98. Wang, Sha, et al. "Super-Strong, Super-Stiff Macrofibers with Aligned, Long Bacterial Cellulose Nanofibers." *Advanced Materials* 29.35 (2017): 1702498.

99. Sehaqui, Houssine, et al. "Cellulose nanofiber orientation in nanopaper and nanocomposites by cold drawing." *ACS applied materials & interfaces* 4.2 (2012): 1043-1049.

100. Ahmed, Syed Rahin, Joseph Cirone, and Aicheng Chen. "Fluorescent Fe3O4 quantum dots for H2O2 detection." *ACS Applied Nano Materials* 2.4 (2019): 2076-2085.

101. Huang, Yanyan, Jinsong Ren, and Xiaogang Qu. "Nanozymes: classification, catalytic mechanisms, activity regulation, and applications." *Chemical reviews* 119.6 (2019): 4357-4412.

102. Abitbol, Tiffany, et al. "Hybrid fluorescent nanoparticles from quantum dots coupled to cellulose nanocrystals." *Cellulose* 24.3 (2017): 1287-1293.

103. Li, Xiaowan, and Yingcheng Hu. "Luminescent films functionalized with cellulose nanofibrils/CdTe quantum dots for anti-counterfeiting applications." *Carbohydrate polymers* 203 (2019): 167-175.

104. Wang, Qinwen, et al. "A tunable photoluminescent composite of cellulose nanofibrils and CdS quantum dots." *Nanomaterials* 6.9 (2016): 164.

105. Zhu, Shoujun, et al. "The photoluminescence mechanism in carbon dots (graphene quantum dots, carbon nanodots, and polymer dots): current state and future perspective." *Nano research* 8.2 (2015): 355-381.

106. Zhu, Shoujun, et al. "The photoluminescence mechanism in carbon dots (graphene quantum dots, carbon nanodots, and polymer dots): current state and future perspective." *Nano research* 8.2 (2015): 355-381.

107. Sekiya, Ryo, et al. "White-Light-Emitting Edge-Functionalized Graphene Quantum Dots." *Angewandte Chemie* 126.22 (2014): 5725-5729.

108. Sekiya, Ryo, et al. "White-Light-Emitting Edge-Functionalized Graphene Quantum Dots." *Angewandte Chemie* 126.22 (2014): 5725-5729.

109. Khabibullin, Amir, et al. "Injectable shear-thinning fluorescent hydrogel formed by cellulose nanocrystals and graphene quantum dots." *Langmuir* 33.43 (2017): 12344-12350.

110. Guo, Jiaqi, et al. "Photoluminescent hybrids of cellulose nanocrystals and carbon quantum dots as cytocompatible probes for in vitro bioimaging." *Biomacromolecules* 18.7 (2017): 2045-2055.

111. Junka, Karoliina, et al. "Modification of cellulose nanofibrils with luminescent carbon dots." *Biomacromolecules* 15.3 (2014): 876-881.

112. 112. Junka, Karoliina, et al. "Modification of cellulose nanofibrils with luminescent carbon dots." *Biomacromolecules* 15.3 (2014): 876-881.

113. Rol, Fleur, et al. “Recent advances in surface-modified cellulose nanofibrils.” *Progress in Polymer Science* 88 (2019): 241-264.

114. Xu, Pengwu, et al. "Effects of modified nanocrystalline cellulose on the hydrophilicity, crystallization and mechanical behaviors of poly (3-hydroxybutyrate-co-3-hydroxyhexanoate)." *New Journal of Chemistry* 42.14 (2018): 11972-11978.

115. de Oliveira Taipina, Marcia, et al. "Surface modification of cotton nanocrystals with a silane agent." *Cellulose* 20 (2013): 217-226.

116. Qian, Shaoping, et al. "Improved properties of PLA biocomposites toughened with bamboo cellulose nanowhiskers through silane modification." *Journal of Materials Science* 53 (2018): 10920-10932.

117. Yin, Yuanyuan, et al. "Cellulose nanocrystals functionalized with amino-silane and epoxy-poly (ethylene glycol) for reinforcement and flexibilization of poly (lactic acid): material preparation and compatibility mechanism." *Cellulose* 25 (2018): 6447-6463.

118. Shojaeiarani, Jamileh, Dilpreet Bajwa, and Greg Holt. "Sonication amplitude and processing time influence the cellulose nanocrystals morphology and dispersion." *Nanocomposites* 6.1 (2020): 41-46.

119. Eriksson, Maria, et al. "The influence of grafting on flow-induced crystallization and rheological properties of poly (ε-caprolactone)/cellulose nanocrystal nanocomposites." *Nanocomposites* 4.3 (2018): 87-101.

120. Pechová, Veronika, et al. "Development of orodispersible films containing benzydamine hydrochloride using a modified solvent casting method." *AAPS PharmSciTech* 19 (2018): 2509-2518.

121. Wang, Long-Feng, Jong-Whan Rhim, and Seok-In Hong. "Preparation of poly (lactide)/poly (butylene adipate-co-terephthalate) blend films using a solvent casting method and their food packaging application." *LWT-Food Science and Technology* 68 (2016): 454-461.

122. Pucić, Irina, and Tanja Jurkin. "FTIR assessment of poly (ethylene oxide) irradiated in solid state, melt and aqeuous solution." *Radiation Physics and Chemistry* 81.9 (2012): 1426-1429.

123. Sato, Harumi, et al. "Crystal structures, thermal behaviors, and CH center dot center dot center dot O= C hydrogen bondings of poly (3-hydroxyvalerate) and poly (3-

hydroxybutyrate) studied by infrared spectroscopy and X-ray diffraction." *Macromolecules* 41.12 (2008): 4305-4312.

124. Frone, Adriana N., et al. "Morphology and thermal properties of PLA–cellulose nanofibers composites." *Carbohydrate polymers* 91.1 (2013): 377-384.

125. Xu, Xuezhu, et al. "Cellulose nanocrystals vs. cellulose nanofibrils: a comparative study on their microstructures and effects as polymer reinforcing agents." *ACS applied materials & interfaces* 5.8 (2013): 2999-3009.

126. Salon, Marie-Christine B., et al. "Studies of interactions between silane coupling agents and cellulose fibers with liquid and solid-state NMR." *Magnetic Resonance in Chemistry* 45.6 (2007): 473-483.

127. Shojaeiarani, Jamileh, et al. "Rheological properties of cellulose nanocrystals engineered polylactic acid nanocomposites." *Composites Part B: Engineering* 161 (2019): 483-489.

128. Andersons, J., E. Spārniņš, and Roberts Joffe. "Stiffness and strength of flax fiber/polymer matrix composites." *Polymer Composites* 27.2 (2006): 221-229.

129. Peijs, Ton, et al. "Thermoplastic composites based on flax fibres and polypropylene: Influence of fibre length and fibre volume fraction on mechanical properties." *Macromolecular Symposia*. Vol. 127. No. 1. Basel: Hüthig & Wepf Verlag, 1998.

130. Bajwa, Dilpreet S., et al. "Role of hybrid nano-zinc oxide and cellulose nanocrystals on the mechanical, thermal, and flammability properties of poly (lactic acid) polymer." *Journal of Composites Science* 5.2 (2021): 43.

131. Shojaeiarani, Jamileh, Dilpreet S. Bajwa, and Nicole M. Stark. "Spin-coating: A new approach for improving dispersion of cellulose nanocrystals and mechanical properties of poly (lactic acid) composites." *Carbohydrate polymers* 190 (2018): 139-147.

132. Iyer, Krishnan A., Gregory T. Schueneman, and John M. Torkelson. "Cellulose nanocrystal/polyolefin biocomposites prepared by solid-state shear pulverization: Superior dispersion leading to synergistic property enhancements." *Polymer* 56 (2015): 464-475.

133. Orr, Matthew P., and Meisha L. Shofner. "Processing strategies for cellulose nanocrystal/polyethylene-co-vinyl alcohol composites." *Polymer* 126 (2017): 211-223.

134. Rahimi, Shahab Kashani, and Joshua U. Otaigbe. "The effects of the interface on microstructure and rheo-mechanical properties of polyamide 6/cellulose nanocrystal nanocomposites prepared by in-situ ring-opening polymerization and subsequent melt extrusion." *Polymer* 127 (2017): 269-285.

135. Bitinis, Natacha, et al. "Poly (lactic acid)/natural rubber/cellulose nanocrystal bionanocomposites Part I. Processing and morphology." *Carbohydrate polymers* 96.2 (2013): 611-620.

136. Ma, Libo, et al. "Preparing cellulose nanocrystal/acrylonitrile-butadiene-styrene nanocomposites using the master-batch method." *Carbohydrate polymers* 125 (2015): 352-359.

137. Codou, Amandine, et al. "Preparation and crystallization behavior of poly (ethylene 2, 5-furandicarboxylate)/cellulose composites by twin screw extrusion." *Carbohydrate polymers* 174 (2017): 1026-1033.

138. Shojaeiarani, Jamileh, Dilpreet S. Bajwa, and Nicole M. Stark. "Spin-coating: A new approach for improving dispersion of cellulose nanocrystals and mechanical properties of poly (lactic acid) composites." *Carbohydrate polymers* 190 (2018): 139-147.

139. Zheng, Ting, et al. "PHBV-graft-GMA via reactive extrusion and its use in PHBV/nanocellulose crystal composites." *Carbohydrate polymers* 205 (2019): 27-34.

140. Inai, N. H., et al. "Interfaces in polyethylene oxide modified cellulose nanocrystal-polyethylene matrix composites." *Composites Science and Technology* 154 (2018): 128-135.

141. Gray, Narges, et al. "Influence of cellulose nanocrystal on strength and properties of low density polyethylene and thermoplastic starch composites." *Industrial Crops and Products* 115 (2018): 298-305.

142. Zheng, Ting, and Srikanth Pilla. "Melt processing of cellulose nanocrystal-filled composites: toward reinforcement and foam nucleation." *Industrial & Engineering Chemistry Research* 59.18 (2020): 8511-8531.

143. Nagalakshmaiah, Malladi, Nadia El Kissi, and Alain Dufresne. "Ionic compatibilization of cellulose nanocrystals with quaternary ammonium salt and their melt extrusion with polypropylene." *ACS applied materials & interfaces* 8.13 (2016): 8755-8764.

144. Kim, Taeho, et al. "Trans crystallization behavior and strong reinforcement effect of cellulose nanocrystals on reinforced poly (butylene succinate) nanocomposites." *RSC advances* 8.28 (2018): 15389-15398.

145. Li, Luyao, et al. "Preparation of polylactic acid/TEMPO-oxidized bacterial cellulose nanocomposites for 3D printing via Pickering emulsion approach." *Composites Communications* 16 (2019): 162-167.

146. Feng, Chiao, and Sheng-Sheng Yu. "3D printing of thermal insulating polyimide/cellulose nanocrystal composite aerogels with low dimensional shrinkage." *Polymers* 13.21 (2021): 3614.

147. Zheng, Ting, Craig M. Clemons, and Srikanth Pilla. "Comparative study of direct compounding, coupling agent-aided and initiator-aided reactive extrusion to prepare cellulose nanocrystal/PHBV (CNC/PHBV) nanocomposite." *ACS Sustainable Chemistry & Engineering* 8.2 (2019): 814-822.

148. Richardson, Joseph J., et al. "Continuous metal–organic framework biomineralization on cellulose nanocrystals: extrusion of functional composite filaments." *ACS Sustainable Chemistry & Engineering* 7.6 (2019): 6287-6294.

149. Leite, Liliane Samara Ferreira, et al. "Morphological investigation of cellulose acetate/cellulose nanocrystal composites obtained by melt extrusion." *Journal of Applied Polymer Science* 133.44 (2016).

150. Fallon, J. J., et al. "Mechanically adaptive thermoplastic polyurethane/cellulose nanocrystal composites: Process-driven structure–property relationships." *Journal of Applied Polymer Science* 136.4 (2019): 46992.

151. Liu, Yuzhu, and Laurent M. Matuana. "Surface texture and barrier performance of poly (lactic acid)–cellulose nanocrystal extruded-cast films." *Journal of Applied Polymer Science* 136.22 (2019): 47594.

152. Gupta, Anju, et al. "Rheological and thermo-mechanical properties of poly (lactic acid)/lignin-coated cellulose nanocrystal composites." *ACS Sustainable Chemistry & Engineering* 5.2 (2017): 1711-1720.

153. Wei, Liqing, et al. "Nanocomposites from lignin-containing cellulose nanocrystals and poly (lactic acid)." *Society of plastic engineers, ISBN* (2017): 978-0.

154. Feng, Xinhao, et al. "Lignin-coated cellulose nanocrystal filled methacrylate composites prepared via 3D stereolithography printing: Mechanical reinforcement and thermal stabilization." *Carbohydrate polymers* 169 (2017): 272-281.

155. Mohanty, Amar Kumar, Manjusri Misra, and L. T. Drzal. "Sustainable bio-composites from renewable resources: opportunities and challenges in the green materials world." *Journal of Polymers and the Environment* 10 (2002): 19-26.

156. Faruk, Omar, et al. "Biocomposites reinforced with natural fibers: 2000–2010." *Progress in polymer science* 37.11 (2012): 1552-1596.

157. Beck-Candanedo, Stephanie, Maren Roman, and Derek G. Gray. "Effect of reaction conditions on the properties and behavior of wood cellulose nanocrystal suspensions." *Biomacromolecules* 6.2 (2005): 1048-1054.

158. Saito, Tsuguyuki, et al. "Cellulose nanofibers prepared by TEMPO-mediated oxidation of native cellulose." *Biomacromolecules* 8.8 (2007): 2485-2491.

159. Kamal, Musa R., and Vahid Khoshkava. "Effect of cellulose nanocrystals (CNC) on rheological and mechanical properties and crystallization behavior of PLA/CNC nanocomposites." *Carbohydrate polymers* 123 (2015): 105-114.

160. Wei, Liqing, and Armando G. McDonald. "A review on grafting of biofibers for biocomposites." *Materials* 9.4 (2016): 303.

161. Wei, Liqing, et al. "Modification of cellulose nanocrystals (CNCs) for use in poly (lactic acid)(PLA)-CNC composite packaging products." *Proceedings, Forest Products Society International Convention*. 2016.

162. Bengtsson, Magnus, Paul Gatenholm, and Kristiina Oksman. "The effect of crosslinking on the properties of polyethylene/wood flour composites." *Composites Science and Technology* 65.10 (2005): 1468-1479.

163. Liu, Quanyi, et al. "Recent advances in the flame retardancy role of graphene and its derivatives in epoxy resin materials." *Composites Part A: Applied Science and Manufacturing* 149 (2021): 106539.

164. Lv, Jinling, et al. "Graphene oxide-cellulose nanocrystal (GO-CNC) composite functionalized PVDF membrane with improved antifouling performance in MBR: Behavior and mechanism." *Chemical Engineering Journal* 352 (2018): 765-773.

165. Kumar, Sunil, Sweety Supriya, and Manoranjan Kar. "Multiple electrical phase transitions in Al substituted barium hexaferrite." *Journal of Applied Physics* 122.22 (2017).

166. Sabo, Ronald, et al. "Nanocellulose-enabled electronics, energy harvesting devices, smart materials and sensors: A review." *J. Renew. Mater., 4 (5): 297-312.* 4.5 (2016): 297-312.

167. Guo, Jiaqi, et al. "Photoluminescent hybrids of cellulose nanocrystals and carbon quantum dots as cytocompatible probes for in vitro bioimaging." *Biomacromolecules* 18.7 (2017): 2045-2055.

168. Khabibullin, Amir, et al. "Injectable shear-thinning fluorescent hydrogel formed by cellulose nanocrystals and graphene quantum dots." *Langmuir* 33.43 (2017): 12344-12350.

169. Mazeau, Karim. "On the external morphology of native cellulose microfibrils." *Carbohydrate polymers* 84.1 (2011): 524-532.

170. Kalashnikova, Irina, et al. "Modulation of cellulose nanocrystals amphiphilic properties to stabilize oil/water interface." *Biomacromolecules* 13.1 (2012): 267-275.

171. Sekiya, Ryo, et al. "White-light-emitting edge-functionalized graphene quantum dots." *Angewandte Chemie International Edition* 53.22 (2014): 5619-5623.

172. Xiong, Rui, et al. "Self-assembly of emissive nanocellulose/quantum dot nanostructures for chiral fluorescent materials." *ACS nano* 13.8 (2019): 9074-9081.

173. Gobi, Navathej, et al. "Infusion of graphene quantum dots to create stronger, tougher, and brighter polymer composites." *ACS omega* 2.8 (2017): 4356-4362.

174. Junka, Karoliina, et al. "Modification of cellulose nanofibrils with luminescent carbon dots." *Biomacromolecules* 15.3 (2014): 876-881.

175. Song, Liqing, et al. "Structure observation of graphene quantum dots by single-layered formation in layered confinement space." *Chemical Science* 6.8 (2015): 4846-4850.

176. Dervishi, Enkeleda, et al. "Raman spectroscopy of bottom-up synthesized graphene quantum dots: size and structure dependence." *Nanoscale* 11.35 (2019): 16571-16581.

177. Liu, Qianwen, et al. "Graphene quantum dots for energy storage and conversion: from fabrication to applications." *Materials Chemistry Frontiers* 4.2 (2020): 421-436.

178. Rosddi, Najwa Norimanina Muhammad, et al. "Cationically modified nanocrystalline cellulose/carboxyl-functionalized graphene quantum dots nanocomposite thin film: Characterization and potential sensing application." *Crystals* 10.10 (2020): 875.

179. Wan Ishak, Wan Hafizi, et al. "Gamma irradiation-assisted synthesis of cellulose nanocrystal-reinforced gelatin hydrogels." *Nanomaterials* 8.10 (2018): 749.

180. Armano, Angelo, and Simonpietro Agnello. "Two-dimensional carbon: a review of synthesis methods, and electronic, optical, and vibrational properties of single-layer graphene." *C* 5.4 (2019): 67.

181. Xu, Li, et al. "Preparation and performance of radiata-pine-derived polyvinyl alcohol/carbon quantum dots fluorescent films." *Materials* 13.1 (2019): 67.

182. Alizadehgiashi, Moien, et al. "Nanocolloidal hydrogel for heavy metal scavenging." *Acs Nano* 12.8 (2018): 8160-8168.

183. Kim, Dong Jin, et al. "Graphene quantum dots from carbonized coffee bean wastes for biomedical applications." *Nanomaterials* 11.6 (2021): 1423.

184. Prabhu, S. Akash, et al. "Graphene quantum dots synthesis and energy application: A review." *Carbon Letters* 31 (2021): 1-12.

185. Wu, Junxiao, et al. "Investigation of the microstructures of graphene quantum dots (GQDs) by surface-enhanced Raman spectroscopy." *Nanomaterials* 8.10 (2018): 864.

186. Trache, Djalal, Vijay Kumar Thakur, and Rabah Boukherroub. "Cellulose nanocrystals/graphene hybrids—a promising new class of materials for advanced applications." *Nanomaterials* 10.8 (2020): 1523.

187. Gupta, Prashant, and Subhendu Bhandari. "Polymer-graphene composites as flame and fire retardant materials." *Polymer Nanocomposites Containing Graphene*. Woodhead Publishing, 2022. 743-776.

188. Vivian Abiaziem, Chioma, et al. "Preparation and characterisation of cellulose nanocrystal from sugarcane peels by XRD, SEM and CP/MAS 13C NMR." *Journal of Physics: Conference Series*. Vol. 1299. No. 1. IOP Publishing, 2019.

189. Aghdam, Taher Rahimi, et al. "Photocatalytic removal of NOx over immobilized BiFeO 3 nanoparticles and effect of operational parameters." *Korean Journal of Chemical Engineering* 35 (2018): 994-999.

190. Kumar, Sumeet, et al. "Tunable (violet to green) emission by high-yield graphene quantum dots and exploiting its unique properties towards sun-light-driven photocatalysis and supercapacitor electrode materials." *Materials Today Communications* 11 (2017): 76-86.

191. Yin, Xiaojie, et al. "Multilayer NiO@ Co 3 O 4@ graphene quantum dots hollow spheres for high-performance lithium-ion batteries and supercapacitors." *Journal of Materials Chemistry A* 7.13 (2019): 7800-7814.

192. Guo, Jinxue, et al. "Boosting the lithium storage performance of MoS 2 with graphene quantum dots." *Journal of Materials Chemistry A* 4.13 (2016): 4783-4789.

193. Park, Jungjin, et al. "Graphene quantum dots: structural integrity and oxygen functional groups for high sulfur/sulfide utilization in lithium sulfur batteries." *NPG Asia Materials* 8.5 (2016): e272-e272.

194. Guo, Jinxue, et al. "Boosting the lithium storage performance of MoS 2 with graphene quantum dots." *Journal of Materials Chemistry A* 4.13 (2016): 4783-4789.

195. Raccichini, Rinaldo, et al. "The role of graphene for electrochemical energy storage." *Nature materials* 14.3 (2015): 271-279.